AWARD NUMBER: W81XWH-16-1-0068

TITLE: Targeting the Mevalonate Pathway and its Restorative Feedback Loop in Breast Cancer

PRINCIPAL INVESTIGATOR: Linda Penn, PhD

CONTRACTING ORGANIZATION: University Health Network, 200 Elizabeth St, Toronto, Ontario, CANADA M5G 2C4

REPORT DATE: April 2019

TYPE OF REPORT: Annual

PREPARED FOR: U.S. Army Medical Research and Materiel Command

Fort Detrick, Maryland 21702-5012

REPORT DOCUMENTATION PAGE

Form Approved
OMB No. 0704-0188

1. REPORT DATE	2. REPORT TYPE	3. DATES COVERED
April 2019	Annual Report	01-APR-2018 to 31-MAR-2019

4. TITLE AND SUBTITLE
Targeting the Mevalonate Pathway and its Restorative Feedback Loop in Breast Cancer

5a. CONTRACT NUMBER

5b. GRANT NUMBER
W81XWH-16-1-0068

5c. PROGRAM ELEMENT NUMBER

6. AUTHOR(S)
Linda Penn, PhD and Dave Cescon, MD/PhD

E-Mail: lpenn@uhnresearch.ca

5d. PROJECT NUMBER

5e. TASK NUMBER

5f. WORK UNIT NUMBER

7. PERFORMING ORGANIZATION NAME(S) AND ADDRESS(ES)
University Health Network
200 Elizabeth St
Toronto, Ontario, CANADA
M5G 2C4

8. PERFORMING ORGANIZATION REPORT NUMBER

9. SPONSORING / MONITORING AGENCY NAME(S) AND ADDRESS(ES)
U.S. Army Medical Research and Materiel Command
Fort Detrick, Maryland 21702-5012

10. SPONSOR/MONITOR'S ACRONYM(S)

11. SPONSOR/MONITOR'S REPORT NUMBER(S)

12. DISTRIBUTION / AVAILABILITY STATEMENT
Approved for Public Release; Distribution Unlimited

13. SUPPLEMENTARY NOTES

14. ABSTRACT During this past year of DOD funding, we have shown that targeting the mevalonate pathway with fluvastatin specifically induces apoptosis in breast cancer (BrCa) cells that have undergone epithelial-to-mesenchyme transition (EMT), a critical process for the initiation of metastasis. Moreover, we have identified that EMT gene expression is bimodally distributed and is a biomarker of fluvastatin sensitivity. Mechanistically, we have shown that fluvastatin can induce apoptosis by limiting geranylgeranyl-pyrophosphate (GGPP) and dolichol, an important end-product of the mevalonate pathway essential for protein N-glycosylation. We have also shown that dipyridamole(DP) potentiates fluvastatin-induced apoptosis of BrCa cells by blocking the statin-induced restorative feedback loop. Unexpectedly, evaluation of the fluvastatin+DP combination was not possible in mouse models of BrCa due to toxicities associated with long-term administration of DP in mice. Importantly, this is not an issue when fluvastatin+DP are co-prescribed in humans. We have also identified additional agents that can potentiate statin-induced BrCa cell death, thereby expanding this class of anti-cancer agents.

15. SUBJECT TERMS
statins, dipyridamole, apoptosis, breast cancer, metastasis, mouse models, therapeutics, FDA-approved agents

16. SECURITY CLASSIFICATION OF:			17. LIMITATION OF ABSTRACT	18. NUMBER OF PAGES	19a. NAME OF RESPONSIBLE PERSON
a. REPORT	b. ABSTRACT	c. THIS PAGE			USAMRMC
U	U	U	UU	103	19b. TELEPHONE NUMBER *(include area code)*

Table of Contents

Page

INTRODUCTION:

Background: In early stage breast cancer (BrCa) treated with frontline therapy, 20-30% reoccur as distant metastases, despite intensive treatment. Metastatic BrCa accounts for nearly all BrCa deaths, and has no cure. Development of new and effective metastasis prevention strategies will clearly mark a key advance. We aim to fill this gap and address two overarching challenges in BrCa: 1) prevention of metastatic BrCa spread and elimination of the mortality associated with metastatic BrCa; and 2) replacing toxic interventions with ones that are safe and effective. Specifically, we aim to provide essential preclinical data to advance the Federal Drug Administration (FDA)-approved drug, statins, as metastatic BrCa prevention agents. Our preliminary data show that statins are cytotoxic to BrCa cells that have undergone epithelial-to-mesenchymal transition (EMT) and mesenchymal-to-epithelial transition (MET), two processes that form the initiation and completion of the invasion-metastasis cascade in malignant tumors. We have also shown that statin exposure triggers tumor cells to activate a feedback loop to restore expression of mevalonate pathway genes to replenish the essential growth and survival products generated by this metabolic pathway, and blocking this feedback loop potentiates the cytotoxic activity of statins. We have identified agents that block this pathway, including dipyridamole (DP). Interrogating the efficacy and mechanism of the statin+DP combination, or statin+other feedback inhibitors, in BrCa will provide preclinical evidence to support further evaluation of this novel drug combination in human clinical trials, and for the development of predictive and dynamic biomarkers of drug sensitivity.

Hypothesis and objectives: We *hypothesize* that statins, alone or in combination with agents that block the restorative feedback pathway, can be effective therapeutics to prevent BrCa recurrence. Our *objectives* are to evaluate statins +/- DP and other feedback inhibitors for their efficacy and mechanism of action in BrCa cells *in vitro,* and *in vivo* in relevant mouse models including a cohort of patient derived xenografts (PDXs). Upon completion of this BCRP grant, we will have pre-clinical evidence of efficacy and biomarkers to support a follow-up, clinical trial to test the use of statins +/- DP and/or other feedback inhibitor to treat metastatic disease. We believe that prescription of these effective, well-tolerated, and inexpensive therapeutics in patients with high risk of metastatic recurrence after surgery, will provide clinical benefit and improve BrCa patient survival and quality of life.

Specific Aims:

1. Delineate the efficacy and mechanism of the fluvastatin+DP combination and fluvastatin+additional feedback inhibitors in BrCa cells that have undergone EMT and/or MET.

2. Delineate the mechanism by which DP and additional feedback inhibitors potentiate statin-induced tumor cell apoptosis.

3. Evaluate the efficacy of fluvastatin+feedback inhibitors in relevant mouse models of BrCa metastasis.

KEYWORDS: statins, dipyridamole, statin-induced feedback inhibitors, apoptosis, breast cancer, metastasis, mouse models, therapeutics, FDA-approved agents

ACCOMPLISHMENTS:

With support from the DOD, the research outlined in the original proposal has progressed in a steady and productive manner as expected for this third year of funding. As is common in research, some unexpected results have occurred and alternative approaches have been initiated to achieve our goals. To delineate the accomplishments to date, the tasks outlined in the original Statement of Work of the proposal are itemized below (italics) and a progress report for each task provided.

Aim 1. Delineate the efficacy and mechanism of the fluvastatin+DP combination in BrCa cells that have undergone EMT and/or MET (months 1-36).
Milestones to Achieve: We will delineate the efficacy and mechanism of the fluvastatin/DP combination in BrCa cells that have undergone EMT (months 1-36).
Progress: 75%. We have delineated the efficacy and mechanism of fluvastatin-induced apoptosis in BrCa cells that have undergone EMT. One manuscript describing these findings and the identification of a biomarker of statins response, and has been published in the journal *Cancer Research* (Yu et al., PMID:29229608). A second manuscript focuses on the mechanism of statin action, which has been reviewed at *Cell Metabolism* (Appendix 1) and we are presently addressing reviewers' comments. A third manuscript focusing on the mechanism of DP action is now being written for submission (Appendix 2).

Our results indicate that BrCa cells that have undergone EMT become more sensitive to the anti-proliferative effects of fluvastatin (Yu et al., PMID:29229608). In this manuscript, we have also shown that expression of genes associated with EMT serve as a robust biomarker of statin sensitivity, not only in BrCa, but across a broad range of cancers. Moreover, we have addressed mechanism and shown that the anti-proliferative effects of fluvastatin on cells undergoing EMT is dependent on a specific product of the mevalonate pathway; geranylgeranyl pyrophosphate (GGPP). Briefly, GGPP can serve as a substrate for protein isoprenylation or as a building block for the production of co-enzyme Q or dolichol. Unexpectedly, the mechanism did not involve protein isoprenylation as anticipated (Appendix 1, Figure 1D). Instead, we have shown that key end-product in cell undergoing EMT is dolichol, which is essential for protein N-glycosylation (Appendix 1, Figure 1E, 2D, 3, 4). We have shown that the EMT re-programs the N-glycosylation profile of the cell surface and fluvastatin blocks this re-programming associated with metastasis. Indeed, we have demonstrated that statins inhibit BrCa metastasis (Appendix 1, Figure 5 and 6). In addressing reviewers comments, we went to repeat the results showing that fluvastatin-induced apoptosis of sensitive breast cancer cell lines could be rescued by the exogenous addition of mevalonate, GGPP or dolichol (Appendix 1, Figure 2D), however much to our surprise, cell death was rescued with mevalonate and GGPP, but not dolichol. The supplier of dolichol used in our previous experiments (Sigma), stopped selling this product, so we purchased this compound from other suppliers. Dolichol (C95-105]-PP) is a member of highly hydrophobic dolichol group of long-chain isoprenoid molecules, and issues with cell uptake of dolichol have been previously reported, however we had overcome this issue and shown that uptake was possible in the absence of serum in the cell medium. With the new source of dolichol, uptake was again a confounder. We are trying to re-optimize cell uptake of dolichol by evaluating various solvents, methods of delivery and media, including Tween, porphysomes, cyhlodextrins, nanoparticles, and Opti-MEM. We have labelled the dolichol to track uptake but have not yet succeeded in achieving dolichol uptake. We are continuing to optimize conditions

by changing dolichol formulations. Dolichol is essential for N-glycosylation of cell surface proteins. We have shown the remodeling of protein N-glycosylation associated with cells undergoing EMT is blocked by fluvastatin (Appendix 1).

Subtask 1: Develop and validate HPLC/MS assays to measure the intracellular concentration of MVA, GGPP and FPP, as well as DP, (Fluvastatin already established), using MCF10A cell lines overexpressing Snail and H-Ras (months 1-12; Site 1, Penn)
Complete. In collaboration with Dr. Eric Chen, we have successfully developed HPLC/MS assays to detect MVA, GGPP, FPP and DP using standard curves with purchased compounds. However, we have not been able to detect these metabolites in living cells, despite several strategies to optimize sensitivity and specificity of this assay. Optimization strategies have been exhausted using this approach, thus we will seek collaborators to work with us to perform these assays, when they are developed by others who may use different instrumentation.

Subtask 2: Establish and validate IHC assays for HMGCS1 and SREBP2, (HMGCR already established) (months 1-12; Site 1, Penn)
Complete. We have established and validated an IHC assay for SREBP2. Assay development for HMGCS1 has been terminated as all commercially available antibodies have failed at the level of sensitivity and/or specificity. Thus, we will go forward with IHC assays for the transcription factors SREBP2 and its target gene HMGCR. While having an IHC assay for another SREBP2 target, HMGCS1, would have been ideal, it is not essential to conduct our research as two out of three probes have been successfully been developed and validated.

Subtask 3: Develop titratable inducible system to express dominant active (DA) alleles, and DA alleles fused to a myristoylation tag (myr-DA) of five isoprenylated proteins (months 1-12; Site 1, Penn)
Complete. To determine whether the need for protein isoprenylation was the key to statin-sensitivity, we evaluate a panel of isoprenylated Ras-family proteins (HRas, KRas, RhoA, RhoB, Rac1, Rap1A) for their ability to increase statin sensitivity of non-transformed MCF10A breast derived cells. Surprisingly, the only isoprenylated Ras-family member that sensitized MCF10A cells to fluvastatin-induced apoptosis, was Ras (Yu et al., PMID:29229608). Thus, we generated and evaluated the myristoylated form of Ras to determine whether isoprenylation was conferring Ras-induced statin-sensitivity. Indeed, this analysis showed that Ras was able to sensitize MCF10A cells to statin-induced kill whether isoprenylated or myristoylated, showing that Ras-induced sensitivity to statins was independent of isoprenylation. This result was unexpected and lead us to discover that the sensitivity conferred by exogenous Ras (whether isoprenylated or myristoylated) was due to Ras-driving epithelial to mesenchyme (EMT) transition. (Yu et al., PMID:29229608).

Subtask 4: Express DA and myr-DA alleles in MCF10A and assay for activity, EMT and fluvastatin sensitivity in 2D and 3D culture conditions (months 6-18; Site 1, Penn).
Complete. Ectopic expression of the DA alleles of four isoprenylated proteins (RhoA, RhoB, Rac1, Rap1A) were able to transform MCF10A cells but unexpectedly did not sensitize these cells to fluvastatin-induced apoptosis or -decreased colony growth (Yu et al., PMID:29229608). Only ectopic activated Ras both transformed and sensitized MCF10A cells to the anti-proliferative activity of fluvastatin. Moreover, expression of the myr-Ras did not overcome sensitivity to fluvastatin-induced death as expected. Taken together, this data suggested that

protein isoprenylation was not contributing to the increased sensitivity to fluvastatin (Yu et al., PMID:29229608).

Subtask 5: Express DA and myr-DA alleles in MCF10A Snail and H-Ras cells and assay for activity, EMT and fluvastatin sensitivity in 2D and 3D culture conditions (months 12-24; Site 1, Penn).
Complete. Based on the results of Aim1, Subtask 4, this series of experiments was no longer required as we have shown that fluvastatin-induced apoptosis in BrCa cells was uncoupled from protein isoprenylation, yet still functionally rescued by exogenous GGPP (Yu et al., PMID:29229608). Indeed, geranylgeranyl transferase inhibitors that target the enzymes that catalyze the isoprenylation reaction do not phenocopy the increased statin sensitivity evident in cells undergoing EMT. Further interrogation showed that GGPP was not required for isoprenylation but for the production of dolichol and protein N-glycosylation (Appendix 1). Thus, the model changed and evaluating the role of these isoprenylated proteins, as originally outlined, became obsolete.

Subtask 6: Conduct RNAseq on cells grown in 3D on Matrigel, this include MCF10A cells that have (Snail, H-ras) and have not undergone EMT (vector control, MycT58A), as well as MCF10A cells expressing DA or myr-DA that undergo EMT (months 6-18; Site 1, Penn).
Complete. The goal of this subtask was to develop a mRNA expression based biomarker of cells that have undergone EMT and are highly sensitive to the anti-proliferative activity of fluvastatin. Indeed, we have identified that expression of genes associated with EMT are bimodally distributed and serve as a robust biomarker of statin sensitivity in BrCa. Moreover, we have shown that this biomarker shows efficacy across large panel of cancer types, beyond BrCa (Yu et al., PMID:29229608). The development of this signature of EMT/ responsiveness permits the further evaluation of this response marker using 3D patient-derived organoid cultures grown in 3D matrigel, as a mitigation strategy for *in vivo* administration of the fluvastatin+DP combination for which tolerability challenges have been encountered.

Subtask 7: Conduct Bioinformatics analysis on RNAseq data (months 9-21; Site 1, Penn).
Complete. Bioinformatics analysis lead to the discovery that EMT gene mRNA expression was robustly bimodally distributed and was associated with statin sensitivity. This discovery was evident in multiple cancer subtypes, including BrCa, and with multiple statin drugs, including fluvastatin, simvastatin and lovastatin (Yu et al., PMID:29229608).

Subtask 8: Evaluate metastatic potential of EMT cells (MCF10As overexpressing Snail or H-Ras) in response to fluvastatin+DP (months 18-24; Site 1, Penn)
Complete. To further evaluate the association of fluvastatin sensitivity with cells having undergone EMT, we have shown that BrCa cells that are epithelial (e.g. MCF-7, HCC1937) or mesenchymal (e.g. MDA-MB-231, HCC1806, BT549) in nature are relatively insensitive and sensitive to fluvastatin-induced apoptosis in tissue culture, respectively (Appendix 1, Figure 2). To model metastasis we therefore used a derivative of the MDA-MB-231 cells that metastasize to the lung (LM2-4) and have shown that fluvastatin decreases metastasis *in vivo* (Appendix 1, Figure 5 and 6). We used this LM2-4 (MDA-MB-231) model system rather than the MCF10A cells expressing exogenous Snail or H-Ras, as originally proposed, as we were concerned that the ability of the MCF10A models to metastasize would not be sufficiently robust, which would delay these experiments as metastatic clones would have to be identified and serially propagated to first establish the model, and then evaluate efficacy of fluvastatin+DP. Thus, the well-established LM2-4 (MDA-MB-231) cells were successfully used to model mesenchymal BrCa

cells that undergo metastasis and show that fluvastatin has anti-metastatic properties (Appendix 1, Figure 5 and 6). When we were evaluating DP dosing, we unexpectedly observed liver-associated toxicities in the cohort of mice receiving DP after 3-4 weeks of daily treatment. Thus, optimization of the dose and treatment schedule for DP was required, which is particularly important for the longer duration treatments planned using the resection/metastases prevention models. Unfortunately, this issue was not able to be resolved. Notably, this phenomenon is not expected to impact the potential clinical translation of our results, as DP is delivered clinically in an oral, extended-release formulation, and the combined use with statins is well established in secondary stroke prevention.

Subtask 9: Determine mechanism of cell death in EMT cells (MCF10As overexpressing Snail or H-Ras) vs non-EMT cells (vector control, MycT58A) (months 18-24; Site 1, Penn)
Complete. The mechanism of fluvastatin-induced cell death in EMT cells is apoptosis due to depletion of GGPP/dolichol (Appendix 1, Figure 2). Non-EMT cells are relatively insensitive to Fluvastatin (Yu et al., PMID:29229608; Appendix 1, Figure 2).

Subtask 10: Validate in independent breast cell systems using the following TNBC cell lines: MDA-MB-231, HCC1500, SUM159PT, SUM149PT, BT20, HCC1937, HS578T, MDAMB468, MDAMB436 (months 24-36; Site 1, Penn)
Complete. Several additional cell lines were evaluated (Yu et al., PMID:29229608; Appendix 1, Figure 2). In addition, to determine whether the fluvastatin+DP combination was synergistic across a panel of 47 breast cancer cell lines, a concentration range of DP was evaluated in combination with a sub-lethal dose of fluvastatin (Figure 1A). From this data a synergy score was determined using the Bliss Index model (Figure 1B). Remarkably the fluvastatin+DP combination was synergistic across the majority of cell lines. Even cell lines that were only weakly sensitive to fluvastatin were responsive to the fluvastatin+DP combination. This is consistent with our previous data showing the mevalonate pathway feedback response was intact across a panel of 25 breast cell lines (Goard et al., PMID:24337703). Interestingly, gene set enrichment analysis demonstrated that an EMT gene signature predicted sensitivity to the fluvastatin+DP combination as well as fluvastatin alone (Figure 1C).

Aim 2: Delineate the mechanism by which DP potentiates statin-induced tumor cell apoptosis (months 1-36).
Milestones To Achieve: We will identify the mechanism of DP action that potentiates fluvastatin induced apoptosis and identify the molecular mechanism at the level of SREBP2 feedback response. Novel agents and pathways that sensitize fluvastatin anti-BrCa activity will be identified (months 1-36).
Original Strategy: Complete. We have shown DP blocks SREBP translocation and the restorative feedback response to statin exposure, however, the mechanism of action remained unclear. To address this gap, our original strategy was to identify agents that blocked each of the many reported activities of DP individually, to determine which of these would phenocopy DP potentiation of statin-induced cell death. We started our analyses in AML and MM as this is where our original identification of DP was discovered and studies could begin without delay (Pandyra, et al.; PMID 24994712). Our data in AML suggested that a PDE inhibitor, cilostazol, phenocopied DP by elevating intracellular cAMP levels (Appendix 2). Since cAMP activates a major signaling cascade through Protein Kinase A (PKA), we further investigated whether modulation of PKA activities played a role in the inhibition of the sterol feedback response and

potentiation of fluvastatin-induced cancer cell death. To our surprise, however, when we functionally assessed whether the activation of PKA was the key response to DP-induced elevated cAMP, we found that PKA activation is not functionally important in DP potentiation of statin activity. The activity of DP and cilostazol was intact in both wild-type and PKA null cells at the level of statin potentiation of tumor cell kill and inhibition of the statin-induced feedback response. Thus, this line of investigation has not been as fruitful as anticipated. To ensure these well-performed experiments are disseminated broadly, so others can further explore the mechanism of DP knowing these results, we are writing a manuscript focused on these data (Appendix 2).

New Strategy: 50% Complete As the primary goal of this Aim was to identify "Novel agents and pathways that sensitize fluvastatin anti-BrCa activity" (Figure 2A) and we could not evaluate statin+DP in mouse models of BrCa as anticipated, we decided to take a pharmacogenomics approach (Figure 2B&C) with Dr. Ben Haibe-Kains to ask which drugs are "DP-like" in terms of i) Structure; by identifying compounds that have a shared chemical structure with DP, ii) Perturbation; by identifying compounds that when exposed to cells triggered similar changes to mRNA expression of six mevalonate pathway genes, determined by interrogating the LINCS L1000 dataset, and iii) Sensitivity Screening; by identifying compounds that triggered a similar profile of cell death to DP across the NCI-60 panel of cell lines. This resulted in a Mevalonate Pathway-specific Drug Network Fusion (MVA-DNF). Twenty-three drugs were identified as hits based on statistical significance. Several have been validated justifying further work to complete this novel approach to identify agents and pathways that sensitize fluvastatin anti-BrCa activity.

Subtask 1: Evaluate pharmacological agents for their ability to phenocopy DP and potentiate fluvastatin anti-BrCa activity (MCF10As overexpressing Snail or H-Ras; other TNBC cell lines including MDA-MB-231, HCC1500, SUM159PT, SUM149PT, BT20, HCC1937, HS578T, MDAMB468, MDAMB436 (months 1-12; Site 1, Penn)

New Strategy: 50% Complete. To investigate whether these drugs identified as DP-like could potentiate fluvastatin induced cell death, we looked to validate the top five hits from the ranked list of drugs similar to DP ($p<0.05$). As Doxorubicin scored as a top hit and we had previously published this agent as a potentiator of lovastatin (Martirosyan et al., PMID:20298590), this provided confidence in our results, and the top four drugs were advanced for validation (selumetinib, nelfinavir, mitoxantrone and honokiol) (Figures 3&4). We investigated the sensitivity to sub-lethal statin exposure in combination with the novel DP-like drugs in a statin-sensitive (MDA-MB-231; Fig3) and insensitive (HCC1937; Fig4) BrCa cell lines. As seen with DP, we observed similar potentiation of statins when combined with nelfinavir, honokiol or selumetinib, but not mitoxantrone (Figure 3&4). To determine the nature of the anti-proliferative activity of statins+drugs, we evaluated cell cycle arrest and cell death by fixed propidium-iodide/flow cytometry and apoptosis by PARP-cleavage, respectively. Our data indicates that all three drug combinations mimic DP with an increase in pre-G1 population (Figure 5).

We will validate this apoptotic cell death by an independent approach, such as evidence of PARP cleavage. Moreover, we will extend our analysis across the 47 BrCa cell line panel to evaluate whether these agents synergize with fluvastatin (as previously conducted with DP, see Figure 1). Given the validation of these hits, we will further validate additional hits from the MVA-DNF analysis and prioritize those that are FDA-approved as they can be fast-tracked to patient care in combination with statins.

Subtask 2: Validate results using independent pharmacological inhibitors and RNAi approach (months 9-24; Site 1, Penn)

New Strategy: Ongoing. Selumetinib is a MEK inhibitor and we had previously shown that statin inhibition of the MAPK-ERK-MEK pathway contributed to the AML cell death in response to lovastatin exposure (Wu et al. PMID:15374955). Moreover, we had shown that the MEK1 inhibitor PD98059 sensitized AML cells to low, physiologically achievable concentrations of lovastatin. Thus, our new data shows another MEK inhibitor (Selumetinib) can potentiate fluvastatin-induced cell death of BrCa cell lines and validates statin+MEKi as a combination for further evaluation. Honokial is a product from Mahogany tree bark and mechanism of action remains unclear, therefore we are not able to further evaluate mechanism at a molecular level using a genetic approach. Nelfinavir is a S1P protease inhibitor, therefore we will further validate by establishing inducible shRNAs targeting this protease to evaluate whether this on-target effect is mechanistically critical for nelfinavir to potentiate fluvastatin tumor cell death. On-target validation using a similar genetic approach will be performed once additional hits from the MVA-DNF screen are validated.

Subtask 3: Determine molecular mechanism of action of novel DP-like molecules that can potentiate fluvastatin-induced apoptosis by assaying statin-induced feedback loop at the molecular level (MCF10As overexpressing Snail or H-Ras) (months 24-36; Site 1, Penn).

Ongoing. Assaying the feedback response to statin exposure by qRT-PCR mRNA expression of mevalonate pathway genes will be performed as before in the presence and absence of fluvastatin alone, DP-like drugs alone or fluvastatin+DP-like drugs in combination.

Subtask 4: Conduct biochemical analyses to determine point of SREBP2 translocation that is blocked by DP (MCF10As overexpressing Snail or H-Ras) (months 1-12; Site 1, Penn).

Ongoing. SREBP2 biochemical fractionation will be performed as before. DP as well as additional inhibitors of the feedback response will be evaluated in the presence and absence of fluvastatin.

Subtask 5: Evaluate precise point of SREBP2 inhibition by DP using fluorescence strategies (months 13-24; Site 1, Penn).

Ongoing. We will use a SCAP-GFP tool to evaluate whether DP and novel inhibitors of SREBP2 translocation are blocking at the stage of ER-to-Golgi translocation in BrCa cells. 25-hydroxy-cholesterol will be used as a positive control. Also we have acquired access to the PathHunter SREBP2 Nuclear Translocation Assay to quantitatively evaluate SREBP2 translocation to the nucleus. DP as well as additional inhibitors of the feedback response will be evaluated +/- fluvastatin.

Subtask 6: Determine whether novel agents and RNAi block at similar or dissimilar points of SREBP2 feedback control (months 24-36; Site 1, Penn).

Ongoing. The on-target effect of the agents under evaluation will be studied by using inducible shRNAs of the drug target (if known) to evaluate whether the statin-triggered feedback loop is blocked.

Aim 3: Evaluate the efficacy of fluvastatin+DP in relevant mouse models of BrCa metastasis (months 1-36).
Milestones To Achieve: Evaluate the effects of fluvastatin +/- DP treatment in cell line and BrCa patient-derived xenografts (PDX) using both a conventional and resection model to evaluate activity on primary and metastatic tumor (months 1-36).
Progress: 35%. We have completed the initial planned experiments evaluating the effects of fluvastatin treatment of cell line xenografts by both the conventional and resection models (Appendix 1, Figures 5 and 6). To evaluate fluvastatin+/- DP combination we first evaluated DP dosing and unexpectedly observed liver-associated toxicities in the cohort of mice receiving DP after 3-4 weeks of daily treatment. Thus, optimization of the dose and treatment schedule for DP was required, which is particularly important for the longer duration treatments planned using the resection/metastases prevention models. Unfortunately, this issue was not able to be resolved. Notably, this phenomenon is not expected to impact the potential clinical translation of our results, as DP is delivered clinically in an oral, slow-release formulation, and the combined use with statins is well established in secondary stroke prevention. Having completed the characterization of the models, and recognizing that synergistic combination therapies are likely to be necessary (vs statin monotherapy), we plan to proceed with a mitigation strategy of evaluating alternative combinations from the DP-like agents (described above) that block the statin-induced feedback response for evaluation as single agents and in combination with fluvastatin in cell line xenograft models as well as PDXs, once these have been validated (ongoing). In addition, the combinations of fluvastatin+DP and fluvastatin+novel combinations can be evaluated in the patient-derived models using 3D organoid approach.

Subtask 1: Conduct dose escalation experiments to identify maximum tolerated and effective dose of fluvastatin in the resection model using two cell lines: Luc+14 and Luc+16 (months 1-2; Site 1, Penn).
Complete. We have shown that in the resection model using LM2-4, a MDA-MB-231 derived cell line, that 50 mg/kg daily oral fluvastatin treatment is effective and well-tolerated for long-term treatment in the post-surgical adjuvant setting in SCID mice. This dose of fluvastatin treatment has been used for all subsequent animal studies (Appendix 1).

Subtask 2: Establish and treat PDX #1-8 in (A) conventional PDX models and (B) resection models (months 3-12; Site 2, Cescon).
20% Complete. While DP optimization was underway, we evaluated the effect of fluvastatin monotherapy in (A) conventional and (B) resection models as proposed. While model characterization has been completed (Subtask 4 below), given the limitations encountered with DP administration and the limited monotherapy data observed as expected with fluvastatin, we await the possibility of an alternative/superior combination to be identified through additional work which could proceed to *in vivo* testing. Development of *in vitro* patient-derived xenograft organoids has proceeded to create alternative models to evaluation the fluvastatin+DP (or other novel) combinations.

Subtask 3: Establish and treat PDX #9-25 with control, fluvastatin+DP (2 treatment arms) in (A) conventional PDX models and (B) resection models (months 8-28; Site 2, Cescon).
To be reassessed, given the limitations as encountered above. Mitigation strategies including PDX-derived organoids and novel DP-like combinations are being evaluated.

Subtask 4: Conduct RNAseq on 25 PDX donor mouse primary tumors (months 3-28; Site 1/2, Penn/Cescon)
Complete. Basal RNAseq data has been collected on 30 PDX models. These will permit the interrogation of gene expression predictors of responsiveness to guide experimental evaluation of statin combinations, including novel combinations *in vivo* as well as statin+DP *in vitro* in PDX derived organoids building on the work completed in Aim 1.

Subtask 5: Conduct Bioinformatics analysis on RNAseq data (months 18-36; Site 1, Penn)
Yet to complete. We will next distinguish patient-derived models with the EMT signature. These will be prioritized for future testing with fluvastatin in combination with feedback inhibitors *in vivo* and/or *in vitro* organoid cultures.

Subtask 6: Measure the intracellular concentration of MVA, GGPP and FPP, as well as fluvastatin and DP, as well as cholesterol, triglycerides; pilot on MDA-MB-231 metastasis model, then evaluate PDX models (month 3-36; Site 1, Penn)
On-going. We have measured fluvastatin in the MDA-MB-231 metastasis model in experiments using the MDA-MB-231 metastasis model (Appendix 1, Figure 5B and 5C). Assay development for DP detection and quantification *in vivo* is on-going. The assay for cholesterol and triglycerides measurement is already developed by our collaborator Dr. Richard Lehner. Detection of these metabolites in the PDX models will be conducted after the PDXs are established and treated with the new fluvastatin+feedback inhibitor regimen.

Subtask 7: Conduct RNA analysis and IHC assays for mevalonate genes including HMGCR, HGMCS1 and SREBP2; pilot on MDA-MB-231 metastasis model, then evaluate PDX models (months 3-36; Site 1, Penn).
On-going. We have collected RNA for HMGCR, HMGCS1 and SREBP2 analysis in the MDA-MB-231 metastasis model. IHC assays for HMGCR and SREBP2 will also been conducted with our validated antibodies. Evaluation of the expression of these genes in the PDX models will be conducted after the PDXs are established and treated with fluvastatin and the new feedback inhibitor regimen.

Subtask 8: Analyze all data and publish papers (months 12-36; Site 1 and 2, Penn and Cescon)
On-going. Funding from the DOD has resulted in the publication of a manuscript in the journal Cancer Research (Yu et al., PMID:29229608), another manuscript has been submitted and reviewed by Cell Metabolism (Appendix 1) and another focused on DP mechanism is in preparation (Appendix 2). We anticipate the results of our MVA-DNF study will be completed in about 1.5 yrs after further validation and testing (Figures 1-5), as outlined above.

IMPACT:

We have shown that fluvastatin specifically induces apoptosis in BrCa cells that have undergone EMT, a critical process for the initiation of metastatic spread. These results have direct medical **impact**, as the addition of fluvastatin to the standard of care for BrCa in the adjuvant setting is novel and an actionable outcome that can be readily and affordably implemented.

We have shown that the mechanism of fluvastatin-induced apoptosis in cells undergoing EMT is independent of protein isoprenylation. These results directly **impact** disciplines involving the study of the anti-cancer effects of statins, isoprenylation of RAS family members, metabolic reprogramming and cancer cell EMT. For decades, it has been unclear whether statins kill tumour cells by inhibiting the synthesis of FPP and GGPP, thereby limiting the function of RAS family oncoproteins. This has been a major obstacle in accelerating statins into the BrCa clinic. Our work resolves the discrepancy surrounding this open question by showing that although statins can inhibit isoprenylation of RAS family members, this is not the cause of statin-induced cell death. Instead, we identify EMT gene expression as robust biomarkers of statin sensitivity, which has **impact** and clinical utility as it will inform which patients are most likely to benefit from statin treatment to inhibit aggressive and/or metastatic cancers.

We have begun to delineate the mechanism of action of DP and additional feedback inhibitors that potentiates fluvastatin induced apoptosis. These results have important conceptual and technical **impact**, i) being the first indication that the MVA pathway and its homeostatic feedback regulation are both essential to cells with increased epithelial-mesenchymal plasticity, and ii) uncovering novel ways to identify new strategies to inhibit the SREBP family of transcription factors that drive expression of mevalonate pathway genes and this statin-induced feedback response.

While we have encountered challenges in the *in vivo* evaluation of the fluvastatin+DP combination therapy, due to mouse-specific delivery/tolerability issues we believe our data characterizing the anticancer effects of these well-tolerated and clinically available (in humans) supports the potential for clinical translation, and we are currently working to develop a clinical study to test this. In addition, we have identified novel agents which may have superior synergy, which can be validated and prioritized using the systems and models developed in this project. By evaluating the efficacy of these therapeutics in relevant mouse models and a large cohort of PDXs in both conventional (primary tumor) and resection models (metastatic disease burden), we closely mimic not only the human disease and course of metastatic spread, but also the patient treatment and recovery experience. These relevant and innovative research approaches significantly **impact** BrCa treatment and metastasis prevention.

We have prepared three manuscripts describing our research progress from this first three years of DOD funding. One has been published in the journal *Cancer Research* (Yu et al., PMID:29229608) and the other has been reviewed at the journal *Cell Metabolism* (Appendix 1). We are addressing reviewers' comments in preparation for re-submission of the latter. We are preparing another for publication (Appendix 2) and have new data identifying additional feedback inhibitors that will be further interrogated and published in the near future. Publishing our work in top-flight journals such as these with wide readership significantly **impacts**

technology transfer, allowing us to communicate our ideas and successes, and to move the tools and treatments we have developed forward to clinical application. Presenting our results in local seminars and international conferences to scientists as well as the lay public also **impacts** society at large by engaging a global and diverse audience.

CHANGES/PROBLEMS:

One of our goals is to address the mechanism of DP action from a bottom-up and top-down approach. To address the former we are using mass spectrometry and image analysis tools that we have developed and revealed that DP blocks SREBP2 translocation from the ER to the Golgi, thus blocking this transcription factor from reaching the nucleus. By taking a top-down approach we anticipated that we could determine which of the many biochemical pathways affected by DP may be important for DPs ability to potentiate statin-induced apoptosis of BrCa cells. We evaluated agents that block each of the pathways downstream of DP and thought that inhibition of phosphodiesterases, leading to elevation of cAMP was the key. However, further work showed that cAMP activation of PKA was not functionally important. Thus, this work was not fruitful and lead to a dead end. To overcome this problem, we are using pharmacogenomics approach to identify other agents that can potentiate statin anti-proliferative activity of BrCa cells by inhibiting the statin-induced feedback response. This strategy will increase the arsenal of inhibitors that can potentiate the anti-BrCa activity of statins.

As noted, chronic DP administration *in vivo* for the duration required to evaluate the effects of interest (on metastases) presented an unexpected challenge. We are addressing this in two ways: (i) separately exploring the potential for clinical studies of fluvastatin+DP, based on our combined results and established safety of this approach and (ii) further characterizing novel DP-like combinations which could offer new therapeutic opportunities.

PRODUCTS:

Manuscript published: Yu R, Longo J, van Leeuwen JE, Mullen PJ, Ba-Alawi W, Haibe-Kains B, Penn LZ. Statin-induced cancer cell death can be mechanistically uncoupled from prenylation of RAS family proteins. Cancer Research 2018; 78(5):1347-1357.

Manuscript submitted and reviewed: Yu R, Longo J, van Leeuwen JE, Zhang C, Zhang W, Cescon D, Chen E, Drake RR, Dennis JW, Penn LZ. Blocking the metabolic mevalonate pathway attenuates breast cancer metastasis by altering dolichol-dependent protein N-glycosylation.

PARTICIPANTS & OTHER COLLABORATING ORGANIZATIONS

Name:	*Linda Penn*
Project Role:	*PI (Site 1)*
Researcher Identifier (e.g. ORCID ID):	0000-0001-8133-5459
Nearest person month worked:	36
Contribution to Project:	*Dr. Penn is the leading PI of this project.*
Funding Support:	Salary is not covered by the DOD grant

Name:	*David Cescon*
Project Role:	*Partnering PI (Site 2)*
Researcher Identifier (e.g. ORCID ID):	
Nearest person month worked:	36
Contribution to Project:	*Dr. Cescon is the partnering PI of this project.*
Funding Support:	Salary is not covered by the DOD grant

Name:	*Joseph Longo*
Project Role:	*Graduate Student*
Researcher Identifier (e.g. ORCID ID):	*n/a*
Nearest person month worked:	36
Contribution to Project:	*Mr. Longo has performed work in delineating the mechanism by which DP potentiates statin-induced tumor cell apoptosis, and evaluating the efficacy of fluvastatin in a relevant mouse model of BrCa metastasis.*
Funding Support:	*CIHR Fellowship + DOD grant*

Name:	*Jenna E. van Leeuwen*
Project Role:	*Graduate Student*
Researcher Identifier (e.g. ORCID ID):	*n/a*
Nearest person month worked:	24
Contribution to Project:	*Ms. van Leeuwen has performed work in delineating the efficacy and mechanism of the fluvastatin+DP combination in BrCa cell lines, and evaluating the efficacy of fluvastatin in a relevant mouse model of BrCa metastasis.*
Funding Support:	*DOD grant*

Name:	*Aaliya Tamachi*
Project Role:	*Research Technician*
Researcher Identifier (e.g. ORCID ID):	*n/a*
Nearest person month worked:	36
Contribution to Project:	*Ms. Tamachi has contributed to this project by supporting the animal work and lab work.*
Funding Support:	*DOD grant*

Name:	*Chantal Tobin*
Project Role:	*Research Technician*
Researcher Identifier (e.g. ORCID ID):	*n/a*
Nearest person month worked:	17
Contribution to Project:	*Ms Tobin has contributed to the development and evaluation of patient-derived xenograft models.*
Funding Support:	*DOD grant*

Name:	*Mohamad Elbaz*
Project Role:	*Post-Doctoral Fellow*
Researcher Identifier (e.g. ORCID ID):	*n/a*
Nearest person month worked:	17
Contribution to Project:	*Dr. Elbaz has performed work to identify DP-like molecules that potentiate Fluvastatin anti-BrCa activity by inhibiting the Fluvastatin restorative feedback response, and evaluating the efficacy of Fluvastatin in a relevant mouse model of BrCa metastasis.*
Funding Support:	*DOD grant*

APPENDICES:

Appendix 1: Yu R, Longo J, van Leeuwen JE, Zhang C, Zhang W, Cescon D, Chen E, Drake RR, Dennis JW, Penn LZ. Blocking the metabolic mevalonate pathway attenuates breast cancer metastasis by altering dolichol-dependent protein N-glycosylation. Submitted.

Appendix 2: Longo, J., Pandyra, A.A., Minden, M.D., Schimmer, A.D., Penn, L.Z. Cyclic AMP-hydrolyzing phosphodiesterase inhibitors potentiate statin-induced cancer cell death

Appendix 3: Additional figures supporting this report.

Graphical Abstract

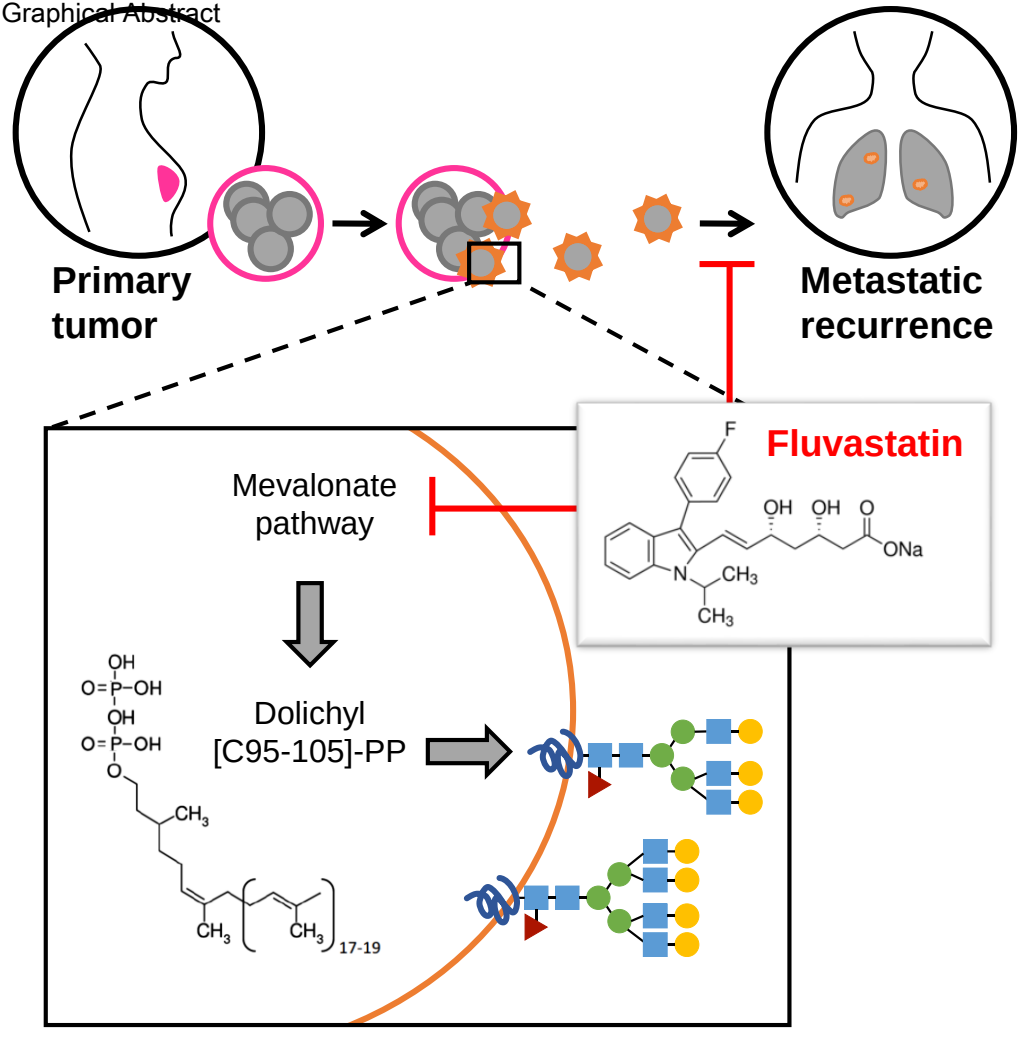

Blocking the metabolic mevalonate pathway attenuates breast cancer metastasis by altering dolichol-dependent protein *N*-glycosylation

Rosemary Yu[1,2], Joseph Longo[1,2], Jenna E. van Leeuwen[1,2], Cunjie Zhang[3,4,5], Wenjiang Zhang[1], David Cescon[1], Eric Chen[1], Richard R. Drake[6], James W. Dennis[3,4,5], Linda Z. Penn[1,2,*]

[1]Princess Margaret Cancer Centre, University Health Network, Toronto, Ontario, Canada M5G 1L7.
[2]Department of Medical Biophysics, University of Toronto, Toronto, Ontario, Canada M5G 1L7.
[3]Lunenfeld-Tanenbaum Research Institute, Mount Sinai Hospital, Toronto, Ontario, Canada M5G 1X5.
[4]Department of Molecular Genetics, University of Toronto, Toronto, Ontario, Canada M5G 1L7.
[5]Department of Laboratory Medicine and Pathobiology, University of Toronto, Toronto, Ontario, Canada M5G 1L7.
[6]Department of Cell and Molecular Pharmacology and Experimental Therapeutics, Medical University of South Carolina, Charleston, South Carolina, United States 29425.

***Corresponding Author and Lead Contact:**
Linda Z. Penn
Princess Margaret Cancer Research Tower
101 College Street, 13-706
Toronto, Ontario, Canada M5G 1L7
416-634-8770
Linda.Penn@uhnresearch.ca

Key words: mevalonate pathway, statins, protein *N*-glycosylation, breast cancer, metastasis, tumor metabolism

Character Count: 53,709

Figures: 6

Summary

Targeting the aberrant tumor metabolism supporting protein post-translational modifications offers a new strategy to combat metastatic breast cancer. We show that the mevalonate pathway is such a vulnerability, and the pathogenic link between this metabolic pathway and breast cancer metastasis is the biosynthesis of dolichol. Dolichol is a class of essential metabolites required to construct donor oligosaccharides for *N*-glycosylation in the protein maturation pathway. Inhibition of the mevalonate pathway by fluvastatin, an FDA-approved drug, reduces *N*-glycosylation at the endoplasmic reticulum and inhibits *N*-glycan remodeling in the Golgi, notably *N*-acetylglucosaminyltransferase V (GnT-V)-mediated branching associated with epithelial-to-mesenchymal transition and metastasis. In a mouse model of post-surgical metastatic breast cancer, adjuvant fluvastatin treatment reduced metastatic burden and improved overall survival. These data support the immediate repurposing of fluvastatin as an adjuvant therapeutic to combat metastatic recurrence in breast cancer, by inhibiting dolichol biosynthesis, in turn reducing *N*-glycosylation site occupancy and altering *N*-glycan branching.

Introduction

The front-line therapy for early stage breast cancer is surgical removal of the tumor followed by adjuvant therapies (Weigelt et al., 2005). Despite aggressive treatment, 15-20% of patients experience recurrence, often as distant metastases (Weigelt et al., 2005). Novel and effective therapeutics to prevent metastatic recurrence will greatly impact breast cancer patient survival. Several retrospective studies have indicated that the risk of post-surgical breast cancer recurrence is reduced by 30-60% in patients who are taking statins (Ahern et al., 2011; Boudreau et al., 2014; Chae et al., 2011; Kwan et al., 2008), a class of approved drugs that are commonly prescribed to lower serum cholesterol. Importantly, increasing duration of adjuvant statin use is associated with decreasing risk of recurrence (Kwan et al., 2008), suggesting that long-term intake of statins in the adjuvant setting can prolong patient survival.

Statins inhibit the metabolic conversion of 3-hydroxy-3-methylglutaryl coenzyme A (HMG-CoA) to mevalonate (MVA), the rate-limiting step of the MVA pathway (Fig. 1A). The MVA pathway synthesizes cholesterol and isoprenoid metabolites including farnesyl pyrophosphate (FPP) and geranylgeranyl pyrophosphate (GGPP), required for post-translational prenylation of proteins such as RAS (Mullen et al., 2016). Previous work has suggested that depletion of FPP and/or GGPP, and consequently inhibition of protein prenylation of RAS family members, underlies statin-induced breast cancer cell death (Mullen et al., 2016). However, mutations in RAS family proteins could not predict response to statins in several prospective clinical trials (Baas et al., 2015a; Baas et al., 2015c; Hong et al., 2014), suggesting that alternative or additional mechanisms are at play. Understanding these mechanisms will be crucial to guide the design of clinical trials, identify biomarkers of statin response, and identify novel anti-cancer pathways for the development of next-generation therapeutics to prevent metastatic breast cancer.

Here, we sought to interrogate the mechanism of statin sensitivity in cell line and *in vivo* models that are reflective of the adjuvant therapeutic space. The endpoint of adjuvant therapies is metastatic outgrowth, which arises from disseminated primary tumor cells (Weigelt et al., 2005). Activation of epithelial-to-

mesenchymal transition (EMT) in cancer cells has been proposed to be the critical initiating step for dissemination, which needs to be reversed at the secondary site to give rise to metastatic outgrowth (Giancotti, 2013). Although it is still debated whether these processes are required for metastasis, the observation that disseminated cancer cells often gain mesenchymal characteristics while losing epithelial features (Giancotti, 2013) suggests that therapeutic targeting of breast cancer cells with mesenchymal phenotypes will reflect utility in the adjuvant setting. Thus, in this manuscript, we first use an EMT model system in breast cancer cell lines to evaluate the mechanism of statin sensitivity *in vitro.* We show that mesenchymal phenotype sensitizes breast cancer cells to fluvastatin-induced cell death, due to an increased dependency on the biosynthesis of dolichol via the MVA pathway (Fig. 1A). Dolichol is a group of long-chain isoprenoids that comprises the lipid component of lipid-linked oligosaccharides (LLO), essential for *N*-linked glycosylation of nascent peptides (Mullen et al., 2016). Previous studies have shown that statin treatment can block *N*-glycosylation on individual proteins such as P-gp (Atil et al., 2016), IGFR (Dricu et al., 1997), EpoR (Hamadmad and Hohl, 2007), and FLT3 (Williams et al., 2012). Here we show that fluvastatin treatment not only reduced the occupancy of LLO-dependent *N*-glycosylation sites, as expected, but also reduced *N*-glycan remodeling in the Golgi; notably *N*-acetylglucosaminyltransferase V (GnT-V; encoded by *MGAT5*)-mediated branching associated with breast cancer EMT and metastasis (Cheung and Dennis, 2007; Lau et al., 2007; Partridge et al., 2004). Finally, using an *in vivo* model of post-surgical metastasis that closely follows the course of human breast cancer progression and treatment (Guerin et al., 2013), we demonstrate that post-surgical adjuvant fluvastatin treatment attenuates breast cancer metastasis and improves overall survival. Taken together, our results warrant the immediate clinical testing of fluvastatin as a safe and effective therapeutic in the adjuvant setting, and suggest the development of novel therapeutics to combat metastatic recurrence in breast cancer by inhibiting aberrant protein *N*-glycosylation.

Results

EMT sensitizes breast cancer cells to fluvastatin and tunicamycin

Fluvastatin was chosen for our studies based on its favorable pharmacokinetic properties and promising anti-breast cancer activities in pre-clinical and clinical pre-operative settings (Garwood et al., 2010; Goard et al., 2014). We used MCF10A breast epithelial cells as our model system, as they possess a highly stable genome, which allows for the evaluation of EMT and statin activity in the absence of gross genetic instability (Soule et al., 1990). Ectopic expression of the EMT-inducing transcription factor SNAIL triggered EMT in MCF10A cells, as shown by downregulation of E-cadherin and upregulation of fibronectin (Fig. 1B). Treatment with fluvastatin readily induced cell death in SNAIL-overexpressing cells, but not vector control cells, as assessed by quantification of DNA content following cell fixation and propidium iodide staining (Fig. 1C). Fluvastatin-induced cell death in SNAIL-overexpressing cells was fully rescued by co-administration with MVA or GGPP, but interestingly not FPP (Fig. 1C), a metabolic intermediate between MVA and GGPP (Fig. 1A). This preferential rescue of statin-induced cell death in tumor cells by GGPP has also been reported in several other cancer cell lines (Kusama et al., 2006; Taylor-Harding et al., 2010), together suggesting that exogenous FPP is shunted towards cholesterol synthesis and away from GGPP synthesis, while disruption of biological processes downstream of GGPP is critical for statin-induced cell death.

GGPP is required for three biological processes: protein prenylation, synthesis of coenzyme Q (CoQ) used in the electron transport chain (ETC), and synthesis of dolichol required for protein *N*-glycosylation (Fig. 1A) (Mullen et al., 2016). We tested whether inhibiting any of these pathways individually using specific inhibitors (Fig. 1A) could phenocopy statins and preferentially kill breast cancer cells with mesenchymal phenotypes. EMT sensitized cells to fluvastatin, as indicated by a lowered IC_{50} value in SNAIL-overexpressing cells (Fig. 1D). To our surprise, EMT did not sensitize cells to geranylgeranyltransferase inhibitors, GGTI-298 or GGTI-2133 (Fig. 1D), suggesting that fluvastatin-induced cell death in this context is independent from inhibition of protein prenylation. The IC_{50} for 2-

thenoyltrifluoroacetone (2-TTFA) and rotenone were similar in both vector and SNAIL-overexpressing cell lines (Fig. 1D), indicating that EMT does not sensitize cells to inhibition of the ETC. Instead, inhibition of LLO assembly downstream of dolichol synthesis by tunicamycin phenocopied fluvastatin by decreasing the IC_{50} in SNAIL-overexpressing cells (Fig. 1D).

These observations were validated in MCF10A cells overexpressing SLUG, TWIST or ZEB1, as well as two independent breast cancer cell lines, MDA-MB-231 and MCF-7 (Fig. S1A-D). Ectopic expression of TWIST or ZEB1 induced EMT in MCF10A cells, as indicated by downregulation of E-cadherin and upregulation of fibronectin or vimentin, while SLUG was unable to induce EMT in the MCF10A cell system (Fig. S1A). Consistently, the mesenchymal TWIST- and ZEB1-expressing cells became more sensitive to fluvastatin and tunicamycin compared to the vector control and the SLUG-expressing cells, which remained epithelial (Fig. S1B). The IC_{50} for GGTIs and ETC inhibitors were unaffected by EMT (Fig. S1B). Similarly, immunoblotting for E-cadherin and vimentin indicated that MCF-7 cells were epithelial and MDA-MB-231 cells were mesenchymal (Fig. S1C). These two cell lines exhibited a 50-fold difference in sensitivity to both fluvastatin and tunicamycin, which could not be phenocopied by GGTI-298, GGTI-2133, 2-TTFA, or rotenone (Fig. S1D). Together, these data indicate that breast cancer cells with mesenchymal phenotypes are more sensitive to fluvastatin or tunicamycin inhibition of dolichol synthesis and function.

Fluvastatin inhibits dolichol-mediated protein *N*-glycosylation

Dolichol is a group of hydrophobic isoprenoid molecules that constitutes the lipid component of LLOs, playing an essential role in the assembly of precursor *N*-glycans used for co-translational protein *N*-glycosylation (Mullen et al., 2016). We therefore tested whether fluvastatin treatment can inhibit protein *N*-glycosylation. EGFR, GP130, and SLC3A2 are three membrane proteins with multiple glycosylation sites. All three membrane proteins became under-glycosylated after 48-72 h of fluvastatin treatment, in both vector and SNAIL-overexpressing cells (Fig. 1E), visualized as lower molecular weight bands by

immunoblotting (Powlesland et al., 2009). As a positive control, tunicamycin inhibition of protein glycosylation was observed after 24 h (Fig. 1E).

As tunicamycin treatment is also known to elicit ER stress, we tested whether the observed effect on protein glycosylation is specific to the inhibition of dolichol biosynthesis and/or function, or an indirect consequence of ER stress. To this end, we treated cells with thapsigargin, a dolichol-independent inducer of ER stress. First, we confirmed that treatment with tunicamycin or thapsigargin induced ER stress, as indicated by upregulation of ER stress markers ERdj4 and BiP, in both vector and SNAIL-overexpressing cells following 24 h of treatment (Fig. S2A). By contrast, treatment with fluvastatin had no significant effect on the expression of ERdj4 and BiP for up to 72 h (Fig. S2A), suggesting that defects in protein glycosylation caused by fluvastatin treatment (Fig. 1E) can be uncoupled from induction of ER stress. Treatment with thapsigargin for up to 72 h did not result in under-glycosylation of EGFR, GP130, or SLC3A2 in either vector or SNAIL-overexpressing cells, although a slight reduction in glycoprotein levels were observed due to ER stress-dependent signaling, as expected (Fig. S2B). Additionally, whereas overexpression of SNAIL sensitized MCF10A cells to fluvastatin and tunicamycin (Fig. 1D), the sensitivity of SNAIL-overexpressing MCF10A cells to thapsigargin remained the same as the vector control cells (Fig. S2C, left panel); the mesenchymal MDA-MB-231 cells were in fact more resistant to thapsigargin than the epithelial MCF-7 cells (Fig. S2C, right panel), further supporting that mesenchymal breast cancer cells are sensitized to fluvastatin and tunicamycin treatment through a dolichol-dependent mechanism.

We next evaluated whether exogenous dolichol can functionally rescue statin-induced cell death across a panel of 5 breast cancer cell lines. Immunoblot of E-cadherin and vimentin showed that MCF-7 and HCC1937 were epithelial, while MDA-MB-231, HCC1806, and BT549 cells displayed mesenchymal characteristics (Fig. 2A). The mesenchymal cell lines were more sensitive to fluvastatin treatment, while the epithelial cell lines were more resistant, as indicated by the fluvastatin IC_{50} of each cell line (Fig. 2B). Exogenous addition of MVA, GGPP, or dolichol (dolichyl[C95]-PP; Fig. 2C) fully rescued viability of

the mesenchymal cell lines in the presence of fluvastatin (Fig. 2D). The presence of serum inhibits dolichol uptake (Palamarczyk and Butters, 1982) and abolished the ability of dolichol to rescue the reduction in cell viability caused by fluvastatin treatment (Fig. S3A-B), which likely explains previous contradicting results regarding the functional role of dolichol in the anti-tumor activity of statins (Bokoch and Prossnitz, 1992; Xia et al., 2001). Taken together, our data suggest that breast cancer cells with mesenchymal characteristics are more sensitive to inhibition of the MVA pathway due to an increased dependency on dolichol-dependent protein *N*-glycosylation.

Fluvastatin reduces protein *N*-glycosylation site occupancy and *N*-glycan remodeling

In the ER, dolichol-dependent protein *N*-glycosylation occurs on asparagine residues (Fig. 3A) on newly synthesized peptides at the consensus sequence NXS/T, where X is not a proline (X≠P). To test whether inhibition of dolichol synthesis by fluvastatin inhibits *N*-glycosylation site occupancy, we performed targeted glycopeptide analysis in HeLa cells where endogenous SLC3A2 has been knocked out, and a single Flp-in insertion site was occupied by tetracyclin (Dox)-inducible FLAG-tagged SLC3A2. FLAG-SLC3A2 became under-glycosylated with increasing time of fluvastatin treatment (Fig. 3B). After FLAG-IP and trypsin digest, three peptides containing asparagine *N*-glycosylation sites were detected and quantified by LC-MS/MS (Table S1). Increasing time of fluvastatin treatment inhibited site occupancy at Asn365 and Asn381, leading to an increase in the unoccupied fraction of these two peptides (Fig. 3C). Interestingly, site occupancy of Asn424 remained unaffected by fluvastatin treatment (Fig. 3C), suggesting site position in the protein fold may differ in sensitivity to LLO levels.

Following LLO-mediated *N*-glycosylation and after successful folding in the ER, glycoproteins enter the Golgi for glycan remodeling and maturation (Fig. 3A). Complex type *N*-glycans are a major subtype of mature *N*-glycans (Fig 3D) that can be further subdivided by the degree of modification by the monosaccharide fucose (F, Fuc) at the core region (Fig 3D, highlighted in box) or at the glycan branches. Analysis of SLC3A2 glycopeptides revealed that fluvastatin treatment reduced the expression of complex type *N*-glycans at all three *N*-glycosylation sites (Fig. 3E-G; Table S1), suggesting that the impact of

fluvastatin treatment extends beyond the efficiency of peptide *N*-glycosylation at the ER, to include Golgi-level effects on *N*-glycan remodeling and maturation as well (Fig. 3A).

Fluvastatin inhibits EMT-associated *N*-glycan remodeling

Oncogene-associated increases in the expression of complex type *N*-glycans are required for cancer cell metastasis (Cheung and Dennis, 2007; Lau et al., 2007; Partridge et al., 2004), We hypothesized that breast cancer cells that have undergone EMT are dependent on altered *N*-glycan expression for their survival, which would explain why SNAIL-overexpressing cells were more sensitive to fluvastatin- and tunicamycin-induced cell death (Fig. 1D), while under-glycosylation of membrane proteins were observed in both vector control cells and SNAIL-overexpressing cells (Fig. 1E). To test this hypothesis, we quantified the total glycome of membrane proteins (Abdel Rahman et al., 2015) in control and SNAIL-overexpressing cells by LC-MS/MS, both basally and after exposure to fluvastatin for 48 h (Table S2).

The MCF10A membrane protein glycome consists of 32% high mannose type *N*-glycans, containing exclusively mannose (M, Man) residues in the glycan antennae (Fig. 4A). Complex type *N*-glycans represented a total of 59% of the MCF10A membrane protein glycome, which can be further subdivided based on fucosylation (F, Fuc) status at the core region and the antennae (Fig. 4A). In MCF10A cells, complex type *N*-glycans were commonly expressed in the unfucosylated and singly fucosylated (core) forms, with a small amount of doubly fucosylated (core and antennae) structures (Fig. 4A). With induction of EMT, the expression of 12 *N*-glycans were significantly upregulated, all of which belonged to the complex type subgroup; and 15 *N*-glycans were downregulated, including all 9 of the doubly fucosylated complex structures detected (Fig. 4B, Table S2). We then examined the effect of fluvastatin treatment on *N*-glycan profiles. Our hypothesis predicts that fluvastatin treatment will inhibit the expression of *N*-glycans that are upregulated by EMT. Indeed, 6 of the 12 complex type *N*-glycans upregulated following induction of EMT were specifically inhibited by fluvastatin treatment in SNAIL-overexpressing cells, but not in control cells (Fig. 4C, black arrowheads), suggesting that tri- and tetra-

antennary *N*-glycans are important mediators of fluvastatin-induced cell death. Of these, the singly fucosylated tri-antennary (N2FM3+N3H3) and singly fucosylated tetra-antennary (N2FM3+N4H4) structures, each representing ~10% of the total surface glycome, remained unchanged with fluvastatin treatment in the vector control cells (Fig. 4D-E). Importantly, SNAIL-overexpressing cells upregulated the expression of these *N*-glycan structures, which was blocked when cells were exposed to fluvastatin (Fig. 4D-E).

The tri- and tetra-antennary complex type *N*-glycans contain β1,6 glycosidic linkages (β1,6GlcNAc-branching) that are produced by the enzyme β1,6-*N*-acetylglucosaminyltransferase V (GnT-V; encoded by *MGAT5*), and are recognized by the lectin phytohaemagglutinin-L (PHA-L; Fig.4F) (Cummings and Kornfeld, 1982). Importantly, these branched *N*-glycans are known to promote tumor progression and metastasis (Cheung and Dennis, 2007; Granovsky et al., 2000; Lau and Dennis, 2008; Lau et al., 2007; Partridge et al., 2004), and positive PHA-L staining in patient samples have been associated with poor prognosis in breast and colon cancers (Drake et al., 2017; Fernandes et al., 1991). By contrast, the enzyme β1,4-*N*-acetylglucosaminyltransferase III (GnT-III; encoded by *MGAT3*) adds a bisecting GlcNAc to the trimannosyl core, which are recognized by phytohaemagglutinin-E (PHA-E) (Cummings and Kornfeld, 1982), and has potential metastasis-suppressing activities (Fig. 4F) (Yoshimura et al., 1995). Consistent with the increase in the tri- and tetra-antennary complex type *N*-glycans with induction of EMT (Fig. 4D-E), we showed that induction of EMT by SNAIL overexpression led to upregulation of GnT-V, while GnT-III expression remained unchanged (Fig. 4G). SNAIL-overexpressing cells showed an upregulation of PHA-L ligands compared to the vector control (Fig. 4H, compare lane 5 to lane 1). Following fluvastatin treatment, PHA-L binding is unaffected in vector cells (compare lane 2 to lane 1), but is decreased in SNAIL-overexpressing cells (compare lane 6 to lane 5). By contrast, PHA-E binding was similar between SNAIL-overexpressing cells and vector control cells, and there was minimal effect of fluvastatin on PHA-E substrates (Fig. 4H). Tunicamycin and thapsigargin were used as positive and negative controls, respectively, for inhibition of protein glycosylation (Fig. 4H).

Fluvastatin impairs protein *N*-glycosylation *in vivo*

Our *in vitro* data indicate that fluvastatin treatment impairs the biosynthesis of dolichol, which is needed to support the expression of complex type branched *N*-glycans associated with EMT and metastasis. To test this mechanism of fluvastatin action *in vivo*, we treated a xenograft model of the aggressive LM2-4 breast cancer cell line, a derivative of MDA-MB-231 cells that preferentially metastasizes to the mouse lung (Guerin et al., 2013), with PBS or 50 mg/kg/d fluvastatin. Since fluvastatin treatment delayed growth of the primary tumor (Fig. 5A), we extended treatment time in the fluvastatin group so that the tumors harvested for further analyses were size-matched (Fig. 5A). Fluvastatin was readily detected by HPLC-MS/MS in both the mouse serum (4.9 ± 0.3 μg/ml or 11.9 ± 0.9 μM) and the xenograft tissue (0.59 ± 0.08 μg/g tissue) (Fig. 5B-C). To the best of our knowledge, this is the first report of fluvastatin detection in extrahepatic tumor tissue to support the model that statins can directly induce cancer cell death *in vivo*.

To test whether fluvastatin can inhibit protein *N*-glycosylation *in vivo*, we performed Matrix Assisted Laser Desorption Ionization Imaging Mass Spectrometry (MALDI-IMS) to spatially quantify *N*-glycans on formalin-fixed tumor sections (Drake et al., 2017; Powers et al., 2014). Tumor tissue slices from PBS (n=6) and fluvastatin (n=5) treated mice were evaluated with this approach, and representative N-glycans are shown in Fig. 5D and 5E. Consistent with our *in vitro* results, we observed that overall levels of tetra-antennary complex type *N*-glycans were lowered in tumors receiving fluvastatin treatment (Fig. 5D), whereas the levels of high mannose type *N*-glycans remained comparable between PBS- and fluvastatin-treated groups (Fig. 5E). As confirmation, we also performed lectin histochemistry (Drake et al., 2017; Fernandes et al., 1991) using PHA-L, and showed that fluvastatin decreased the number of cells staining positive for PHA-L in proliferative regions of tumor sections (Fig. 5F-G). We confirmed that LM2-4 xenografts will readily metastasize to the mouse lung by identifying lung lesions that stained positive for human EGFR (hEGFR) (Fig. 5H). In the PBS treated group, 3 out of 6 mice (50%) had one or more lung lesions (Fig. 5I). In the fluvastatin treated group, 1 out of 5 mice (20%) had hEGFR-positive metastatic lesions, providing the first indication that fluvastatin treatment could decrease breast cancer metastasis in

this model (Fig. 5I). Thus, fluvastatin treatment *in vivo* inhibits the expression of *N*-glycans associated with breast cancer metastasis.

Post-surgical adjuvant fluvastatin treatment delays metastatic outgrowth and prolongs survival

To test the efficacy of fluvastatin treatment in the post-surgical adjuvant setting, we allowed LM2-4 xenografts to reach ~500 mm^3, then surgically removed the primary tumors to mimic front-line treatment in breast cancer patients (Fig. S4A) (Guerin et al., 2013). This experimental design also serves to uncouple the effect of fluvastatin on metastatic outgrowth from delay of metastasis due to inhibition of primary tumor growth. After surgery, mice were randomly assigned to receive PBS or 50 mg/kg/d fluvastatin orally (Fig. 6A), mimicking a typical p.o./q.d. (*per os/quaque die*, by mouth/once a day) prescription. Adjuvant fluvastatin treatment significantly prolonged overall survival in this mouse model (Fig. 6B).

To evaluate the potential anti-metastatic activity of fluvastatin, we analyzed lung samples at three time points during the course of the experiment: (i) at time of surgery; (ii) at 8-9 days post-surgery; and (iii) at endpoint (Fig. 6A). At time of surgery, we confirmed that this model accurately represented early stage breast cancer, as the majority of mice did not have any observable metastases, and 2/8 mice had very small lung lesions (Fig. 6C). At 8-9 days post-surgery, analysis of a small cohort of animals showed that adjuvant fluvastatin treatment effectively inhibited metastatic outgrowth from disseminated breast cancer cells after the primary tumor was removed (Fig. 6D). Finally, at endpoint, we showed that fluvastatin treatment decreased the proportion of mice with heavy (>50 colonies per slice) or medium (5-50 colonies per slice) metastatic load, while increasing the proportion of mice with light metastatic load (<5 colonies per slice; Fig. 6E-G). Consistently, autopsy at endpoint indicated that the majority of PBS-treated mice reached endpoint due to lung metastases, whereas fluvastatin-treated mice largely reached endpoint from primary tumor regrowth (Fig. S4B). We have thus demonstrated using a post-surgical metastatic breast

cancer model that closely follows the course of human disease, that adjuvant fluvastatin use can delay metastatic spread and prolong overall survival.

Discussion

Metastatic recurrence is the main cause of breast cancer deaths (Weigelt et al., 2005). Since statins are already approved, inexpensive, and have excellent safety profiles allowing for long-term use, they are ideal candidates to be repurposed as metastasis-prevention agents. Statins were previously thought to induce apoptosis in cancer cells by inhibiting FPP and GGPP synthesis, thereby disrupting the membrane localization of RAS family members (Mullen et al., 2016). However, mutations in RAS family members have been poor biomarkers of statin response (Baas et al., 2015a; Baas et al., 2015c; Hong et al., 2014), suggesting not only that an alternative mechanism is at play, but also that accurate biomarkers need to be developed to identify patients that will benefit from statin treatment. Here, we address this important gap by demonstrating that sensitivity to fluvastatin in the context of breast cancer cell EMT is mediated by depletion of dolichol, a class of metabolites downstream of FPP and GGPP, which functions as the essential lipid carrier of glycans prior to protein *N*-glycosylation (Mullen et al., 2016). Fluvastatin treatment impaired the expression of β1,6GlcNAc-branched tri- and tetra-antennary *N*-glycans associated with breast cancer EMT and metastasis (Cheung and Dennis, 2007; Lau et al., 2007; Partridge et al., 2004), both in cell culture and *in vivo*. Adjuvant use of fluvastatin delayed breast cancer metastasis and prolonged overall survival, supporting the immediate repurposing of fluvastatin into the breast cancer clinic, and further suggest the development of novel therapeutics to prevent metastatic recurrence in breast cancer by targeting dolichol synthesis and aberrant protein *N*-glycosylation.

Altered protein *N*-glycosylation, notably the upregulation of GnT-V (*MGAT5*), is pivotal to EMT (Miyoshi et al., 1995; Partridge et al., 2004; Terao et al., 2011). The tri- and tetra-antennary β1,6GlcNAc-branched *N*-glycans produced by GnT-V are potent modulators of metastatic potential (Cheung and Dennis, 2007; Granovsky et al., 2000; Lau and Dennis, 2008; Lau et al., 2007; Partridge et al., 2004).

Indeed, high levels of tri- and tetra-antennary complex *N*-glycans are associated with disease progression and poor prognosis in breast and colon cancer patients (Drake et al., 2017; Fernandes et al., 1991). Importantly, in polyomavirus middle T transgene (MMTV-PyMT) mouse and the *Pten*$^{+/-}$ mouse, mammary tumor growth is delayed and metastasis reduced when *Mgat5* is knocked out (Cheung and Dennis, 2007; Granovsky et al., 2000). PyMT *Mgat5*$^{-/-}$ mammary tumors were deficient in surface receptors for EGF and TGF-β and failed to undergo EMT, which was rescued by restoring *Mgat5* expression (Granovsky et al., 2000; Partridge et al., 2004). Here we demonstrate that EMT-associated upregulation of GnT-V-mediated *N*-glycan branching is dependent on dolichol biosynthesis and can be targeted by inhibition of the MVA pathway using fluvastatin. GnT-V activity is highly regulated at several levels, including gene expression (Miyoshi et al., 1995), protein turnover (Voss et al., 2014), and UDP-GlcNAc substrate concentration (Lau et al., 2007); importantly, GnT-V itself is *N*-glycosylated at six asparagine sites, and fluvastatin treatment may also be reducing their occupancy and thus enzyme activity.

The relationship between the effects of fluvastatin on ER and Golgi levels of *N*-glycosylation has not been explored. At the ER, the assembly of each precursor *N*-glycan to be transferred to nascent peptides requires 8 dolichol molecules (Varki et al., 2009), and the observation that dolichol cannot be efficiently recycled (Breitling and Aebi, 2013) and accumulates with aging (Parentini et al., 2005) indicates cells must continuously synthesize dolichol to meet this demand. Our results here clearly show that fluvastatin exploits this metabolic vulnerability in metastatic breast cancer cells by inhibiting LLO biosynthesis, in turn reducing *N*-glycan site occupancy and *N*-glycan branching.

Further evidence supporting the utility of statins as anti-breast cancer agents include two prospective window-of-opportunity clinical trials that evaluated the impact of statin use in the neo-adjuvant setting (Bjarnadottir et al., 2013; Garwood et al., 2010). Comparing tumor samples at biopsy and at surgery, both studies reported a decrease in Ki67 staining after fluvastatin (Garwood et al., 2010) or atorvastatin (Bjarnadottir et al., 2013) treatment. Here, we have chosen a mouse model of post-surgical metastatic

breast cancer that closely mimics front-line treatment and disease progression (Guerin et al., 2013), to test the efficacy of fluvastatin when used in the adjuvant setting to prevent metastasis, where long-term use of this safe and inexpensive drug will likely have clinical benefit. Adjuvant fluvastatin treatment effectively delayed metastasis and prolonged survival at a daily dose of 50 mg/kg in the mouse, equivalent to a well-tolerated daily dose of 4 mg/kg in human patients (Sabia et al., 2001). Our study was also the first to measure the concentration of fluvastatin in the xenograft tissue, with a treatment route and regimen closely mimicking what would be prescribed to human patients (p.o./q.d.). A serum concentration of 4.9 μg/ml (11.9 μM) fluvastatin was achieved in our mouse experiments (Fig. 5B). In comparison, in human volunteers, up to 7 μM fluvastatin was achieved when treated at 1 mg/kg/d (Siekmeier et al., 2001), and up to 12.3 μM lovastatin, another lipophilic statin family member, was achievable when prescribed at 10 mg/kg/d (Holstein et al., 2006). Additionally, a fluvastatin concentration of 586.2 ng/g tissue was measured in the tumor xenograft (Fig. 5C). Assuming a tissue density of 1 g/ml, this is equivalent to a fluvastatin concentration of approximately 1.4 μM, demonstrating that fluvastatin can reach extrahepatic tumor tissues to exert direct anti-cancer effects. Together, these results warrant the immediate clinical evaluation of fluvastatin at this well-tolerated dose in the adjuvant setting in breast cancer patients. Moreover, this work reinforces that targeting aberrant tumor metabolism is a fruitful strategy for the development of novel, effective anti-cancer agents.

Author contributions

RY conceived the hypothesis, designed and performed the experiments, analyzed and interpreted the data, and wrote the manuscript. JL and JEV helped perform the animal experiments. CZ and JWD performed total glycan analysis by LC-MS/MS. WZ and EC performed fluvastatin quantification by HPLC-MS/MS. DC contributed to data interpretation. RRD performed MALDI-IMS. LZP conceived the hypothesis, led the project, interpreted the data, and wrote the manuscript.

Acknowledgements

We thank Drs. Robert Kerbel, Roberta Maestro, and Senthil Muthuswamy for providing reagents, Dr. Meegan Larsen for pathology support, Dr. Thomas Kislinger for helpful discussion, Aaliya Tamachi for

technical assistance, and all members of the Penn lab for helpful discussion and critical review of the manuscript.

Financial Support: This work was supported by funding from the Canada Research Chairs Program (LZP), Canadian Institutes of Health Research (LZP), Terry Fox Research Institute (LZP), CIHR Canada Graduate Scholarship (RY), Ontario Graduate Scholarship (JL), and Ontario Student Opportunity Trust Fund (JEV).

This work was also supported by the Office of the Assistant Secretary of Defense for Health Affairs, through the Breast Cancer Research Program under Award No. W81XWH-16-1-0068. Opinions, interpretations, conclusions and recommendations are those of the author and are not necessarily endorsed by the Department of Defense.

Conflict of Interest: The authors declare no potential conflicts of interest.

References

Abdel Rahman, A.M., Ryczko, M., Nakano, M., Pawling, J., Rodrigues, T., Johswich, A., Taniguchi, N., and Dennis, J.W. (2015). Golgi N-glycan branching N-acetylglucosaminyltransferases I, V and VI promote nutrient uptake and metabolism. Glycobiology *25*, 225-240.

Ahern, T.P., Pedersen, L., Tarp, M., Cronin-Fenton, D.P., Garne, J.P., Silliman, R.A., Sorensen, H.T., and Lash, T.L. (2011). Statin prescriptions and breast cancer recurrence risk: a Danish nationwide prospective cohort study. J Natl Cancer Inst *103*, 1461-1468.

Atil, B., Berger-Sieczkowski, E., Bardy, J., Werner, M., and Hohenegger, M. (2016). In vitro and in vivo downregulation of the ATP binding cassette transporter B1 by the HMG-CoA reductase inhibitor simvastatin. Naunyn Schmiedebergs Arch Pharmacol *389*, 17-32.

Baas, J.M., Krens, L.L., Bos, M.M., Portielje, J.E., Batman, E., van Wezel, T., Morreau, H., Guchelaar, H.J., and Gelderblom, H. (2015a). Safety and efficacy of the addition of simvastatin to panitumumab in previously treated KRAS mutant metastatic colorectal cancer patients. Anticancer Drugs *26*, 872-877.

Baas, J.M., Krens, L.L., ten Tije, A.J., Erdkamp, F., van Wezel, T., Morreau, H., Gelderblom, H., and Guchelaar, H.J. (2015c). Safety and efficacy of the addition of simvastatin to cetuximab in previously treated KRAS mutant metastatic colorectal cancer patients. Invest New Drugs *33*, 1242-1247.

Bjarnadottir, O., Romero, Q., Bendahl, P.O., Jirstrom, K., Ryden, L., Loman, N., Uhlen, M., Johannesson, H., Rose, C., Grabau, D., *et al.* (2013). Targeting HMG-CoA reductase with statins in a window-of-opportunity breast cancer trial. Breast Cancer Res Treat *138*, 499-508.

Bokoch, G.M., and Prossnitz, V. (1992). Isoprenoid metabolism is required for stimulation of the respiratory burst oxidase of HL-60 cells. J Clin Invest *89*, 402-408.

Boudreau, D.M., Yu, O., Chubak, J., Wirtz, H.S., Bowles, E.J., Fujii, M., and Buist, D.S. (2014). Comparative safety of cardiovascular medication use and breast cancer outcomes among women with early stage breast cancer. Breast Cancer Res Treat *144*, 405-416.

Breitling, J., and Aebi, M. (2013). N-linked protein glycosylation in the endoplasmic reticulum. Cold Spring Harb Perspect Biol *5*, a013359.

Chae, Y.K., Valsecchi, M.E., Kim, J., Bianchi, A.L., Khemasuwan, D., Desai, A., and Tester, W. (2011). Reduced risk of breast cancer recurrence in patients using ACE inhibitors, ARBs, and/or statins. Cancer Invest *29*, 585-593.

Cheung, P., and Dennis, J.W. (2007). Mgat5 and Pten interact to regulate cell growth and polarity. Glycobiology *17*, 767-773.

Cummings, R.D., and Kornfeld, S. (1982). Characterization of the structural determinants required for the high affinity interaction of asparagine-linked oligosaccharides with immobilized Phaseolus vulgaris leukoagglutinating and erythroagglutinating lectins. J Biol Chem *257*, 11230-11234.

Drake, R.R., Powers, T.W., Jones, E.E., Bruner, E., Mehta, A.S., and Angel, P.M. (2017). MALDI Mass Spectrometry Imaging of N-Linked Glycans in Cancer Tissues. Adv Cancer Res *134*, 85-116.

Dricu, A., Wang, M., Hjertman, M., Malec, M., Blegen, H., Wejde, J., Carlberg, M., and Larsson, O. (1997). Mevalonate-regulated mechanisms in cell growth control: role of dolichyl phosphate in expression of the insulin-like growth factor-1 receptor (IGF-1R) in comparison to Ras prenylation and expression of c-myc. Glycobiology *7*, 625-633.

Fernandes, B., Sagman, U., Auger, M., Demetrio, M., and Dennis, J.W. (1991). Beta 1-6 branched oligosaccharides as a marker of tumor progression in human breast and colon neoplasia. Cancer Res *51*, 718-723.

Garwood, E.R., Kumar, A.S., Baehner, F.L., Moore, D.H., Au, A., Hylton, N., Flowers, C.I., Garber, J., Lesnikoski, B.A., Hwang, E.S., *et al.* (2010). Fluvastatin reduces proliferation and increases apoptosis in women with high grade breast cancer. Breast Cancer Res Treat *119*, 137-144.

Giancotti, F.G. (2013). Mechanisms governing metastatic dormancy and reactivation. Cell *155*, 750-764.

Goard, C.A., Chan-Seng-Yue, M., Mullen, P.J., Quiroga, A.D., Wasylishen, A.R., Clendening, J.W., Sendorek, D.H., Haider, S., Lehner, R., Boutros, P.C., *et al.* (2014). Identifying molecular features that distinguish fluvastatin-sensitive breast tumor cells. Breast Cancer Res Treat *143*, 301-312.

Granovsky, M., Fata, J., Pawling, J., Muller, W.J., Khokha, R., and Dennis, J.W. (2000). Suppression of tumor growth and metastasis in Mgat5-deficient mice. Nat Med *6*, 306-312.

Guerin, E., Man, S., Xu, P., and Kerbel, R.S. (2013). A model of postsurgical advanced metastatic breast cancer more accurately replicates the clinical efficacy of antiangiogenic drugs. Cancer Res *73*, 2743-2748.

Hamadmad, S.N., and Hohl, R.J. (2007). Lovastatin suppresses erythropoietin receptor surface expression through dual inhibition of glycosylation and geranylgeranylation. Biochem Pharmacol *74*, 590-600.

Holstein, S.A., Knapp, H.R., Clamon, G.H., Murry, D.J., and Hohl, R.J. (2006). Pharmacodynamic effects of high dose lovastatin in subjects with advanced malignancies. Cancer Chemother Pharmacol *57*, 155-164.

Hong, J.Y., Nam, E.M., Lee, J., Park, J.O., Lee, S.C., Song, S.Y., Choi, S.H., Heo, J.S., Park, S.H., Lim, H.Y., *et al.* (2014). Randomized double-blinded, placebo-controlled phase II trial of simvastatin and gemcitabine in advanced pancreatic cancer patients. Cancer Chemother Pharmacol *73*, 125-130.

Kusama, T., Mukai, M., Tatsuta, M., Nakamura, H., and Inoue, M. (2006). Inhibition of transendothelial migration and invasion of human breast cancer cells by preventing geranylgeranylation of Rho. Int J Oncol *29*, 217-223.

Kwan, M.L., Habel, L.A., Flick, E.D., Quesenberry, C.P., and Caan, B. (2008). Post-diagnosis statin use and breast cancer recurrence in a prospective cohort study of early stage breast cancer survivors. Breast Cancer Res Treat *109*, 573-579.

Lau, K.S., and Dennis, J.W. (2008). N-Glycans in cancer progression. Glycobiology *18*, 750-760.

Lau, K.S., Partridge, E.A., Grigorian, A., Silvescu, C.I., Reinhold, V.N., Demetriou, M., and Dennis, J.W. (2007). Complex N-glycan number and degree of branching cooperate to regulate cell proliferation and differentiation. Cell *129*, 123-134.

Miyoshi, E., Nishikawa, A., Ihara, Y., Saito, H., Uozumi, N., Hayashi, N., Fusamoto, H., Kamada, T., and Taniguchi, N. (1995). Transforming growth factor beta up-regulates expression of the N-acetylglucosaminyltransferase V gene in mouse melanoma cells. J Biol Chem *270*, 6216-6220.

Mullen, P.J., Yu, R., Longo, J., Archer, M.C., and Penn, L.Z. (2016). The interplay between cell signalling and the mevalonate pathway in cancer. Nat Rev Cancer *16*, 718-731.

Palamarczyk, G., and Butters, T.D. (1982). Uptake of dolichol into cultured cells. FEBS Lett *143*, 241-246.

Parentini, I., Cavallini, G., Donati, A., Gori, Z., and Bergamini, E. (2005). Accumulation of dolichol in older tissues satisfies the proposed criteria to be qualified a biomarker of aging. J Gerontol A Biol Sci Med Sci *60*, 39-43.

Partridge, E.A., Le Roy, C., Di Guglielmo, G.M., Pawling, J., Cheung, P., Granovsky, M., Nabi, I.R., Wrana, J.L., and Dennis, J.W. (2004). Regulation of cytokine receptors by Golgi N-glycan processing and endocytosis. Science *306*, 120-124.

Powers, T.W., Neely, B.A., Shao, Y., Tang, H., Troyer, D.A., Mehta, A.S., Haab, B.B., and Drake, R.R. (2014). MALDI imaging mass spectrometry profiling of N-glycans in formalin-fixed paraffin embedded clinical tissue blocks and tissue microarrays. PLoS One *9*, e106255.

Powlesland, A.S., Hitchen, P.G., Parry, S., Graham, S.A., Barrio, M.M., Elola, M.T., Mordoh, J., Dell, A., Drickamer, K., and Taylor, M.E. (2009). Targeted glycoproteomic identification of cancer cell glycosylation. Glycobiology *19*, 899-909.

Sabia, H., Prasad, P., Smith, H.T., Stoltz, R.R., and Rothenberg, P. (2001). Safety, tolerability, and pharmacokinetics of an extended-release formulation of fluvastatin administered once daily to patients with primary hypercholesterolemia. J Cardiovasc Pharmacol *37*, 502-511.

Siekmeier, R., Lattke, P., Mix, C., Park, J.W., and Jaross, W. (2001). Dose dependency of fluvastatin pharmacokinetics in serum determined by reversed phase HPLC. J Cardiovasc Pharmacol Ther *6*, 137-145.

Soule, H.D., Maloney, T.M., Wolman, S.R., Peterson, W.D., Jr., Brenz, R., McGrath, C.M., Russo, J., Pauley, R.J., Jones, R.F., and Brooks, S.C. (1990). Isolation and characterization of a spontaneously immortalized human breast epithelial cell line, MCF-10. Cancer Res *50*, 6075-6086.

Taylor-Harding, B., Orsulic, S., Karlan, B.Y., and Li, A.J. (2010). Fluvastatin and cisplatin demonstrate synergistic cytotoxicity in epithelial ovarian cancer cells. Gynecol Oncol *119*, 549-556.

Terao, M., Ishikawa, A., Nakahara, S., Kimura, A., Kato, A., Moriwaki, K., Kamada, Y., Murota, H., Taniguchi, N., Katayama, I., *et al.* (2011). Enhanced epithelial-mesenchymal transition-like phenotype in N-acetylglucosaminyltransferase V transgenic mouse skin promotes wound healing. J Biol Chem *286*, 28303-28311.

Varki, A., Cummings, R.D., Esko, J.D., Freeze, H.H., Stanley, P., Bertozzi, C.R., Hart, G.W., and Etzler, M.E. (2009). Essentials of Glycobiology, 2010/03/20 edn.

Voss, M., Kunzel, U., Higel, F., Kuhn, P.H., Colombo, A., Fukumori, A., Haug-Kroper, M., Klier, B., Grammer, G., Seidl, A., *et al.* (2014). Shedding of glycan-modifying enzymes by signal peptide peptidase-like 3 (SPPL3) regulates cellular N-glycosylation. EMBO J *33*, 2890-2905.

Weigelt, B., Peterse, J.L., and van 't Veer, L.J. (2005). Breast cancer metastasis: markers and models. Nat Rev Cancer *5*, 591-602.

Williams, A.B., Li, L., Nguyen, B., Brown, P., Levis, M., and Small, D. (2012). Fluvastatin inhibits FLT3 glycosylation in human and murine cells and prolongs survival of mice with FLT3/ITD leukemia. Blood *120*, 3069-3079.

Xia, Z., Tan, M.M., Wong, W.W., Dimitroulakos, J., Minden, M.D., and Penn, L.Z. (2001). Blocking protein geranylgeranylation is essential for lovastatin-induced apoptosis of human acute myeloid leukemia cells. Leukemia *15*, 1398-1407.

Yoshimura, M., Nishikawa, A., Ihara, Y., Taniguchi, S., and Taniguchi, N. (1995). Suppression of lung metastasis of B16 mouse melanoma by N-acetylglucosaminyltransferase III gene transfection. Proc Natl Acad Sci U S A *92*, 8754-8758.

Figure legends

Figure 1. Induction of EMT by SNAIL overexpression increases cell sensitivity to inhibition of dolichol-dependent protein *N*-glycosylation by fluvastatin and tunicamycin.

A, a simplified schematic of the mevalonate (MVA) pathway. Inhibitors of specific components of the pathway are represented in red. CoA, coenzyme A; HMG-CoA, 3-hydroxy-3-methylglutaryl coenzyme A; MVA, mevalonate; FPP, farnesyl pyrophosphate; GGPP, geranylgeranyl pyrophosphate; LLO, lipid-

linked oligosaccharides; GGTI, geranylgeranyltransferase inhibitor; CoQ, coenzyme Q; ETC, electron transport chain; 2-TTFA, 2-thenoyltrifluoroacetone.

B, immunoblot (IB) of E-cadherin, an epithelial cell marker, and fibronectin, a mesenchymal cell marker, revealed that overexpression of SNAIL induced EMT in MCF10A cells. Tubulin is used as loading control. See also Fig. S1.

C, Flow cytometric quantification of % dead cells (% pre-G1 population) with propidium iodide DNA staining after fixation. Fluvastatin treatment for 72 h induced cell death in MCF10A cells overexpressing SNAIL, but not in vector control cells. Fluvastatin-induced cell death was fully rescued by co-administration with MVA or GGPP, but not FPP, at the indicated doses. Bars are mean + SD, n=3. *, $p<0.05$; **, $p<0.01$ (one-way ANOVA with a Dunnett post-test, comparing all columns vs. fluvastatin column).

D, SNAIL overexpression sensitized cells to fluvastatin and tunicamycin, but not inhibitors of other components of the MVA pathway. IC_{50} values as calculated based on MTT assays after cells were treated with 8 doses of each drug for 72 h. Bars are mean + SD, n=3-4. *, $p<0.05$; **, $p<0.01$; (unpaired, two-tailed *t* test, comparing SNAIL vs. vector columns). See also Fig. S1.

E, IB for EGFR, GP130, and SLC3A2 for glycosylation status indicates that fluvastatin treatment for 48-72 h led to under-glycosylation of EGFR, GP130, and SLC3A2 in both vector control and SNAIL-overexpressing cells as indicated by the appearance of lower-molecular weight bands. Tunicamycin treatment for 24 h was a positive control for protein under-glycosylation. Ku80 is used as a loading control. Representative images are shown, n=3-4. See also Fig. S2.

Figure 2. Inhibition of dolichol synthesis underlies fluvastatin sensitivity in mesenchymal breast cancer cell lines.

A, IB of E-cadherin, an epithelial cell marker, and vimentin, a mesenchymal cell marker, indicates that MCF-7 and HCC1937 cells are more epithelial, while MBA-MB-231, HCC1806, and BT549 cells are more mesenchymal. Ku80 is used as a loading control.

B, fluvastatin preferentially killed the more mesenchymal MDA-MB-231, HCC1806, and BT549 cells, compared to the more epithelial MCF-7 and HCC1937 cells. IC_{50} values are calculated based on MTT assays after cells were treated with 8 doses of each drug for 72 h in Opti-MEM serum reduced media. Bars are mean + SD, n=3.

C, chemical structure of dolichyl[C95-105]-PP, a member of the dolichol group of long-chain isoprenoid molecules.

D, MTT assays reveal that fluvastatin treatment for 72 h in Opti-MEM serum reduced media reduced cell viability in mesenchymal cells, but not in epithelial cell lines. Fluvastatin-induced reduction in cell viability was fully rescued by co-administration with MVA, GGPP, or dolichol (dolichyl[C95]-PP), at the indicated doses. Bars are mean + SD, n=3-4. *, $p<0.05$; **, $p<0.01$ (one-way ANOVA with a Dunnett post-test, comparing all columns vs. fluvastatin column). See also Fig. S3.

E, a simplified schematic of the function of dolichol. MVA, mevalonate; GlcNAc, *N*-acetylglucosamine; Asn, asparagine.

Figure 3. Fluvastatin treatment blocks dolichol-dependent protein *N*-glycosylation with complex type *N*-glycans.

A, a simplified schematic of the dolichol-dependent protein *N*-glycosylation process. MVA, mevalonate; GlcNAc, *N*-acetylglucosamine; Asn, asparagine.

B, In HeLa cells with Dox-inducible FLAG-SLC3A2 expression, IB for FLAG indicates that fluvastatin treatment led to under-glycosylation of SLC3A2 as indicated by the appearance of lower-molecular weight bands. actin was used as a loading control. Representative images are shown, n=3.

C, levels of unoccupied Asn residues in SLC3A2 are quantified by FLAG-IP followed by LC-MS/MS. Fluvastatin treatment for up to 48 h increased the levels of unoccupied Asn at residues 365 and 381, but not 424. Three biological replicates were analyzed with two technical replicates each. ns, not significant; *, $p<0.05$ (two-way ANOVA with a Dunnett post-test, comparing each treatment column vs. control column).

D, schematic representation of complex type *N*-glycans that decorate SLC3A2 on Asn residues 365, 381, and 424, that are represented in the following panels.

E-G, fluvastatin treatment for up to 48 h decreases the levels of *N*-glycosylation with complex type *N*-glycans. Bars are mean + SD, n=3. ns, not significant; *, $p<0.05$ (two-way ANOVA with a Dunnett post-test, comparing each treatment column vs. control column).

Figure 4. Fluvastatin treatment decreases complex branched *N*-glycans associated with EMT.

A, schematic representation of high mannose type and complex type *N*-glycans, the two major classes of *N*-glycans (top), and distribution of major classes of *N*-glycans in the total cell surface glycome in MCF10A cells quantified by LC-MS/MS (bottom).

B, heatmap of the expression of complex *N*-glycans following SNAIL-induced EMT. Data presented are the mean of 3 biological replicates with 1-2 technical replicates each. *, q<0.0301 (unpaired, 2-tailed *t* test with Benjamini-Hochberg FDR correction). See also Table S1.

C, heatmap of the expression of complex *N*-glycans following treatment with 20 μM fluvastatin in vector cells (left column) and SNAIL-overexpressing cells (right column). Black arrowheads indicate glycan species that are significantly upregulated in EMT (**B**) and downregulated by fluvastatin treatment in SNAIL-overexpressing cells (**C**, right column), but not affected by fluvastatin treatment in control cells (**C**, left column). Data presented are the mean of 3 biological replicates with 1-2 technical replicates each. *, q<0.0108 (unpaired, 2-tailed *t* test with Benjamini-Hochberg FDR correction). See also Table S1.

D-E, LC-MS/MS quantification of the β1,6-branched, tri-antennary (**D**) and tetra-antennary (**E**) *N*-glycans indicate that these *N*-glycan species are upregulated in EMT, which is inhibited by 20 μM fluvastatin treatment for 48 h. Bars are mean + SD, n=3. ns, not significant; *, p<0.05 (one-way ANOVA with a Bonferroni post-test, comparing selected pairs of columns). See also Table S1.

F, schematic representation of two mutually exclusive *N*-glycan branching pathways, catalyzed by different enzymes, recognized by different lectins, and with opposing effects on metastasis.

G, IB of GnT-III *(MGAT3)* and GnT-V *(MGAT5)* showed that SNAIL-overexpressing cells upregulated GnT-V while GnT-III expression was unchanged, compared to vector control cells. Actin was used as a loading control. Representative images are shown, n=3.

H, lectin blotting revealed that PHA-L ligand was upregulated in SNAIL-overexpressing cells, and was decreased by fluvastatin after 48 h. PHA-E ligand was expressed at comparable levels between the two cell lines and was not affected by fluvastatin treatment. Treatment with tunicamycin for 48 h was used as a positive control that decreased expression of both PHA-L and PHA-E ligands in both cell lines. Treatment with thapsigargin for 48 h was used as a negative control. Actin was used as a loading control. Representative images are shown, n=4.

Figure 5. Fluvastatin treatment decreases complex branched *N*-glycans *in vivo*.

A, fluvastatin delayed growth of the primary tumor. One million LM2-4 cells were subcutaneously implanted in SCID mice and treated with PBS or 50 mg/kg/d fluvastatin by oral gavage. Mice were

sacrificed 6 days (PBS) or 12 days after treatment (fluvastatin) to ensure tumors from the two groups were size-matched for downstream analyses. Data points are mean ± SD, n=5-6.

B-C, at time of sacrifice, mouse serum and a piece of tumor xenograft were flash-frozen in liquid N_2, and fluvastatin was extracted and quantified by HPLC-MS/MS. Data points are mean ± SD, n=4-6.

D-E, at time of sacrifice, a piece of tumor xenograft was formalin-fixed and paraffin-embedded (FFPE). Spatial profiling of *N*-glycans by MALDI indicated that expression of tetra-antennary complex type *N*-glycans were decreased with fluvastatin treatment, while high mannose type *N*-glycans were unaffected.

F-G, lectin histochemistry of tumor xenografts indicated that PHA-L ligand in Ki67-positive tissue areas was decreased with fluvastatin treatment. Representative images are shown, n=5. Scale bars = 50 μm. Data points are mean ± SD, n=5. **, $p<0.01$ (unpaired, two-tailed *t* test, comparing fluvastatin treatment vs. PBS control).

H-I, fluvastatin treatment decreased proportion of mice with metastatic lesions in the lungs at the time of sacrifice. At time of sacrifice, mouse lungs were resected and FFPE. Two sequential slices were obtained every 200 μm for three depths containing all five lobes, and stained for H&E or hEGFR (**H**) Scale bars = 100 μm**.** Metastatic colonies were identified by hEGFR and confirmed by H&E. Each lung slice was independently reviewed by two personnel. Representative images are shown, n=5-6.

Figure 6. Post-surgical adjuvant fluvastatin treatment delays metastasis and prolongs survival.

A, schematic of the mouse model and the time points where mice were sacrificed. See also Fig. S4.

B, fluvastatin treatment at 50 mg/kg/d orally significantly prolonged survival of mice with post-surgical metastatic breast cancer. *, $p<0.05$ (Log-rank test, n=12). See also Fig. S4.

C-E, At the indicated time point, mice were sacrificed and lungs were resected for FFPE. Two sequential slices were obtained every 200 μm for three depths containing all five lobes, and stained for H&E or hEGFR. Metastatic colonies were identified by hEGFR staining and confirmed by H&E. At time of surgery, mouse lungs were clear of metastatic colonies or had very small lesions (**C**). Scale bar = 20 μm. At 8-9 days post-surgery, mice receiving fluvastatin treatment had less metastatic tumor load than mice receiving PBS control (**D)**. At endpoint, fluvastatin treatment decreased the proportion of mice with heavy (>50 colonies per slice) or intermediate metastatic load (5-50 colonies per slice). The proportion of mice with light metastatic load (<5 colonies per slice) were increased (**E**). Each lung slice was independently reviewed by two personnel. Representative images are shown.

F-G, quantification of metastatic load by colony count (**F**) or by hEGFR positivity (**G**) both showed lowered metastatic load in fluvastatin-treated mice.

STAR Methods

Contact for Reagent and Resource Sharing

Further information and requests for resources and reagents should be directed to and will be fulfilled by the corresponding author, Dr. Linda Z. Penn (Linda.Penn@uhnresearch.ca).

Experimental Model and Subject Details

Mice

Animal work was carried out with the approval of the Princess Margaret Cancer Centre Ethics Review Board in accordance to the regulations of the Canadian Council on Animal Care. In conducting research using animals, the investigators adhered to the laws of the United States and regulations of the Department of Agriculture. Female SCID mice were obtained from the in-house breeding colony at the Princess Margaret Cancer Centre and at 6-8 weeks of age. All mice were maintained under specific pathogen-free conditions with a 12-hour light-dark cycle. Food and water were provided *ad libitum*.

Cell lines

MCF10A cells were a kind gift of Dr. Senthil Muthuswamy. MDA-MB-231 and LM2-4 cells were a kind gift of Dr. Robert Kerbel. BT549, HCC1806, HCC1937, HEK293Tv, LM2-4, MCF-7, MCF10A, and MDA-MB-231 cells were cultured at 37°C in a humidified atmosphere at 5% CO_2 in supplemented growth media as previously described (Goard et al., 2014; Guerin et al., 2013; Pandyra et al., 2015). All cell lines were authenticated by short-tandem repeat (STR) profiling, and tested to be free of mycoplasma. Transgene expression was stably introduced into MCF10A cells using retroviral insertion with pLPC, a kind gift of Dr. Roberta Maestro, or pBabePuro as previously described (Pandyra et al., 2015). In the conduct of research utilizing recombinant DNA, the investigators adhered to NIH Guidelines for research involving recombinant DNA molecules. Cells were imaged on a Leica Stereomicroscope (Leica MZ FLIII).

Method details

Reagents

Fluvastatin was purchased from US Biologicals (F5277-76). TGF-β was purchased from PeproTech (100-21). PNGase F was purchased from NEB (P0704). cOmplete protease inhibitor was purchased from Roche (11697498001). RapiGest SF was purchased from Waters (186001861). Sialidase was purchased

from Glyko (GK80040). Dolichyl[C95]-PP was purchased from American Radiolabeled Chemicals Inc (ARCD 1056). All other chemicals were purchased from Sigma unless otherwise specified. In the conduct of research involving hazardous organisms or toxins, the investigators adhered to the CDC-NIH Guide for Biosafety in Microbiological and Biomedical Laboratories.

MTT assays

3-(4,5-dimethylthiazol-2-yl)-2,5-diphenyltetrazolium bromide (MTT) assays were performed as previously described (Goard et al., 2014). Cells were seeded at 750-5,000 cells/well in 96-well plates and treated in triplicate with 8 doses of drugs or the solvent control for 72 h, either in growth media or in Opti-MEM serum reduced media as indicated. IC_{50} values were computed using GraphPad Prism with a bottom constraint equal to 0.

Immunoblotting

Lysates were prepared by lysing in RIPA lysis buffer (25 mM Tris pH 7.4, 150 mM NaCl, 0.5% sodium deoxycholate, 1% NP-40, protease inhibitors). The following antibodies were used for detection: c-MYC (MAb 9E10, in-house), E-Cadherin (CST 3195), vimentin (CST 5741), fibronectin (Abcam ab32419), actin (Sigma A2066), tubulin (Millipore CP06), GP130 (SCB sc-655), EGFR (CST 2232), SLC3A2 (SCB sc-7095), Ku80 (CST 2180), GnT-III (Thermo PA5-12156), GnT-V (Thermo MA5-24325), PHA-L (EY Labs H-1801-1), PHA-E (EY labs H-1802-1).

Immunohistochemistry

Tissue samples were formalin-fixed and paraffin-embedded by standard protocols. For tumors, three sequential slices were stained for H&E, Ki67 (Novus NB110-90592), or biotin-PHA-L (EY Labs BA-1801-2). The number of PHA-L positive cells were counted at 20x magnification in Ki67-positive regions with a minimum of four views per slice. For lungs, two sequential slices were obtained every 200 μm for three depths containing all five lobes, and stained for H&E or hEGFR (Zymed 28005). Metastatic colonies were identified by hEGFR staining and confirmed by H&E. Each lobe was individually outlined and total hEGFR positivity was computed using ImageScope.

Cell death assay

Cells were seeded at 250,000/plate overnight, then treated with as indicated for 72 h. Cells were fixed in 70% ethanol overnight, stained with propidium iodide (Sigma), and analyzed for the sub-diploid DNA ("pre-G1") population as previously described (Goard et al., 2014).

qRT-PCR

Total RNA was harvested from subconfluent cells using TRIzol Reagent (Invitrogen). cDNA was synthesized from 500 ng of RNA using SuperScript III (Invitrogen). Real-time quantitative RT-PCR was performed using SYBR Green (Applied Biosystems) with the following primers:

BiP_fw 3'- TGACATTGAAGACTTCAAAGCT-5'

BiP_rv 3'- CTGCTGTATCCTCTTCACCAGT-5'

ERdj4_fw 3'- AAAATAAGAGCCCGGATGCT-5'

ERdj4_rv 3'- CGCTTCTTGGATCCAGTGTT-5'

18S_rRNA_fw 5'-GTAACCCGTTGAACCCCATT-3'

18S_rRNA_fw 3'-CCATCCAATCGGTAGTAGCG-3'

Sample preparation for glycopeptide analysis

A total of 10 million cells were harvested after indicated treatment. Cells were lysed in 1ml IP lysis buffer (1% Triton-100, 20 mM Tris pH 7.5, 150 mM NaCl, 1 mM EDTA, 1mM EGTA, cOmplete protease inhibitor), and centrifuged at 14,000 rpm for 30 min at 4^{o}C. Lysates were normalized to 2.5 mg/ml and 1 ml was incubated with 20 µl of FLAG beads at 4^{o}C overnight. Beads were washed thoroughly in TBS (50 mM Tris pH 7.5, 150 mM NaCl) and 50 mM ammonium bicarbonate and on-bead trypsin digest was carried out using 0.5 µg of trypsin at 37^{o}C overnight. Glycopeptides were extracted using 0.5% formic acid, vacuumed to dry, and desialidated with 0.5 µl of sialidase at 37^{o}C overnight.

Glycopeptide analysis by LC-MS/MS

Peptides were applied to a nano-HPLC Chip using a Agilent 1200 series microwell-plate autosampler, and interface with a Agilent 6550 Q-TOF MS (Agilent Technologies, Inc., Santa Clara, CA). The reverse-phase nano-HPLC Chip (G4240-62002) had a 40 nL enrichment column and a 75 µm x 150mm separation column packed with 5 µm Zorbax 300SB-C18. The mobile phase was 0.1% formic acid in water (v/v) as solvent A, and 0.1% formic acid in ACN (v/v) as solvent B. The flow rate at 0.3 µL/min with gradient schedule; 3% B (0−1 min); 3−40% B (1−90 min); 40−80% B(90−95 min); 80% B (95−100 min) and 80-3% B (100-105 min). Mascot search was used to identify proteins and peptide sequences coverage. Extract glycopeptide were identified by Agilent Masshunter Quanlititive Analysis software by the presence of hexose and N-acetylhexosamine. Glycan structures were predicted for extracted

glycopeptides by online GlycoMod (http://web.expasy.org/glycomod/). Glycan structure by MS/MS and occupancy of NXS/T N-glycosylation sites were determined manually.

N-glycan extraction

A total of 15 million cells were seeded overnight and treated as indicated for 48 h. Cells were harvested, suspended 1 mL of HEPES homogenization buffer (0.25 M sucrose, 50 mM HEPES pH 7.5, 5 mM NaF, 5 mM EDTA, 2 mM DTT, cOmplete protease inhibitor), and lysed using a probe sonicator. Homogenate was cleared at 2,000 xg for 20 min at 4°C, then ultracentrifuged at 115,000 xg for 70 min at 4°C. The pellet was vigorously suspended in 650 µL Tris buffer (0.8% Triton X-114, 50 mM Tris pH 7.5, 0.1 mM NaCl, 5 mM EDTA, 5 mM NaF, 2 mM DTT, cOmplete protease inhibitor). The homogenate was chilled on ice for 10 min, incubated at 37°C for 20 min, then phase partitioned at 1,950 xg for 2 min at room temperature. The upper phase was discarded. Membrane proteins in the lower phase was precipitated with 1 mL acetone at -20°C overnight.

Precipitated proteins were suspended in 60 µL of suspension buffer (0.25% RapiGest SF, 50 mM ammonium bicarbonate, 5 mM DTT). The completely dissolved solution was heated for 3 min at 85°C. Approximately 30 µg proteins was mixed with 0.5 µL of PNGase F, 0.7 µL of sialidase, and 20 µL of 50 mM ammonium bicarbonate, and incubated at 42°C for 2 h followed by 37°C overnight. Released *N*-glycans were extracted with 4-5 volumes of 100% ethanol at -80°C for 2 hours. The supernatant containing released *N*-glycans was speed vacuumed to dry.

Home-made porous graphitized carbon (PGC) microtips containing 10 mg PGC in a bed volume of 50 µL was washed with 500 µL of ddH_2O, 500 µL of 80% acetonitrile (ACN), and equilibrated with 500 µL 0.1% trifluoroacetic acid (TFA). *N*-glycan pellets were dissolved in 50 µL of 0.1% TFA and slowly loaded into microtips at a flow rate of ~100 µL/min. Microtips were washed with 500 µL 0.1% TFA. *N*-glycans were eluted several times with 500 µL of elution buffer (0.05% TFA, 40% ACN). The eluted *N*-glycans were speed vacuumed to dry.

Global glycan analysis by LC-MS/MS

Analysis of the eluted *N*-glycans was modified from a previous method (Abdel Rahman et al., 2015). Total glycan samples were applied to a nano-HPLC Chip using an Agilent 1200 series microwell-plate autosampler, and interface with an Agilent 6550 Q-TOF MS (Agilent Technologies, Inc., Santa Clara, CA). The HPLC Chip (glycan Chip) had a 40 nL enrichment column and a 75 µm x 43 mm separation column packed with 5 µm graphitized carbon as stationary phase. The mobile phase was 0.1% formic acid in water (v/v) as solvent A, and 0.1% formic acid in ACN (v/v) as solvent B. The flow rate at 0.3 µL/min with gradient schedule; 5% B (0−1 min); 5−20% B (1−15 min); 20−70% B (15−16 min); 70% B (16−19

min) and 70-5% B (19-20 min). Free glycans released by PNGase F were identified by Agilent Masshunter Quanlititive Analysis software by the presence of hexose and *N*-acetylhexosamine. Glycan structures were predicted by online GlycoMod (http://web.expasy.org/glycomod/). Agilent Masshunter Quantitative Analysis software was used to quantify the extracted glycan peaks.

Animal models

Animal work was carried out with the approval of the Princess Margaret Hospital ethics review board in accordance to the regulations of the Canadian Council on Animal Care. In conducting research using animals, the investigators adhered to the laws of the United States and regulations of the Department of Agriculture. LM2-4 cells (1 million cells in 50 μL) were implanted subcutaneously in female SCID mice (6-8 wks), obtained in-house from the University Health Network animal colony. Primary tumors were measured every two days and calculated by (width x width x length)/2. After surgical removal of the primary tumors, animals were monitored daily for endpoint, including signs of metastatic load in the lung (laboured breathing). Treatment was given daily orally with PBS or 50 mg/kg/d fluvastatin. Necropsy was performed at endpoint where any tissues with evidence of metastatic disease is rapidly excised and fixed in formalin for histopathology.

Fluvastatin quantification by HPLC-MS/MS

Fluvastatin concentrations were determined by a modified HPLC-MS/MS method with atorvastatin as the internal standard (IS). Mouse serum or xenograft tissue were incubated with methyl tert-butyl ether for 30 min followed by centrifugation at 3000 rpm for 30 min. The supernatant was separated, dried at room temperature, and reconstituted in methanol/water (1:1). The HPLC system consisted of a Shimadzu LC-20AD pump and a Shimadzu LC-20 AC autosampler (Shimadzu Corporation, Columbia, MD). The column used was a Phenomex hyperclone BDS C18 column (50 × 2.0mm, 5 μm, Torrance, CA). The binary mobile phase consisted of mobile phase A: 5 mM ammonium acetate in water and mobile phase B: 5 mM ammonium acetate in acetonitrile. The gradient conditions for the mobile phase were as follows: 0.0-1.0 min, 20-100% B; 1.0-3.0 min, 100% B; 3.0-3.2 min, 100-10% B; 3.2-6.0 min, 20% B. The flow rate was 0.5 ml/min. The HPLC system was interfaced to an Applied Biosystem MDS Sciex triple quadrupole mass spectrometer (API 3200) (Applied Biosystems, Foster City, CA) operating in the negative electrospray ionization mode. For multiple-reaction monitoring, the transitions monitored were *m*/*z* 410.3 to 209.9 for fluvastatin, and *m*/*z* 557.0 to 278.1 for the IS (atorvastatin). Data collection, peak integration, and calculation were performed using Applied Biosystem MDS Analyst 1.4.2 software.

MALDI-IMS

PBS-treated and fluvastatin-treated tumor tissue samples were formalin-fixed and paraffin-embedded by standard protocols and sliced at 5 μM thickness on positively charged slides. Antigen retrieval followed by application of recombinant PNGaseF with an HTX TM Sprayer and 2 h incubation was done as previously described (Drake et al., 2017; Powers et al., 2014). CHCA (α-cyano-4-hydroxycinnamic acid) matrix was sprayed on the tissue, followed by analysis of released N-glycans using a 7T solariX dual-source MALDI-FTICR mass spectrometer (Bruker Daltonics, Billerica, MA) as previously described (Drake et al., 2017; Powers et al., 2014). Two-dimensional glycan image maps were visualized using FlexImaging 4.1 software (Bruker Daltonics, Billerica, MA).

Quantification and Statistical Analysis

Statistical analysis was performed using GraphPad Prism 6 and R software. Statistical testing and significance are performed as indicated in the legend of each figure. Histopathological analyses were independently reviewed by two personnel blinded to group allocation at the time of analysis. Quantification of histochemical analyses was performed using ImageScope software. *In vitro* experiments were not feasible for randomization or blinding due to the nature of the experiments.

Supplemental Items

Figure S1, related to Figure 1. Induction of EMT increases cell sensitivity to fluvastatin and tunicamycin.

Figure S2, related to Figure 1. Fluvastatin effect is independent from induction of ER stress.

Figure S3, related to Figure 2. Exogenous addition of dolichol (dolichyl[C95]-PP) did not rescue viability of MDA-MB-231 or MCF-7 cells with fluvastatin treatment in DMEM supplemented with 10% FBS.

Table S1, related to Figure 3. LC-MS/MS quantification of SLC3A2 glycopeptides after dox induction in HeLa cells with fluvastatin treatment.

Table S1, related to Figure 4. Total membrane protein N-glycans in vector and SNAIL-overexpressing MCF10A cells with fluvastatin treatment.

Figure S4, related to Figure 6. Characteristics of primary tumor growth and post-surgical endpoint.

Figure 1.

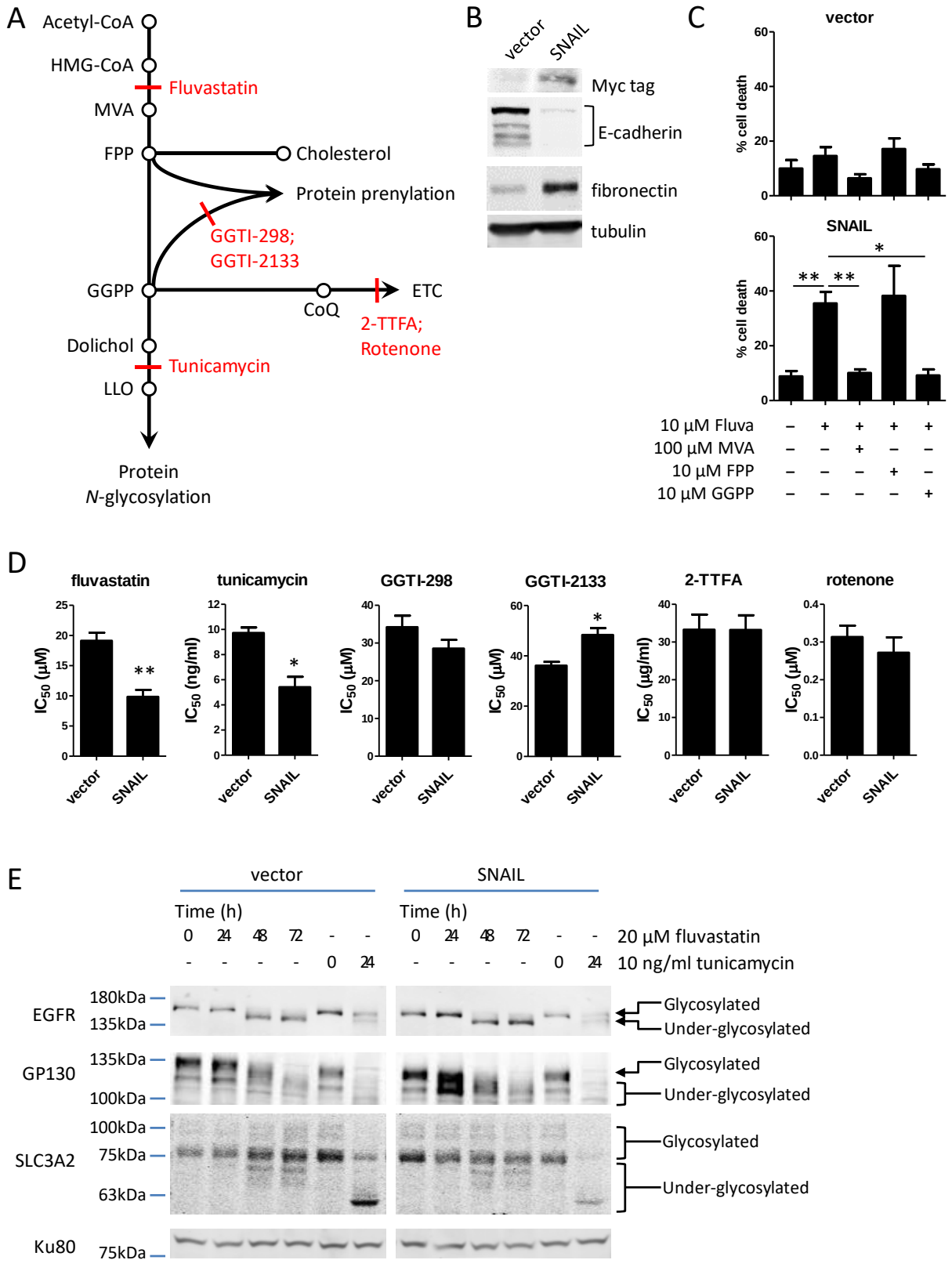
A
Acetyl-CoA
HMG-CoA
Fluvastatin
MVA
FPP
Cholesterol
Protein prenylation
GGTI-298;
GGTI-2133
GGPP
ETC
CoQ
2-TTFA;
Rotenone
Dolichol
Tunicamycin
LLO
Protein
N-glycosylation
B
vector
SNAIL
Myc tag
E-cadherin
fibronectin
tubulin
C
vector
% cell death
SNAIL
10 µM Fluva
100 µM MVA
10 µM FPP
10 µM GGPP
D
fluvastatin
tunicamycin
GGTI-298
GGTI-2133
2-TTFA
rotenone
IC50 (µM)
IC50 (ng/ml)
IC50 (µg/ml)
vector
SNAIL
E
vector
SNAIL
Time (h)
20 µM fluvastatin
10 ng/ml tunicamycin
EGFR
GP130
SLC3A2
Ku80
180kDa
135kDa
100kDa
75kDa
63kDa
Glycosylated
Under-glycosylated

Figure 1. Induction of EMT by SNAIL overexpression increases cell sensitivity to inhibition of dolichol-dependent protein *N*-glycosylation by fluvastatin and tunicamycin. **A**, a simplified schematic of the mevalonate (MVA) pathway. Inhibitors of specific components of the pathway are represented in red. CoA, coenzyme A; HMG-CoA, 3-hydroxy-3-methylglutaryl coenzyme A; MVA, mevalonate; FPP, farnesyl pyrophosphate; GGPP, geranylgeranyl pyrophosphate; LLO, lipid-linked oligosaccharides; GGTI, geranylgeranyltransferase inhibitor; CoQ, coenzyme Q; ETC, electron transport chain; 2-TTFA, 2-thenoyltrifluoroacetone. **B**, immunoblot (IB) of E-cadherin, an epithelial cell marker, and fibronectin, a mesenchymal cell marker, revealed that overexpression of SNAIL induced EMT in MCF10A cells. Tubulin is used as loading control. **C**, Flow cytometric quantification of % dead cells (% pre-G1 population) with propidium iodide DNA staining after fixation. Fluvastatin treatment for 72 h induced cell death in MCF10A cells overexpressing SNAIL, but not in vector control cells. Fluvastatin-induced cell death was fully rescued by co-administration with MVA or GGPP, but not FPP, at the indicated doses. Bars are mean + SD, n=3. *, $p<0.05$; **, $p<0.01$ (one-way ANOVA with a Dunnett post-test, comparing all columns vs. fluvastatin column). **D**, SNAIL overexpression sensitized cells to fluvastatin and tunicamycin, but not inhibitors of other components of the MVA pathway. IC_{50} values as calculated based on MTT assays after cells were treated with 8 doses of each drug for 72 h. Bars are mean + SD, n=3-4. *, $p<0.05$; **, $p<0.01$; (unpaired, two-tailed *t* test, comparing SNAIL vs. vector columns). **E**, IB for EGFR, GP130, and SLC3A2 for glycosylation status indicates that fluvastatin treatment for 48-72 h led to under-glycosylation of EGFR, GP130, and SLC3A2 in both vector control and SNAIL-overexpressing cells as indicated by the appearance of lower-molecular weight bands. Tunicamycin treatment for 24 h was a positive control for protein under-glycosylation. Ku80 is used as a loading control. Representative images are shown, n=3-4.

Figure 2.

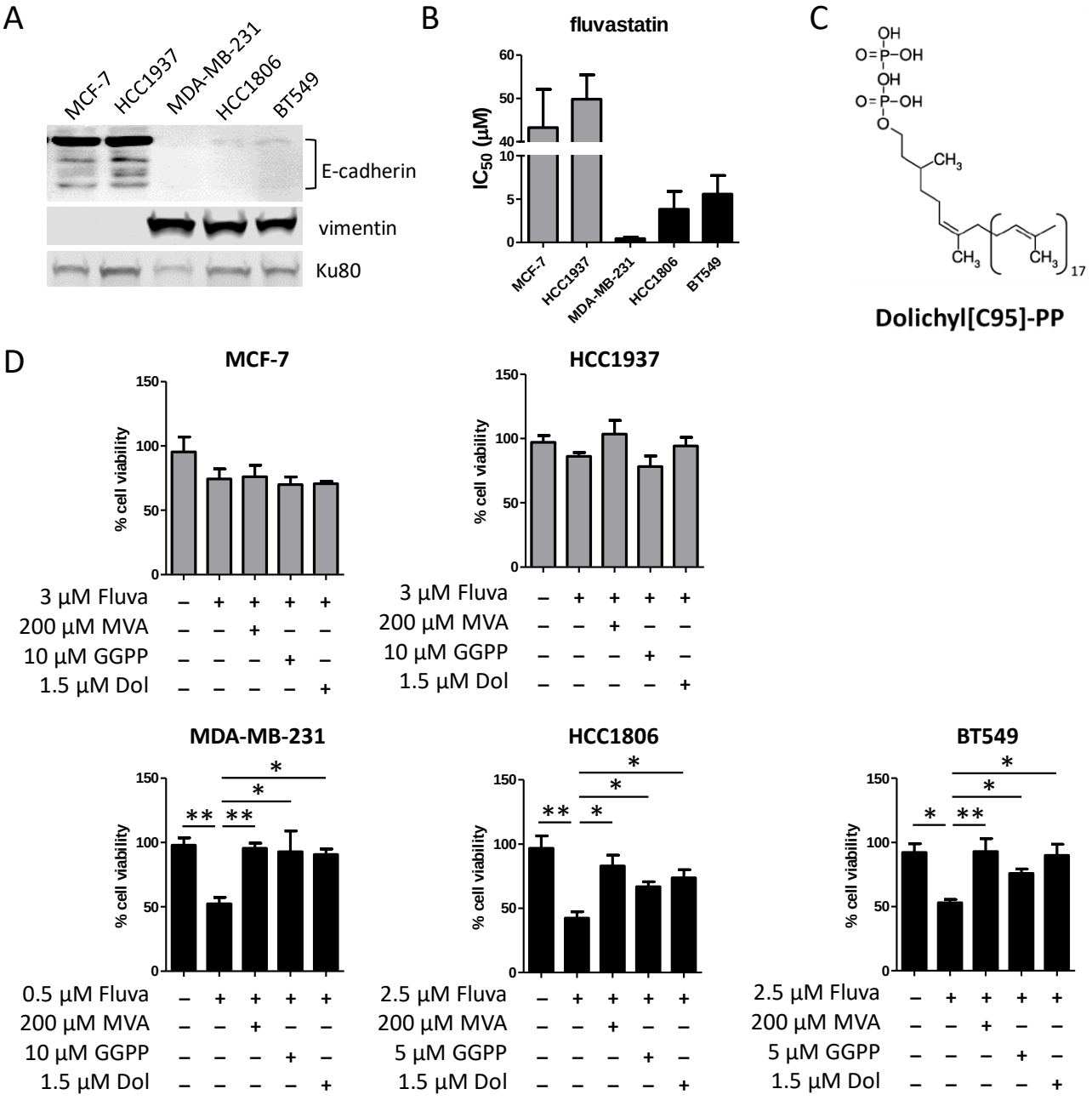
A
MCF-7
HCC1937
MDA-MB-231
HCC1806
BT549
E-cadherin
vimentin
Ku80
B
fluvastatin
IC50 (μM)
C
Dolichyl[C95]-PP
D
MCF-7
% cell viability
3 μM Fluva
200 μM MVA
10 μM GGPP
1.5 μM Dol
HCC1937
MDA-MB-231
0.5 μM Fluva
HCC1806
2.5 μM Fluva
5 μM GGPP
BT549

Figure 2. Inhibition of dolichol synthesis underlies fluvastatin sensitivity in mesenchymal breast cancer cell lines. **A**, IB of E-cadherin, an epithelial cell marker, and vimentin, a mesenchymal cell marker, indicates that MCF-7 and HCC1937 cells are more epithelial, while MBA-MB-231, HCC1806, and BT549 cells are more mesenchymal. Ku80 is used as a loading control. **B**, fluvastatin preferentially killed the more mesenchymal MDA-MB-231, HCC1806, and BT549 cells, compared to the more epithelial MCF-7 and HCC1937 cells. IC_{50} values are calculated based on MTT assays after cells were treated with 8 doses of each drug for 72 h in Opti-MEM serum reduced media. Bars are mean + SD, n=3. **C**, chemical structure of dolichyl[C95-105]-PP, a member of the dolichol group of long-chain isoprenoid molecules. **D**, MTT assays reveal that fluvastatin treatment for 72 h in Opti-MEM serum reduced media reduced cell viability in mesenchymal cells, but not in epithelial cell lines. Fluvastatin-induced reduction in cell viability was fully rescued by co-administration with MVA, GGPP, or dolichol (dolichyl[C95]-PP), at the indicated doses. Bars are mean + SD, n=3-4. *, $p<0.05$; **, $p<0.01$ (one-way ANOVA with a Dunnett post-test, comparing all columns vs. fluvastatin column). **E**, a simplified schematic of the function of dolichol. MVA, mevalonate; GlcNAc, *N*-acetylglucosamine; Asn, asparagine.

Figure 3.

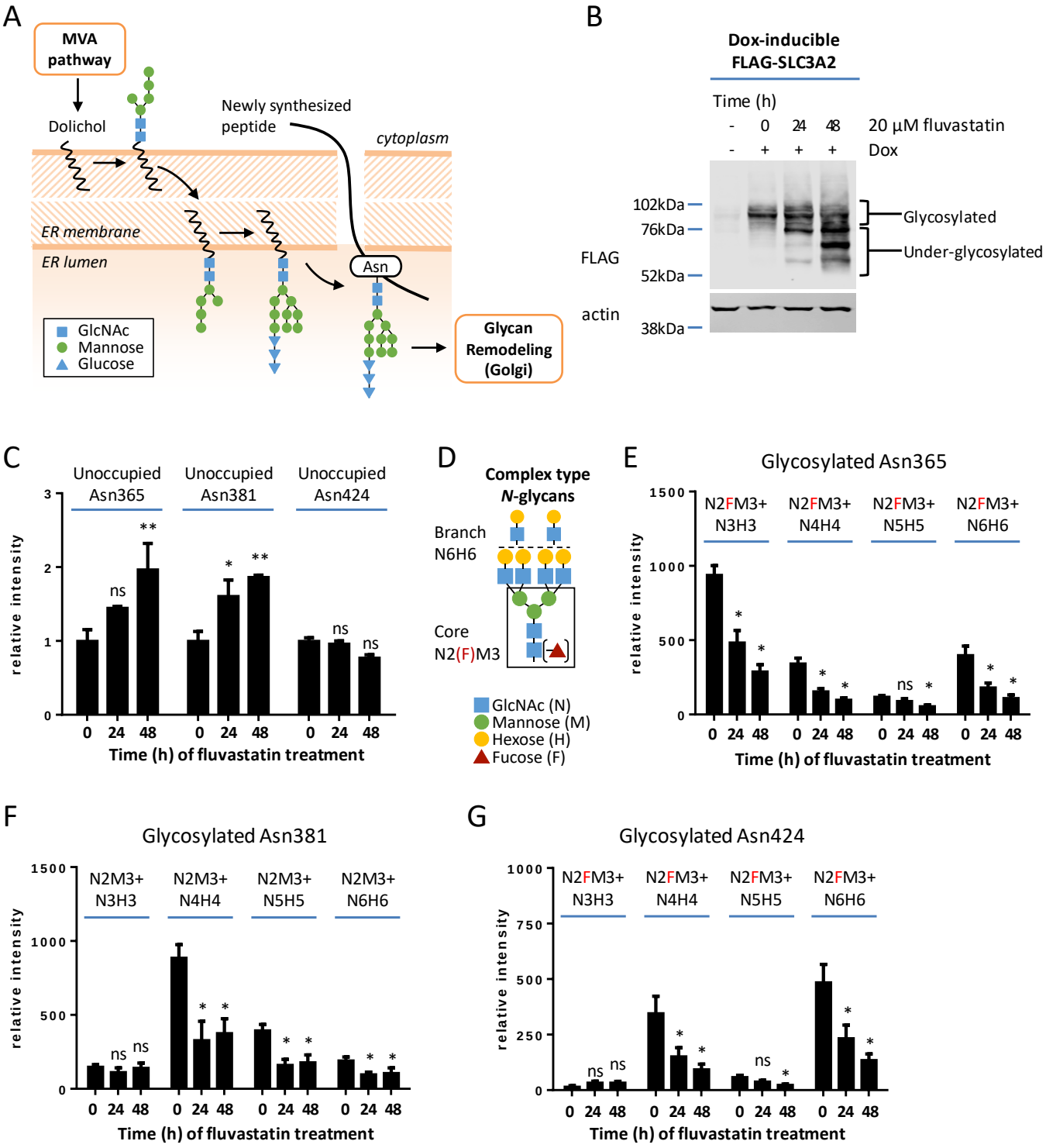
A
MVA pathway
Dolichol
Newly synthesized peptide
cytoplasm
ER membrane
ER lumen
Asn
GlcNAc
Mannose
Glucose
Glycan Remodeling (Golgi)
B
Dox-inducible FLAG-SLC3A2
Time (h)
- 0 24 48 20 μM fluvastatin
- + + + Dox
102kDa
76kDa
52kDa
FLAG
Glycosylated
Under-glycosylated
actin
38kDa
C
Unoccupied Asn365
Unoccupied Asn381
Unoccupied Asn424
relative intensity
Time (h) of fluvastatin treatment
D
Complex type N-glycans
Branch N6H6
Core N2(F)M3
GlcNAc (N)
Mannose (M)
Hexose (H)
Fucose (F)
E
Glycosylated Asn365
N2FM3+ N3H3
N2FM3+ N4H4
N2FM3+ N5H5
N2FM3+ N6H6
relative intensity
Time (h) of fluvastatin treatment
F
Glycosylated Asn381
N2M3+ N3H3
N2M3+ N4H4
N2M3+ N5H5
N2M3+ N6H6
relative intensity
Time (h) of fluvastatin treatment
G
Glycosylated Asn424
N2FM3+ N3H3
N2FM3+ N4H4
N2FM3+ N5H5
N2FM3+ N6H6
relative intensity
Time (h) of fluvastatin treatment

Figure 3. Fluvastatin treatment blocks dolichol-dependent protein *N*-glycosylation with complex type *N*-glycans. **A**, a simplified schematic of the dolichol-dependent protein *N*-glycosylation process. MVA, mevalonate; GlcNAc, *N*-acetylglucosamine; Asn, asparagine. **B**, In HeLa cells with Dox-inducible FLAG-SLC3A2 expression, IB for FLAG indicates that fluvastatin treatment led to under-glycosylation of SLC3A2 as indicated by the appearance of lower-molecular weight bands. actin was used as a loading control. Representative images are shown, n=3. **C**, levels of unoccupied Asn residues in SLC3A2 are quantified by FLAG-IP followed by LC-MS/MS. Fluvastatin treatment for up to 48 h increased the levels of unoccupied Asn at residues 365 and 381, but not 424. Three biological replicates were analyzed with two technical replicates each. ns, not significant; *, $p<0.05$ (two-way ANOVA with a Dunnett post-test, comparing each treatment column vs. control column). **D**, schematic representation of complex type *N*-glycans that decorate SLC3A2 on Asn residues 365, 381, and 424, that are represented in the following panels. **E-F**, fluvastatin treatment for up to 48 h decreases the levels of *N*-glycosylation with complex type *N*-glycans. Bars are mean + SD, n=3. ns, not significant; *, $p<0.05$ (two-way ANOVA with a Dunnett post-test, comparing each treatment column vs. control column).

Figure 4.

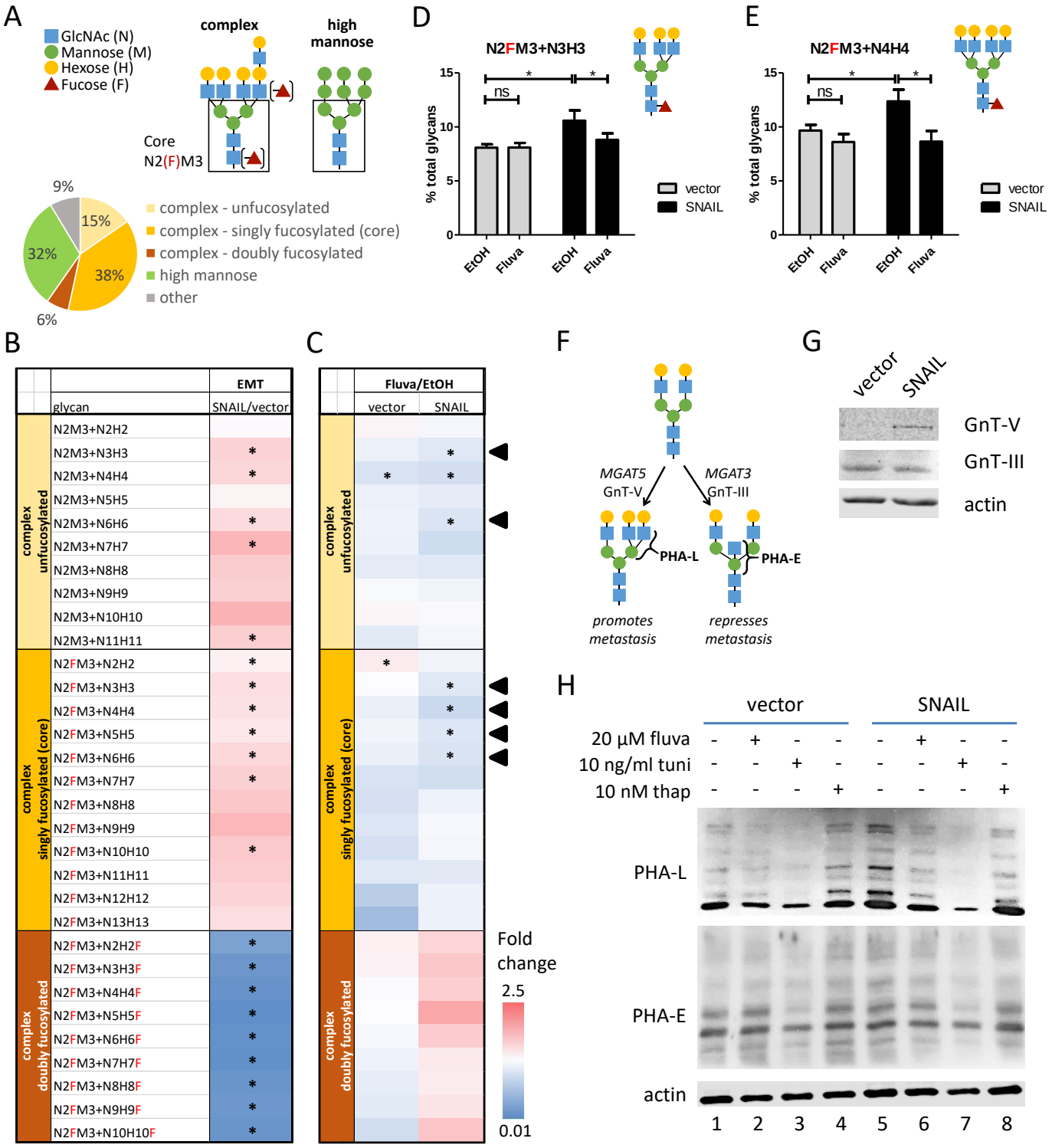
A
GlcNAc (N)
Mannose (M)
Hexose (H)
Fucose (F)
complex
high mannose
Core
N2(F)M3
9%
15%
32%
38%
6%
complex - unfucosylated
complex - singly fucosylated (core)
complex - doubly fucosylated
high mannose
other
D
N2FM3+N3H3
% total glycans
ns
*
*
vector
SNAIL
EtOH
Fluva
EtOH
Fluva
E
N2FM3+N4H4
% total glycans
ns
*
*
vector
SNAIL
EtOH
Fluva
EtOH
Fluva
B
EMT
glycan
SNAIL/vector
complex unfucosylated
N2M3+N2H2
N2M3+N3H3 *
N2M3+N4H4 *
N2M3+N5H5
N2M3+N6H6 *
N2M3+N7H7 *
N2M3+N8H8
N2M3+N9H9
N2M3+N10H10
N2M3+N11H11 *
complex singly fucosylated (core)
N2FM3+N2H2 *
N2FM3+N3H3 *
N2FM3+N4H4 *
N2FM3+N5H5 *
N2FM3+N6H6 *
N2FM3+N7H7 *
N2FM3+N8H8
N2FM3+N9H9
N2FM3+N10H10 *
N2FM3+N11H11
N2FM3+N12H12
N2FM3+N13H13
complex doubly fucosylated
N2FM3+N2H2F *
N2FM3+N3H3F *
N2FM3+N4H4F *
N2FM3+N5H5F *
N2FM3+N6H6F *
N2FM3+N7H7F *
N2FM3+N8H8F *
N2FM3+N9H9F *
N2FM3+N10H10F *
C
Fluva/EtOH
vector
SNAIL
complex unfucosylated
complex singly fucosylated (core)
complex doubly fucosylated
Fold change
2.5
0.01
F
MGAT5
GnT-V
MGAT3
GnT-III
PHA-L
PHA-E
promotes metastasis
represses metastasis
G
vector
SNAIL
GnT-V
GnT-III
actin
H
vector
SNAIL
20 µM fluva - + - - - + - -
10 ng/ml tuni - - + - - - + -
10 nM thap - - - + - - - +
PHA-L
PHA-E
actin
1 2 3 4 5 6 7 8

Figure 4. Fluvastatin treatment decreases complex branched *N*-glycans associated with EMT. **A**, schematic representation of complex type and high mannose type *N*-glycans (top), the two major classes of *N*-glycans, and distribution of major classes of *N*-glycans in the total cell surface glycome in MCF10A cells quantified by LC-MS/MS (bottom). **B**, heatmap of the expression of complex *N*-glycans following SNAIL-induced EMT. Data presented are the mean of 3 biological replicates with 1-2 technical replicates each. *, q<0.0301 (unpaired, 2-tailed *t* test with Benjamini-Hochberg FDR correction). **C**, heatmap of the expression of complex *N*-glycans following treatment with 20 μM fluvastatin in vector cells (left column) and SNAIL-overexpressing cells (right column). Black arrowheads indicate glycan species that are significantly upregulated in EMT (**B**) and downregulated by fluvastatin treatment in SNAIL-overexpressing cells (**C**, right column), but not affected by fluvastatin treatment in control cells (**C**, left column). Data presented are the mean of 3 biological replicates with 1-2 technical replicates each. *, q<0.0108 (unpaired, 2-tailed *t* test with Benjamini-Hochberg FDR correction). **D-E**, LC-MS/MS quantification of the β1,6-branched, tri-antennary (**D**) and tetra-antennary (**E**) *N*-glycans indicate that these *N*-glycan species are upregulated in EMT, which is inhibited by 20 μM fluvastatin treatment for 48 h. Bars are mean + SD, n=3. ns, not significant; *, p<0.05 (one-way ANOVA with a Bonferroni post-test, comparing selected pairs of columns). **F**, schematic representation of two mutually exclusive *N*-glycan branching pathways, catalyzed by different enzymes, recognized by different lectins, and with opposing effects on metastasis. **G**, IB of GnT-III *(MGAT3)* and GnT-V *(MGAT5)* showed that SNAIL-overexpressing cells upregulated GnT-V while GnT-III expression was unchanged, compared to vector control cells. Actin was used as a loading control. Representative images are shown, n=3. **H**, lectin blotting revealed that PHA-L ligand was upregulated in SNAIL-overexpressing cells, and was decreased by fluvastatin after 48 h. PHA-E ligand was expressed at comparable levels between the two cell lines and was not affected by fluvastatin treatment. Treatment with tunicamycin for 48 h was used as a positive control that decreased expression of both PHA-L and PHA-E ligands in both cell lines. Treatment with thapsigargin for 48 h was used as a negative control. Actin was used as a loading control. Representative images are shown, n=4.

Figure 5.

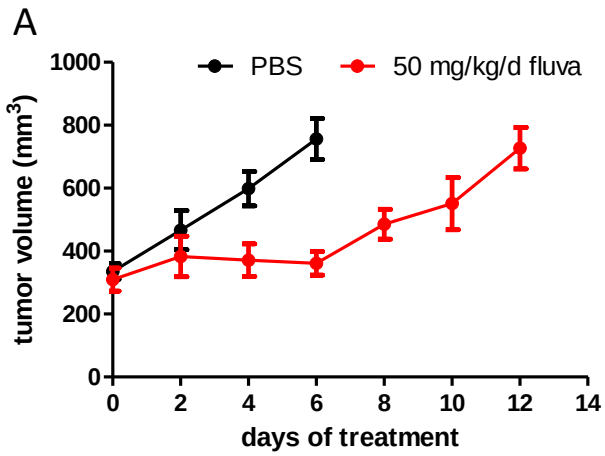

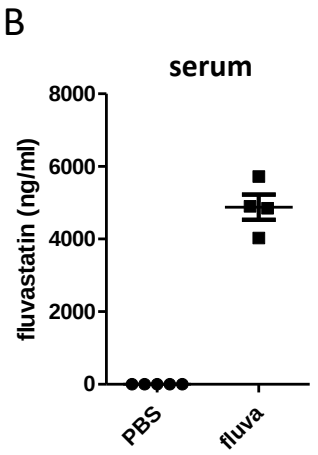

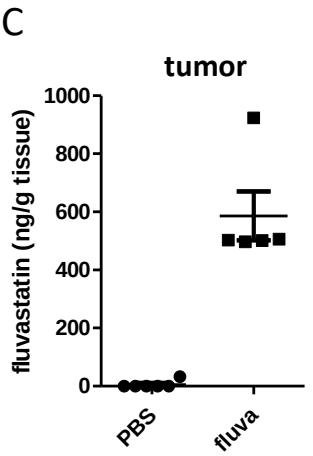

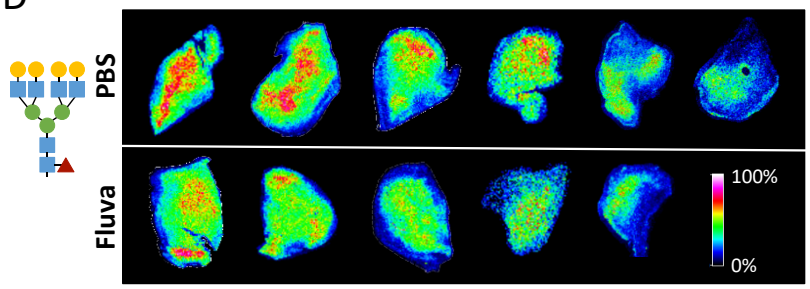

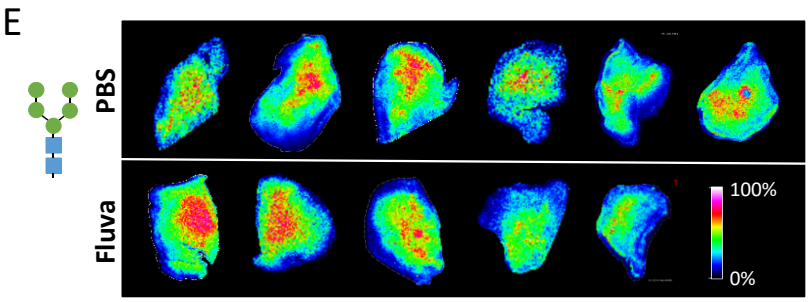

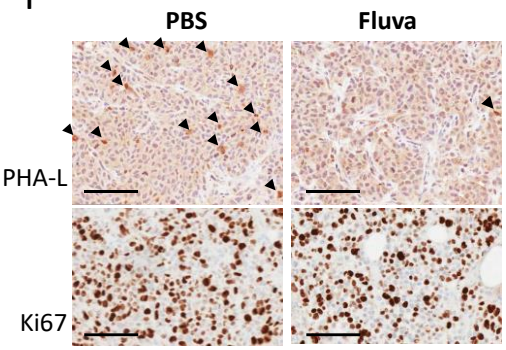

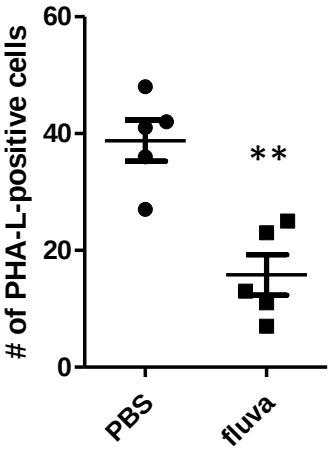

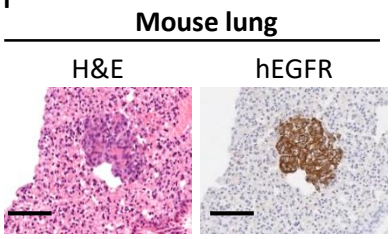

I

	Number of mice with metastasis (%)
PBS	3/6 (50%)
Fluva	1/5 (20%)

Figure 5. Fluvastatin treatment decreases complex branched *N*-glycans *in vivo*. **A**, fluvastatin delayed growth of the primary tumor. One million LM2-4 cells were subcutaneously implanted in SCID mice and treated with PBS or 50 mg/kg/d fluvastatin by oral gavage. Mice were sacrificed 6 days (PBS) or 12 days after treatment (fluvastatin) to ensure tumors from the two groups were size-matched for downstream analyses. Data points are mean ± SD, n=5-6. **B-C**, at time of sacrifice, mouse serum and a piece of tumor xenograft were flash-frozen in liquid N_2, and fluvastatin was extracted and quantified by HPLC-MS/MS. Data points are mean ± SD, n=4-6. **D-E**, at time of sacrifice, a piece of tumor xenograft was formalin-fixed and paraffin-embedded (FFPE). Spatial profiling of *N*-glycans by MALDI indicated that expression of tetra-antennary complex type *N*-glycans were decreased with fluvastatin treatment, while high mannose type *N*-glycans were unaffected. **F-G**, lectin histochemistry of tumor xenografts indicated that PHA-L ligand in Ki67-positive tissue areas was decreased with fluvastatin treatment. Representative images are shown, n=5. Scale bars = 50 µm. Data points are mean ± SD, n=5. **, $p<0.01$ (unpaired, two-tailed *t* test, comparing fluvastatin treatment vs. PBS control). **H-I**, fluvastatin treatment decreased proportion of mice with metastatic lesions in the lungs at the time of sacrifice. At time of sacrifice, mouse lungs were resected and FFPE. Two sequential slices were obtained every 200 µm for three depths containing all five lobes, and stained for H&E or hEGFR (**H**) Scale bars = 100 µm**.** Metastatic colonies were identified by hEGFR and confirmed by H&E. Each lung slice was independently reviewed by two personnel. Representative images are shown, n=5-6.

Figure 6.

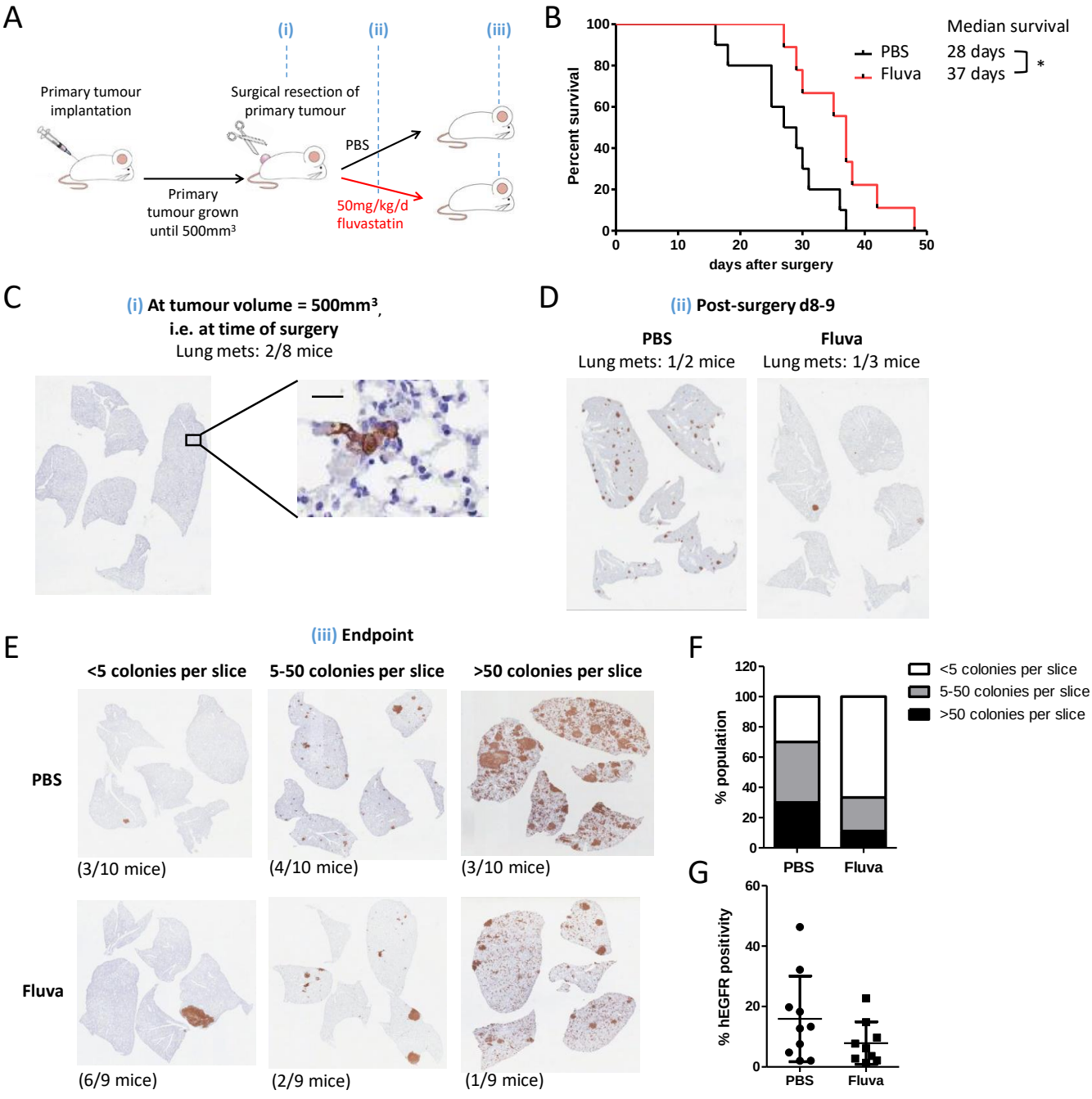
A
(i)
(ii)
(iii)
Primary tumour implantation
Surgical resection of primary tumour
PBS
Primary tumour grown until 500mm³
50mg/kg/d fluvastatin
B
Percent survival
days after surgery
PBS
Fluva
Median survival
28 days
37 days
*
C
(i) At tumour volume = 500mm³, i.e. at time of surgery
Lung mets: 2/8 mice
D
(ii) Post-surgery d8-9
PBS
Lung mets: 1/2 mice
Fluva
Lung mets: 1/3 mice
E
(iii) Endpoint
<5 colonies per slice
5-50 colonies per slice
>50 colonies per slice
PBS
(3/10 mice)
(4/10 mice)
(3/10 mice)
Fluva
(6/9 mice)
(2/9 mice)
(1/9 mice)
F
% population
<5 colonies per slice
5-50 colonies per slice
>50 colonies per slice
PBS
Fluva
G
% hEGFR positivity
PBS
Fluva

Figure 6. Post-surgical adjuvant fluvastatin treatment delays metastasis and prolongs survival. **A**, schematic of the mouse model and the time points where mice were sacrificed. **B**, fluvastatin treatment at 50 mg/kg/d orally significantly prolonged survival of mice with post-surgical metastatic breast cancer. *, $p<0.05$ (Log-rank test, n=12). **C-E**, At the indicated time point, mice were sacrificed and lungs were resected for FFPE. Two sequential slices were obtained every 200 µm for three depths containing all five lobes, and stained for H&E or hEGFR. Metastatic colonies were identified by hEGFR staining and confirmed by H&E. At time of surgery, mouse lungs were clear of metastatic colonies or had very small lesions (**C**). Scale bar = 20 µm. At 8-9 days post-surgery, mice receiving fluvastatin treatment had less metastatic tumor load than mice receiving PBS control (**D)**. At endpoint, fluvastatin treatment decreased the proportion of mice with heavy (>50 colonies per slice) or intermediate metastatic load (5-50 colonies per slice). The proportion of mice with light metastatic load (<5 colonies per slice) were increased (**E**). Each lung slice was independently reviewed by two personnel. Representative images are shown. **F-G**, quantification of metastatic load by colony count (**F**) or by hEGFR positivity (**G**) both showed lowered metastatic load in fluvastatin-treated mice.

Key Resources Table

REAGENT or RESOURCE	SOURCE	IDENTIFIER
Antibodies		
c-MYC	ATCC	CRL-1729
E-Cadherin	CST	3195
vimentin	CST	5741
fibronectin	Abcam	Ab32419
GP130	SCB	sc-655
EGFR (for IB)	CST	2232
EGFR (for IHC)	Zymed	28005
SLC3A2	SCB	Sc-7095
GnT-III	Thermo	PA5-12156
GnT-V	Thermo	MA5-24325
PHA-L (for IB)	EY Labs	H-1801-1
biotin-PHA-L (for IHC)	EY Labs	BA-1801-2
PHA-E	EY Labs	H-1802-1
Chemicals, Peptides, and Recombinant Proteins		
Fluvastatin	US Biologicals	F5277-76
RapiGest SF	Waters	186001861
Dolichyl[C95]-PP	American Radiolabeled Chemicals Inc	ARCD 1056
Trypsin	Promega	V5113
Sialidase A	Glyko	GK80040
Experimental Models: Cell Lines		
MCF10A	Soule et al., 1990	n/a
LM2-4	Guerin et al., 2013	n/a
Experimental Models: Organisms/Strains		
Mouse/SCID	Princess Margaret Cancer Centre in-house breeding colony	n/a
Oligonucleotides		

BiP_fw 3'- TGACATTGAAGACTTCAAAGCT-5'	This paper	n/a
BiP_rv 3'- CTGCTGTATCCTCTTCACCAGT-5'	This paper	n/a
ERdj4_fw 3'- AAAATAAGAGCCCGGATGCT-5'	This paper	n/a
ERdj4_rv 3'- CGCTTCTTGGATCCAGTGTT-5'	This paper	n/a
18S_rRNA_fw 5'-GTAACCCGTTGAACCCCATT-3'	This paper	n/a
18S_rRNA_fw 3'-CCATCCAATCGGTAGTAGCG-3'	This paper	n/a
Recombinant DNA		
pLPC-Myc-TWIST	This paper	n/a
pLPC-SNAIL1-Myc	This paper	n/a
pLPC-SNAIL2-Myc	This paper	n/a
pBabeHygro-Zeb1	This paper	n/a

Figure S1, related to Figure 1.

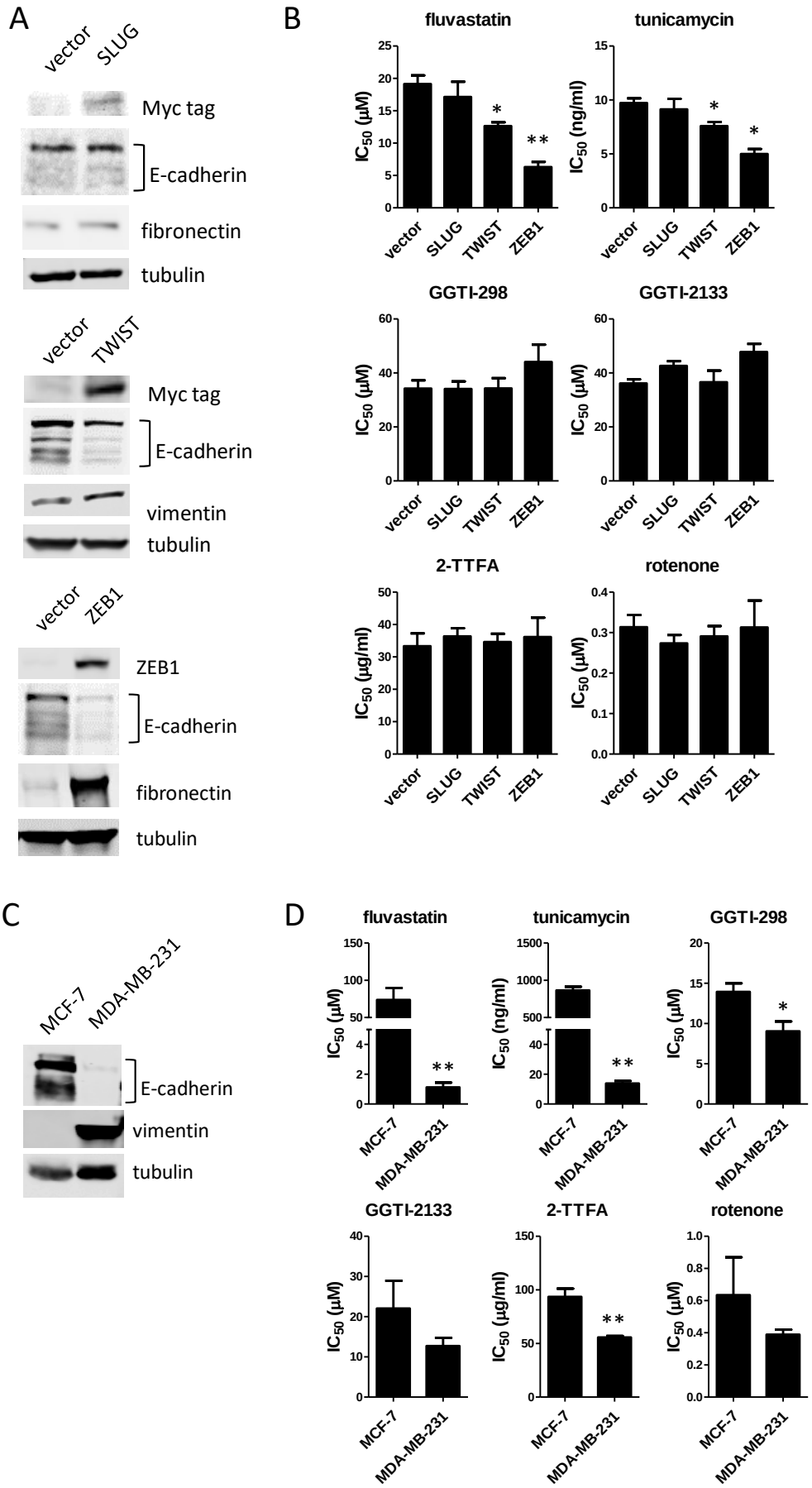

Figure S1, related to Figure 1. Induction of EMT increases cell sensitivity to fluvastatin and tunicamycin. **A**, IB of E-cadherin, an epithelial cell marker, and fibronectin, a mesenchymal cell marker, revealed that MCF10A vector control and SLUG-overexpressing cells remained epithelial, while TWIST- and ZEB1-overexpressing cells underwent EMT. Tubulin is used as a loading control. **B**, Induction of EMT by TWIST or ZEB1 overexpression sensitized cells to fluvastatin and tunicamycin, but not inhibitors of other components of the MVA pathway. IC_{50} values as calculated based on MTT assays after cells were treated with 8 doses of each drug for 72 h. Bars are mean + SD, n=3-4. *, $p<0.05$; **, $p<0.01$ (one-way ANOVA with a Dunnett post-test, comparing all columns vs. vector column). **C**, IB of E-cadherin, an epithelial cell marker, and vimentin, a mesenchymal cell marker, revealed that MCF-7 cells are more epithelial, while MBA-MB-231 cells are more mesenchymal. Tubulin is used as a loading control. **D**, Fluvastatin and tunicamycin preferentially killed the more mesenchymal MDA-MB-231 cells, compared to the more epithelial MCF-7 cells, by approximately 50-fold. This difference could not be phenocopied by GGTI-298, GGTI-2133, 2-TTFA, or rotenone. IC_{50} values are calculated based on MTT assays after cells were treated with 8 doses of each drug for 72 h. Bars are mean + SD, n=3. *, $p<0.05$; **, $p<0.01$ (unpaired, two-tailed *t* test, comparing MDA-MB-231 and MCF-7 columns).

Figure S2, related to Figure 1.

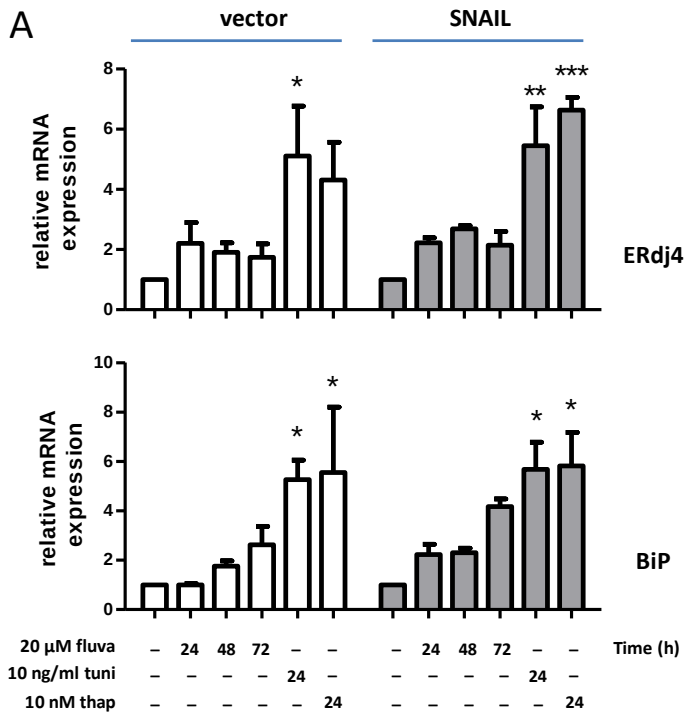

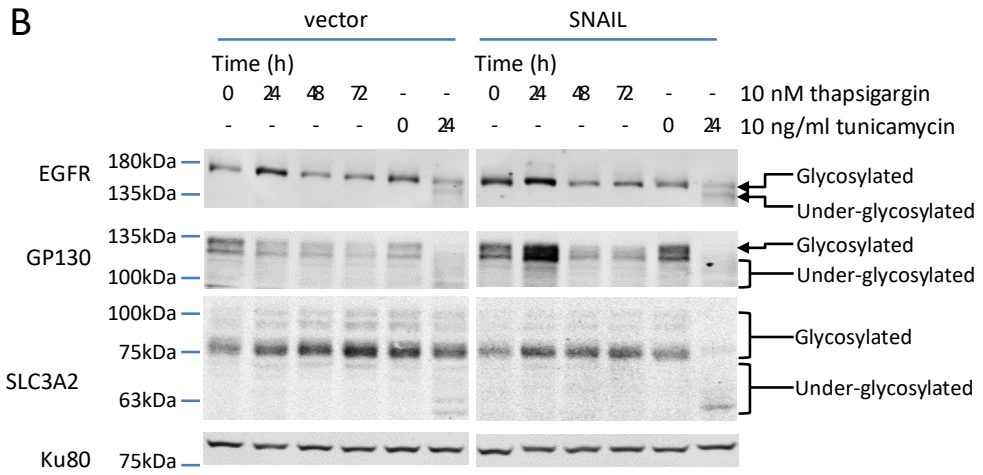

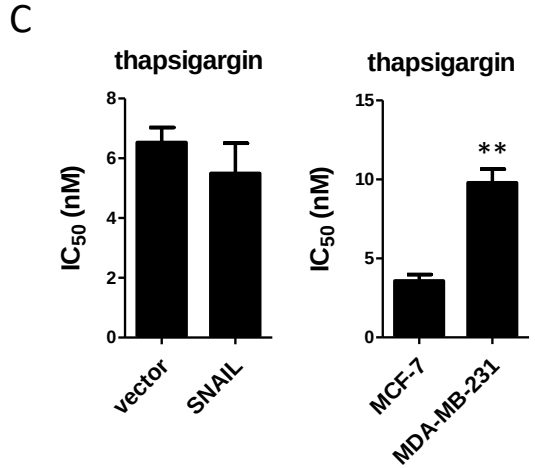

Figure S2, related to Figure 1. Fluvastatin effect is independent from induction of ER stress. **A**, qRT-PCR of ER stress markers ERdj4 and BiP revealed that fluvastatin treatment for up to 72 h did not induce ER stress, while tunicamycin and thapsigargin treatment both induced ER stress after 24 h of treatment. qRT-PCR of 18S rRNA was used as a housekeeping control. Bars are mean + SD, n=3. *, $p<0.05$; **, $p<0.01$; ***, $p<0.001$ (one-way ANOVA with a Dunnett post-test, comparing all columns vs. solvent control). **B**, IB for EGFR, GP130, and SLC3A2 for glycosylation status indicates that thapsigargin treatment for up to 72 h did not affect glycosylation status of these proteins in both vector control and SNAIL-overexpressing cells. Tunicamycin treatment for 24 h was a positive control for protein under-glycosylation. Ku80 is used as a loading control. Representative images are shown, n=3-4. **C**, IC_{50} values as calculated based on MTT assays after cells were treated with 8 doses of thapsigargin for 72 h, showed that sensitivity to thapsigargin was not modulated by EMT. Bars are mean + SD, n=3. **, $p<0.01$ (unpaired, two-tailed *t* test, comparing MDA-MB-231 and MCF-7 columns).

Figure S3, related to Figure 2.

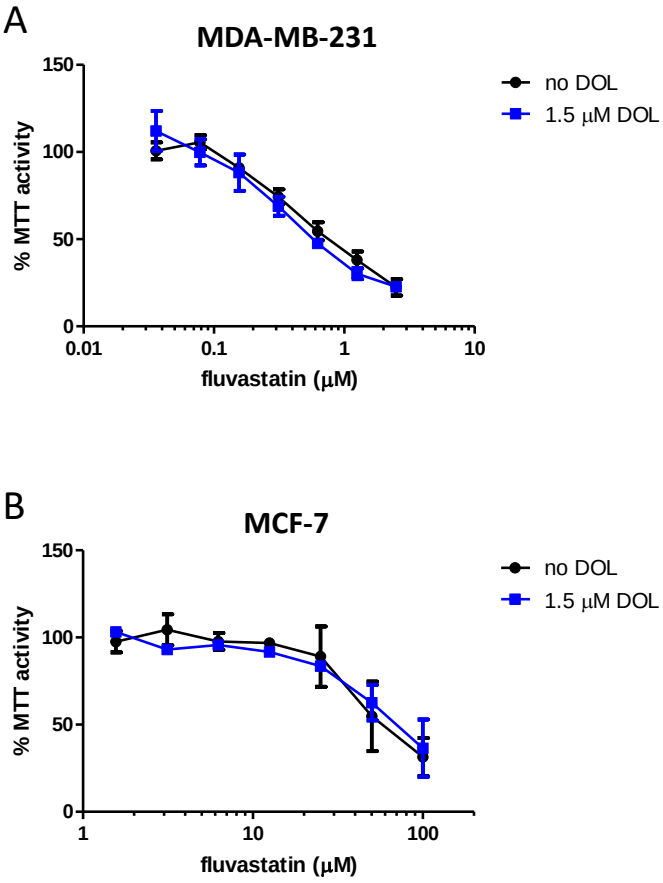

Figure S3, related to Figure 2. Exogenous addition of dolichol (dolichyl[C95]-PP) did not rescue viability of MDA-MB-231 (**A**) or MCF-7 cells (**B**) with fluvastatin treatment in DMEM supplemented with 10% FBS. Cell viability was calculated based on MTT assays after cells were treated with 7 doses of fluvastatin for 72 h. Data points are mean ± SD, n=3.

Table S1, Related to Figure 3.

LC-MS/MS Quantification of SLC3A2 glycopeptides after Dox induction in HeLa cells with fluvastatin treatment.

Peptide	type	glycan	Mean intensity		
			untreated	24h fluva	48h fluva
DASSFLAEWQN365ITK	unoccupied	-	142.90	207.84	306.55
DASSFLAEWQN365ITK	complex	N2M3+N2H2	23.13	113.31	79.74
DASSFLAEWQN365ITK	complex	N2M3+N2H2F	283.98	348.61	229.22
DASSFLAEWQN365ITK	complex	N2M3+N3H3	23.12	44.47	30.23
DASSFLAEWQN365ITK	complex	N2M3+N3H3F	939.05	484.57	289.79
DASSFLAEWQN365ITK	complex	N2M3+N3H3F2	180.96	143.17	89.14
DASSFLAEWQN365ITK	complex	N2M3+N4H4	23.99	24.83	15.73
DASSFLAEWQN365ITK	complex	N2M3+N4H4F	343.22	156.20	99.29
DASSFLAEWQN365ITK	complex	N2M3+N4H4F2	128.65	76.28	49.73
DASSFLAEWQN365ITK	complex	N2M3+N5H5F	119.98	90.36	55.08
DASSFLAEWQN365ITK	complex	N2M3+N6H6	18.57	16.98	10.56
DASSFLAEWQN365ITK	complex	N2M3+N6H6F	398.81	182.38	111.15
DASSFLAEWQN365ITK	complex	N2M3+N6H6F2	188.76	111.19	67.51
DASSFLAEWQN365ITK	complex	N2M3+N8H8F	138.71	73.66	42.61
DASSFLAEWQN365ITK	complex	N2M3+N8H8F2	83.46	52.22	34.31
DASSFLAEWQN365ITK	complex	N2M3+N10H10F	63.60	40.81	24.16
DASSFLAEWQN365ITK	high mannose	N2M3+H1	3.80	14.62	38.88
DASSFLAEWQN365ITK	high mannose	N2M3+H2	6.75	97.69	270.60
DASSFLAEWQN365ITK	high mannose	N2M3+H3	16.03	189.98	154.67
DASSFLAEWQN365ITK	incomplete	N2M3	8.23	10.69	64.55
DASSFLAEWQN365ITK	incomplete	N2M3+N1	41.50	48.42	568.66
DASSFLAEWQN365ITK	incomplete	N2M3+N2	73.18	87.74	255.07
DASSFLAEWQN365ITK	incomplete	N2M3+NF	24.45	32.00	596.94
DASSFLAEWQN365ITK	incomplete	N2M3+N2F	9.09	54.61	517.83
DASSFLAEWQN365ITK	incomplete	N2M3+N3F	11.78	47.25	379.22
DASSFLAEWQN365ITK	incomplete	N2M3+N4F	8.45	19.73	209.22
DASSFLAEWQN365ITK	incomplete	N2M3+NHF	24.50	52.81	190.58
DASSFLAEWQN365ITK	incomplete	N2M3+F	2.45	4.30	60.56
DASSFLAEWQN365ITK	incomplete	N2M3+FH	2.16	1.46	12.32
LLIAGTN381SSDLQQILSLLESNK	unoccupied	-	26.55	31.80	51.22
LLIAGTN381SSDLQQILSLLESNK	complex	N2M3+N2H2	16.99	42.09	72.11
LLIAGTN381SSDLQQILSLLESNK	complex	N2M3+N3H3	149.49	113.71	142.42
LLIAGTN381SSDLQQILSLLESNK	complex	N2M3+N4H4	886.65	329.28	377.49
LLIAGTN381SSDLQQILSLLESNK	complex	N2M3+N4H4F	42.54	20.22	25.03
LLIAGTN381SSDLQQILSLLESNK	complex	N2M3+N5H5	395.55	161.84	179.24
LLIAGTN381SSDLQQILSLLESNK	complex	N2M3+N6H6	191.52	97.70	106.93

LLIAGTN381SSDLQQILSLLESNK	complex	N2M3+N7H7	79.02	54.51	59.41
LLIAGTN381SSDLQQILSLLESNK	complex	N2M3+N8H8	15.77	15.47	17.17
LLIAGTN381SSDLQQILSLLESNK	high mannose	N2M3+H1	4.97	4.07	31.82
LLIAGTN381SSDLQQILSLLESNK	high mannose	N2M3+H2	5.89	46.58	120.15
LLIAGTN381SSDLQQILSLLESNK	high mannose	N2M3+H3	2.88	35.32	25.63
LLIAGTN381SSDLQQILSLLESNK	high mannose	N2M3+H4	6.03	89.98	42.42
LLIAGTN381SSDLQQILSLLESNK	incomplete	N2M3	0.92	0.86	7.79
LLIAGTN381SSDLQQILSLLESNK	incomplete	N2M3+N1	6.82	44.46	345.40
LLIAGTN381SSDLQQILSLLESNK	incomplete	N2M3+N2	2.71	83.02	572.48
LLIAGTN381SSDLQQILSLLESNK	incomplete	N2M3+N3	9.45	52.12	370.71
LLIAGTN381SSDLQQILSLLESNK	incomplete	N2M3+N4	4.10	39.21	81.35
LLIAGTN381SSDLQQILSLLESNK	incomplete	N2M3+NH	1.77	23.89	111.63
LLIAGTN381SSDLQQILSLLESNK	incomplete	N2M3+NH2	1.84	29.06	79.58
LLIAGTN381SSDLQQILSLLESNK	incomplete	N2M3+NH3	3.56	14.14	27.49
LLIAGTN381SSDLQQILSLLESNK	incomplete	N2M3+N2H1	4.27	7.97	81.50
LLIAGTN381SSDLQQILSLLESNK	incomplete	N2M3+N3H1	5.71	5.03	59.58
LLIAGTN381SSDLQQILSLLESNK	incomplete	N2M3+N3H2	1.49	3.16	15.88
LLIAGTN381SSDLQQILSLLESNK	incomplete	N2M3+N4H1	6.14	16.57	17.71
SLVTQYLN424ATGNR	unoccupied	-	153.15	149.05	137.47
SLVTQYLN424ATGNR	complex	N2M3+N2H2F	10.11	43.45	44.12
SLVTQYLN424ATGNR	complex	N2M3+N3H3F	14.31	33.62	33.09
SLVTQYLN424ATGNR	complex	N2M3+N4H4	33.73	26.49	16.50
SLVTQYLN424ATGNR	complex	N2M3+N4H4F	341.92	152.12	91.64
SLVTQYLN424ATGNR	complex	N2M3+N4H4F2	57.14	34.16	22.70
SLVTQYLN424ATGNR	complex	N2M3+N5H5F	56.60	39.82	23.74
SLVTQYLN424ATGNR	complex	N2M3+N5H5F2	26.25	20.75	12.47
SLVTQYLN424ATGNR	complex	N2M3+N6H6	45.00	31.12	16.51
SLVTQYLN424ATGNR	complex	N2M3+N6H6F	473.39	230.99	131.68
SLVTQYLN424ATGNR	complex	N2M3+N6H6F2	115.45	69.76	43.95
SLVTQYLN424ATGNR	complex	N2M3+N7H7F	106.57	65.47	37.10
SLVTQYLN424ATGNR	complex	N2M3+N7H7F2	28.22	24.05	13.62
SLVTQYLN424ATGNR	complex	N2M3+N8H8F2	53.44	40.32	22.86
SLVTQYLN424ATGNR	complex	N2M3+N8H8F	172.57	97.61	54.17
SLVTQYLN424ATGNR	complex	N2M3+N9H9F1	52.50	38.69	20.82
SLVTQYLN424ATGNR	complex	N2M3+N10H10F1	69.89	47.82	26.19
SLVTQYLN424ATGNR	complex	N2M3+N10H10F2	32.23	22.95	13.87
SLVTQYLN424ATGNR	high mannose	N2M3+H1	4.87	9.92	16.39
SLVTQYLN424ATGNR	high mannose	N2M3+H2	5.94	52.15	96.36
SLVTQYLN424ATGNR	high mannose	N2M3+H3	18.36	148.30	75.30
SLVTQYLN424ATGNR	incomplete	N2M3	7.44	10.12	28.74
SLVTQYLN424ATGNR	incomplete	N2M3+N1	1.98	7.90	36.20

SLVTQYLN424ATGNR	incomplete	N2M3+N2	13.78	28.73	126.16
SLVTQYLN424ATGNR	incomplete	N2M3+NF	1.71	14.86	97.98
SLVTQYLN424ATGNR	incomplete	N2M3+N2F	26.69	93.80	515.61
SLVTQYLN424ATGNR	incomplete	N2M3+N3F	13.26	96.48	788.40
SLVTQYLN424ATGNR	incomplete	N2M3+N4F	7.71	36.34	125.08
SLVTQYLN424ATGNR	incomplete	N2M3+NHF	7.22	23.11	72.45
SLVTQYLN424ATGNR	incomplete	N2M3+F	1.98	5.31	46.34
SLVTQYLN424ATGNR	incomplete	N2M3+NH	3.87	9.69	13.15
SLVTQYLN424ATGNR	incomplete	N2M3+NH2F	4.66	19.61	47.78
SLVTQYLN424ATGNR	incomplete	N2M3+N2H1F	1.14	3.57	19.69

Table S2, Related to Figure 4.
Total membrane protein N-glycans in vector and SNAIL-overexpressing MCF10A cells with fluvastatin treatment.

Type	glycan	charge/"m/z" (retention time)	Mean glycan quantification (% total)			
			vector EtOH	vector Fluva	SNAIL EtOH	SNAIL Fluva
complex	N2M3+N2H2	2+/821.3034 (10-13)	8.01	8.78	8.40	8.02
complex	N2FM3+N2H2	2+/894.3335 (11.2-15)	16.23	19.09	18.22	16.89
complex	N2FM3+N2H2F	2+/967.36245 (10.5-14)	2.08	2.35	0.46	0.65
complex	N2M3+N3H3	2+/1003.872 (10.5-15)	3.09	2.80	4.40	3.66
complex	N2FM3+N3H3	2+/1076.8981 (12-15.5)	8.07	8.10	10.58	8.80
complex	N2FM3+N3H3F	2+/1149.9352 (12-16)	1.00	1.10	0.14	0.21
complex	N2FM3+N3H3F	3+/766.9568 (12-16)	0.28	0.32	0.02	0.04
complex	N2M3+N4H4	2+/1186.4468 (12.3-16.5)	1.72	1.35	2.57	1.85
complex	N2M3+N4H4	3+/791.2955 (12.3-16.5)	1.09	0.86	1.33	1.07
complex	N2FM3+N4H4	2+/1259.464 (13.8-17)	4.58	4.33	6.61	4.49
complex	N2FM3+N4H4	3+/839.9795 (13.8-17)	5.09	4.28	5.75	4.16
complex	N2FM3+N4H4F	2+/1332.5011 (13-17.5)	0.52	0.54	0.04	0.06
complex	N2FM3+N4H4F	3+/888.6664 (13-17.5)	0.96	0.93	0.09	0.13
complex	N2M3+N5H5	2+/1369.0029 (13.8-17.5)	0.22	0.20	0.25	0.21
complex	N2M3+N5H5	3+/913.0102 (13.8-17.5)	0.66	0.59	0.72	0.64
complex	N2FM3+N5H5	2+/1442.0326 (14.2-17.5)	0.47	0.44	0.61	0.50
complex	N2FM3+N5H5	3+/961.6884 (14.2-17.5)	1.75	1.63	2.12	1.72
complex	N2FM3+N5H5F	2+/1515.0601 (15-17.5)	0.11	0.12	0.00	0.01
complex	N2FM3+N5H5F	3+/1010.3798 (15-17.5)	0.58	0.57	0.03	0.06
complex	N2M3+N6H6	2+/1551.584 (15-17.5)	0.03	0.03	0.04	0.03
complex	N2M3+N6H6	3+/1034.715 (15-17.5)	0.31	0.29	0.42	0.34
complex	N2FM3+N6H6	2+/1624.6012 (16-17.5)	0.10	0.09	0.14	0.11
complex	N2FM3+N6H6	3+/1083.4008 (16-17.5)	0.94	0.84	1.29	1.02
complex	N2FM3+N6H6F	3+/1132.0819 (15.5-17.5)	0.39	0.38	0.03	0.04
complex	N2M3+N7H7	3+/1156.435 (16-17.5)	0.10	0.09	0.17	0.13
complex	N2FM3+N7H7	3+/1205.1132 (17-17.5)	0.32	0.25	0.46	0.34
complex	N2FM3+N7H7F	3+/1253.8046 (16.5-17.4)	0.19	0.17	0.01	0.01
complex	N2M3+N8H8	3+/1278.1325 (17.5)	0.04	0.03	0.05	0.04
complex	N2FM3+N8H8	3+/1326.8256 (17.5)	0.17	0.13	0.27	0.24
complex	N2FM3+N8H8F	3+/1375.517 (17.5)	0.10	0.09	0.01	0.01
complex	N2M3+N9H9	3+/1399.8598 (17.5)	0.02	0.02	0.03	0.03
complex	N2FM3+N9H9	3+/1448.538 (17.5)	0.10	0.08	0.17	0.16
complex	N2FM3+N9H9F	3+/1497.2294 (17.5)	0.05	0.05	0.01	0.01
complex	N2M3+N10H10	3+/1521.5622 (17.5)	0.01	0.01	0.01	0.01
complex	N2FM3+N10H10	3+/1570.2405 (17.5)	0.05	0.05	0.09	0.09
complex	N2FM3+N10H10	4+/1177.9378 (17.5)	0.08	0.06	0.11	0.11
complex	N2FM3+N10H10F	4+/1214.4596 (17.5)	0.05	0.03	0.01	0.01
complex	N2M3+N11H11	3+/1643.2721 (17.5)	0.03	0.02	0.04	0.04
complex	N2FM3+N11H11	3+/1691.9628 (17.5)	0.03	0.02	0.04	0.03
complex	N2FM3+N12H12	4+/1360.5064 (17.5)	0.05	0.03	0.07	0.06
complex	N2FM3+N13H13	4+/1451.7907 (17.5)	0.04	0.02	0.05	0.04
high mannose	N2M3+H2(M5)	2+/618.2244 (8.2-11.5)	2.37	2.63	1.95	2.62
high mannose	N2M3+H2(M5)	1+/1235.4411 (8.2-11.5)	1.28	2.53	1.13	1.91
high mannose	N2M3+H3(M6)	2+/699.2515 (8.2-10.5)	2.86	3.09	2.50	3.21
high mannose	N2M3+H3(M6 ammonium adduct)	2+/707.768 (8.2-10.5)	1.55	1.57	1.26	1.81
high mannose	N2M3+H3(M6)	1+/1397.4939 (8.2-10.5)	1.67	1.90	1.35	1.95
high mannose	N2M3+H4(M7)	2+/780.2879 (8.2-10.5)	3.73	3.85	3.38	3.97
high mannose	N2M3+H4(M7 ammonium adduct)	2+/788.7886 (8.2-10.5)	1.57	1.89	1.49	1.86
high mannose	N2M3+H4(M7)	1+/1559.5467 (8.2-10.5)	0.45	0.68	0.43	0.52
high mannose	N2M3+H5(M8)	2+/861.3047 (8-10.8)	4.79	3.86	4.29	4.68
high mannose	N2M3+H5(M8 ammonium adduct)	2+/869.8157 (8-10.8)	2.69	2.42	2.73	3.34
high mannose	N2M3+H6(M9)	2+/942.3285 (8-10.5)	4.77	2.79	3.45	2.11
high mannose	N2M3+H6(M9 ammonium adduct)	2+/950.8421 (8-10.5)	2.61	1.57	2.00	1.21
high mannose	N2M3+H7(M10)	2+/1023.356 (8.6-10.6)	0.69	0.29	0.36	0.20
high mannose	N2M3+H7(M10 ammonium adduct)	2+/1031.869 (8.6-10.6)	0.35	0.15	0.21	0.11
high mannose	N2M3+H6(M9 dimer)	3+/1256.106 (8-9.6)	0.10	0.04	0.05	0.02
high mannose	N2M3+H6(M9 M8 dimer)	3+/1202.087 (8-9.5)	0.25	0.14	0.15	0.12

hybrid	N2M3+N1H2	2+/719.7605 (8-12)	1.63	1.69	1.61	2.01
hybrid	N2FM3+N1H2	2+/792.791 (8.5-12.5)	0.72	0.90	0.54	1.00
hybrid	N2M3+N1H3	2+/800.79645 (9-12)	2.06	1.81	1.73	2.16
hybrid	N2FM3+N1H3	2+/873.8254 (10.5-13)	0.41	0.67	0.27	0.57
hybrid	N2M3+N1H4	2+/881.8194 (8.6-10.5)	0.27	0.23	0.24	0.21
hybrid	N2M3+N2H3	2+/902.3314 (8.5-13.5)	0.29	0.25	0.37	0.33
hybrid	N2FM3+N2H3	2+/975.3618 (11-14.5)	0.27	0.34	0.27	0.30
hybrid	N2M3+N2H4	2+/983.36245 (11.5-14)	0.06	0.05	0.10	0.11
hybrid	N2FM3+N3H4	2+/1157.9311 (13.5-16)	0.09	0.09	0.11	0.09
hybrid	N2FM3+N6H8	3+/1191.436 (15.5-17)	0.01	0.01	0.03	0.02
incomplete	N2FM3+N1H1	2+/711.7674 (11-16)	0.73	0.78	0.40	0.78
incomplete	N2FM3+N2	2+/732.2813 (10.2-12.5)	0.76	1.06	0.52	2.95
incomplete	N2FM3+N3	2+/833.821 (10.1-13)	0.13	0.18	0.13	0.90
incomplete	N2FM3+N2H1	2+/813.3077 (9.5-13.5)	0.74	0.98	0.61	1.99
incomplete	N2FM3+N3H2	2+/995.8738 (10.5-15.5)	0.30	0.32	0.32	0.68
incomplete	N2FM3+N4H3	2+/1178.4399 (13.5-15)	0.15	0.14	0.19	0.23
total			100.00	100.00	100.00	100.00

Figure S4, related to Figure 6.

A

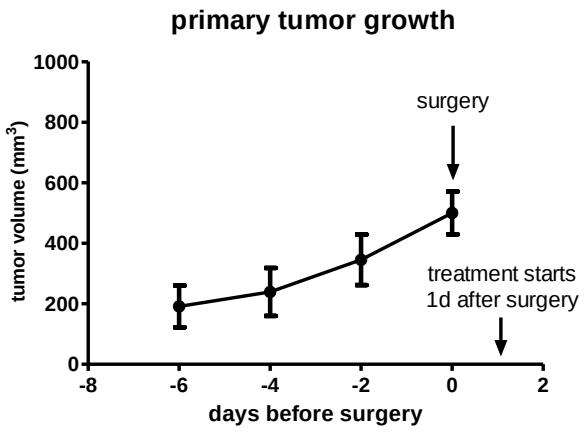

B

Cause of endpoint	PBS	Fluva
Difficulty breathing[1]	6	1
Distended abdomen[2]	2	1
Lymph node mass and/or primary site regrowth[3]	2	7
Total number of mice	10	9

[1] Endpoint when observed 3 consecutive days, combined with poor body condition score
[2] Immediate endpoint when observed
[3] Endpoint when total tumour mass approach 1000mm^3

Figure S4, related to Figure 6. Characteristics of primary tumor growth and post-surgical endpoint. **A,** SCID mice were injected subcutaneously with 1 million LM2-4 cells. Tumors were allowed to grow without treatment to approximately 500 mm^3. Mice were randomized to receive surgery removing the primary tumor, or to be sacrificed. The former group were further randomized to receive PBS or 50 mg/kg/d fluvastatin by oral gavage, starting 1 after surgery. Data points are mean ± SD, n=32. **B**, breakdown of the cause of endpoint. Whereas the majority of mice receiving PBS control reached endpoint from lung events, most of fluvastatin-treated mice reached endpoint due to primary tumor regrowth.

Highlights

- Mevalonate (MVA) pathway is a targetable vulnerability of metastatic breast cancer
- MVA pathway produces dolichol, essential for protein *N*-glycosylation
- Fluvastatin inhibits dolichol synthesis and metastasis-associated *N*-glycosylation
- Adjuvant therapy with fluvastatin attenuates metastasis and improves survival

eTOC blurb

Yu et al. show that metastatic breast cancer cells are dependent on the mevalonate (MVA) pathway to support dolichol biosynthesis and dolichol-dependent protein *N*-glycosylation. Inhibition of the MVA pathway by fluvastatin attenuates metastasis in a mouse model of post-surgical metastatic breast cancer. Immediate clinical testing of fluvastatin is warranted.

Cyclic AMP-hydrolyzing phosphodiesterase inhibitors potentiate statin-induced cancer cell death

Joseph Longo[1,2*], Aleksandra A. Pandyra[1,2,3,4*], Mark D. Minden[1,2], Aaron D. Schimmer[1,2], Linda Z. Penn[1,2]

[1]Princess Margaret Cancer Centre, University Health Network, Toronto, Ontario, Canada
[2]Department of Medical Biophysics, University of Toronto, Toronto, Ontario, Canada
[3]Department of Molecular Medicine II, Medical Faculty, Heinrich Heine University, Düsseldorf, Germany
[4]Department of Gastroenterology, Hepatology, and Infectious Diseases, Heinrich Heine University, Düsseldorf, Germany
*Authors contributed equally to this work

Corresponding Author:
Dr. Linda Z. Penn
Princess Margaret Cancer Research Tower
101 College Street, 13-706
Toronto, Ontario, Canada M5G 1L7
lpenn@uhnresearch.ca
(416)-634-8770

Running title: Statins & PDE inhibitors induce cancer cell death

Keywords: Statins, mevalonate pathway, SREBP2, phosphodiesterase inhibitor, dipyridamole, cilostazol

Abbreviations: AML, acute myeloid leukemia; ANOVA, analysis of variance; cAMP, cyclic adenosine monophosphate; GGPP, geranylgeranyl pyrophosphate; HMG-CoA, 3-hydroxy-3-methylglutaryl Coenzyme A; HMGCR, HMG-CoA reductase; MM, multiple myeloma; MVA, mevalonate; PDE, phosphodiesterase; PKA, protein kinase A; SREBP, sterol regulatory element-binding protein.

Abstract

The anti-platelet drug dipyridamole has been shown to synergize with statins to induce cancer cell-specific apoptosis; however, given the polypharmacology of dipyridamole, the precise mechanism by which it potentiates statin-induced apoptosis remains unclear. Here, we applied a pharmacological approach to identify the specific activity of dipyridamole responsible for its synergistic anti-cancer interaction with statins. We evaluated compounds that phenocopy the individual activities of dipyridamole and assessed whether they were able to potentiate statin-induced cell death. Notably, agents that function to increase levels of intracellular cyclic adenosine monophosphate (cAMP), including the phosphodiesterase (PDE) inhibitor cilostazol, phenocopied dipyridamole and potentiated statin-induced cell death in acute myeloid leukemia (AML) and multiple myeloma (MM) cell lines. This response was independent of protein kinase A (PKA), one of the main effectors of cAMP, as both dipyridamole and cilostazol potentiated statin-induced cell death in PKA-deficient cells. Furthermore, we demonstrate that both dipyridamole and cilostazol inhibit statin-induced activation of sterol regulatory element-binding protein 2 (SREBP2), the main transcription factor that is activated in response to cholesterol depletion to restore homeostasis. Taken together, we provide evidence to support that cAMP-hydrolyzing PDE inhibitors, such as dipyridamole and cilostazol, potentiate statin-induced cancer cell death. Given that a number of PDE inhibitors are clinically-approved for various indications, they are immediately available for testing in combination with statins for the treatment of hematological malignancies.

1. Introduction

The synthesis of cholesterol and other isoprenoids via the mevalonate (MVA) pathway is tightly regulated to maintain homeostasis. In many cancer cells, an increased dependency on isoprenoid biosynthesis for growth and survival confers sensitivity to the statin family of drugs, which inhibits the rate-limiting enzyme of the MVA pathway, HMG-CoA reductase (HMGCR) (Mullen *et al.*, 2016). In normal and many cancer cells, however, treatment with statins activates the transcription factor sterol regulatory element-binding protein 2 (SREBP2), which functions to upregulate genes involved in MVA metabolism to restore homeostasis. Activation of this feedback response has been associated with statin resistance in cancer cells (Clendening *et al.*, 2010; Göbel *et al.*, 2019; Longo *et al.*, 2019). By contrast, subsets of cancer cells that fail to induce this feedback loop following statin treatment undergo apoptosis in response to statin exposure (Clendening *et al.*, 2010; Göbel *et al.*, 2019; Longo *et al.*, 2019).

We recently demonstrated that inhibition of this feedback response via RNAi-mediated knockdown of SREBP2 potentiates statin-induced cell death in lung and breast cancer cell lines (Pandyra *et al.*, 2015). Moreover, through a drug screening approach, our lab identified that the drug dipyridamole, an anti-platelet agent approved for secondary stroke prevention, can synergize with statins to induce apoptosis in acute myeloid leukemia (AML) and multiple myeloma (MM) cells (Pandyra *et al.*, 2014). We further demonstrated that dipyridamole inhibits statin-induced SREBP2 cleavage and activation, thus abrogating the restorative feedback loop of the MVA pathway (**Figure 1**) (Pandyra *et al.*, 2014). Since these initial observations in AML and MM, dipyridamole has been shown to inhibit statin-induced SREBP2 activation and potentiate statin-induced cell death in breast (Göbel *et al.*, 2019) and prostate (Longo *et al.*, 2019) cancer; however, the mechanism by which dipyridamole inhibits SREBP2 and potentiates statin-induced cancer cell death remains poorly characterized.

In this manuscript, we present data to suggest that the ability of dipyridamole to function as a phosphodiesterase (PDE) inhibitor and increase intracellular cyclic adenosine monophosphate (cAMP) levels, at least in part, contributes to its ability to inhibit SREBP2 cleavage/activation and potentiate statin-induced cancer cell death.

2. Material and methods

2.1 Cell culture and compounds

KMS11, LP1, OCI-AML-2 and OCI-AML-3 cell lines were cultured as described previously (Pandyra *et al.*, 2014). S49 wildtype (CCLZR352) and kin- (CCLZR347) cells were purchased from the University of California, San Francisco (UCSF) Cell Culture Facility and were cultured in Dulbecco's Modified Eagle Medium (DMEM) supplemented with 10% heat-inactivated horse serum, 100 units/mL penicillin and 100 µg/mL streptomycin. Cell lines were routinely confirmed to be mycoplasma-free using the MycoAlert Mycoplasma Detection Kit (Lonza). Atorvastatin calcium (21CEC Pharmaceuticals Ltd.) and fluvastatin sodium (US Biological) were dissolved in ethanol. Dipyridamole (Sigma), cilostazol (Tocris Bioscience), *S*-(4-nitrobenzyl)-6-thioinosine (NBMPR (Tocris Bioscience), 4-{[3′,4′-(methylenedioxy)benzyl]amino}-6-methoxyquinazoline (MBMQ) (Calbiochem), fasentin (Sigma) and forskolin (Sigma) were dissolved in DMSO. Mevalonate and dibutyryl-cAMP (db-cAMP) were purchased from Sigma and dissolved in water. Geranylgeranyl pyrophosphate (GGPP) (methanol:ammonia solution) was purchased from Sigma.

2.2 Cell viability assays

3-(4,5-dimethylthiazol-2-yl)-2,5-diphenyltetrazolium bromide (MTT) assays were performed as previously described (Dimitroulakos *et al.*, 2001). Briefly, cells were seeded at 15,000-20,000 cells/well in 96-well plates and treated as indicated for 48 hours. Percent cell viability was calculated relative to cells treated with solvent control(s). Fluvastatin dose-response curves were plotted and area under the dose-response curve (AUC) values were computed using GraphPad Prism v6 software.

2.3 Cell death assays

Cells were seeded at 750,000 cells/well in 6-well plates and treated as indicated for 48 hours. For propidium iodide staining, cells were fixed in 70% ethanol for at least 24 hours, stained with PI and analyzed by flow cytometry for the % pre-G1 DNA population as a measure of cell death, as previously described (Clendening *et al.*, 2010). For Annexin V staining, cells were processed and stained using the Annexin V-FITC Apoptosis Kit (BioVision Inc.) as per the manufacturer's protocol. Apoptosis assays using primary AML cells were performed as described previously (Pandyra *et al.*, 2014). Patient samples were obtained with informed consent under a protocol

approved by the University Health Network Research Ethics Board in accordance with the Declaration of Helsinki.

2.4 CCLE data mining

RNA sequencing expression data for the selected AML and MM human cell lines from the Cancer Cell Line Encyclopedia (CCLE) (Barretina *et al.*, 2012) was analyzed using the Xena Functional Genomics Explorer (Goldman *et al.*, 2015).

2.5 CRISPR/Cas9-mediated gene knockout

Independent small guide RNAs (sgRNAs) that target *PRKACA* were cloned into lentiCRISPR v2 (Addgene plasmid #52961). A sgRNA targeting a random locus on chromosome 10 was used as a negative control. HEK-293Tv cells were co-transfected with the sgRNA constructs, pMD2.G and psPAX2 using calcium-phosphate. LP1 cells were transduced with the lentiviral supernatants in the presence of 8 μg/mL polybrene, after which they were selected with 1 μg/mL puromycin. The sequences for the sgRNAs were obtained from (Hart *et al.*, 2015) and are as follows:

gC10 Random: AAACATGTATAACCCTGCGC

g*PRKACA* #1: ACGAATCAAGACCCTCGGCA

g*PRKACA* #2: AGATGTTCTCACACCTACGG

2.6 Immunoblotting

Immunoblotting was performed as previously described (Longo *et al.*, 2019), using the following primary antibodies: SREBP2 (1:250; BD Biosciences, 557037), Actin (1:3,000; Sigma, A2066), PKA C-α (Cell Signaling Technology, #4782), α-Tubulin (1:3,000; Calbiochem, CP06).

2.7 Quantitative RT-PCR

Total RNA was isolated from sub-confluent cells using TRIzol Reagent (Invitrogen). cDNA was synthesized from 500 ng RNA using SuperScript III (Invitrogen). Quantitative reverse transcription PCR (qRT-PCR) was performed using TaqMan probes (Applied Biosystems) for the following genes: *HMGCR* (Hs00168352), *HMGCS1* (Hs00266810), *INSIG1* (Hs01650979) and *GAPDH* (Hs99999905).

3. Results

3.1 The cAMP-hydrolyzing PDE3 inhibitor cilostazol phenocopies dipyridamole to potentiate statin-induced cancer cell death

Dipyridamole has been reported to play a number of diverse intracellular roles, such as functioning as an inhibitor of nucleoside transport (King *et al.*, 2006), glucose uptake (Steinfelder and Joost, 1988) and PDEs (Bender and Beavo, 2006) (**Figure 2A**). To test which, if any, of these reported functions of dipyridamole may be important for potentiating statin-induced cancer cell death, we assayed additional compounds with similar activities for their ability to phenocopy dipyridamole. For these experiments, we evaluated the following compounds: fasentin (glucose transporter 1 (GLUT1) inhibitor), NBMPR (equilibrative nucleoside transporter 1 (ENT1) inhibitor), MBMQ (cGMP-hydrolyzing PDE5 inhibitor) and cilostazol (cAMP-hydrolyzing PDE3 inhibitor). AML (OCI-AML-2, OCI-AML-3) and MM (KMS11) cells were treated with each compound alone or in combination with atorvastatin. The concentrations of each compound were chosen such that they had minimal single-agent effects on cell viability (< 20%), but were still within the range known to inhibit the target under investigation (Boleti *et al.*, 1997; Bouley *et al.*, 2005; Hourani *et al.*, 2001; M.-J. Kim *et al.*, 2005; J. Lu *et al.*, 2018; Shakur *et al.*, 2002; Wood *et al.*, 2008). Of the 4 compounds evaluated, only the combination of atorvastatin and cilostazol was observed to decrease AML and MM cell viability in all 3 cell lines (**Figure 2B**). We further demonstrated that these effects were not specific to atorvastatin, as a similar decrease in cell viability was observed when cilostazol was combined with fluvastatin, another member of the statin family of drugs (**Figure 3A**). Importantly, the addition of exogenous MVA or geranylgeranyl-pyrophosphate (GGPP) was able to fully rescue the decrease in cell viability caused by the statin-cilostazol combination (**Figure 3A**), supporting that these effects were due to MVA pathway inhibition.

3.2 Compounds that increase cAMP levels phenocopy dipyridamole and cilostazol to potentiate statin-induced apoptosis

PDEs catalyze the hydrolysis of cyclic adenosine monophosphate (cAMP) and cyclic guanosine monophosphate (cGMP), thereby regulating the intracellular concentrations of these secondary messengers. There are 11 PDE proteins that can be expressed in mammalian cells, which differ in their cellular functions, structures, expression patterns and affinities for cAMP and cGMP (Baillie *et al.*, 2019; Maurice *et al.*, 2014). Dipyridamole is known to inhibit multiple cAMP- and cGMP-hydrolyzing PDEs with varying affinities (Baillie *et al.*, 2019; Bender and Beavo, 2006). By

contrast, cilostazol is reported to be a specific inhibitor of PDE3, which is a cAMP-hydrolyzing PDE (Bender and Beavo, 2006; Maurice *et al.*, 2014). Given our observation that the statin-cilostazol combination was uniquely able to decrease the viability of AML and MM cells, we hypothesized that inhibition of cAMP hydrolysis by dipyridamole may be responsible for its ability to synergize with statins to induce apoptosis. To evaluate whether the PDEs targeted by dipyridamole and cilostazol are expressed in AML and MM cells, we mined the Cancer Cell Line Encyclopedia (CCLE) database (Barretina *et al.*, 2012). Indeed, multiple PDEs, including isoforms of PDE3, PDE5, PDE6, PDE7 and PDE8, are highly expressed in both AML and MM cell lines (**Figure 3B**). We subsequently evaluated the ability of other compounds that increase intracellular cAMP, including an adenylate cyclase activator (forskolin) and cell-permeable analog of cAMP (db-cAMP), to potentiate statin-induced apoptosis. Indeed, the combination of fluvastatin with dipyridamole, cilostazol, forskolin or db-cAMP was able to significantly induce apoptosis in OCI-AML-2 and OCI-AML-3 cells, whereas no significant apoptosis was observed when each compound was used as a single agent (**Figure 3C**). To determine whether primary AML cells were similarly sensitive to the combination of a statin and PDE inhibitor, we treated primary cells with fluvastatin and/or cilostazol for 48 hours, after which apoptosis was quantified by Annexin V staining using flow cytometry. Indeed, the fluvastatin-cilostazol combination significantly induced apoptosis in primary AML cells (**Figure 3D**). This is consistent with our previous report that the statin-dipyridamole combination can induce apoptosis in primary AML cells (Pandyra *et al.*, 2014). Notably, we evaluated the statin-cilostazol combination in three of the same patients as in our previous report with dipyridamole, and observed concordant results (Pandyra *et al.*, 2014). Collectively, these data suggest that elevating intracellular levels of cAMP may be an effective way to sensitize hematological cancer cells to statin-induced apoptosis.

3.3 Potentiation of statin-induced cancer cell death by dipyridamole or cilostazol is independent of protein kinase A (PKA)

cAMP can activate several effectors, the most well studied of which is the cAMP-dependent protein kinase A (PKA). PKA has been shown to phosphorylate a multitude of proteins with diverse roles in signal transduction, metabolism, ion transport and transcription regulation (Sassone-Corsi, 2012). Hence, we next evaluated whether activation of PKA was necessary for the ability of dipyridamole and cilostazol to potentiate statin-induced cancer cell death. To test this,

we took advantage of the murine S49 lymphoma cell system. Exposure of S49 cells to increasingly higher concentrations of cAMP allowed for the isolation of a mutant cell line (kin-) that is resistant to the cytotoxic effects of elevated cAMP (Orellana and McKnight, 1990). In particular, kin- cells have no detectable PKA activity due to improper *cis*-autophosphorylation at serine 338 during translation, which renders the catalytic subunit of PKA insoluble (Keshwani *et al.*, 2012). Interestingly, the combination of fluvastatin with either dipyridamole or cilostazol significantly induced cell death in both wildtype (WT) and kin- S49 cells (**Figures 4A-B**), suggesting that the ability of dipyridamole and cilostazol to potentiate statin-induced cell death is independent of PKA.

As an independent approach, we used CRISPR-Cas9 technology to knock out the alpha catalytic subunit of PKA (PKA-Cα, encoded by *PRKACA*) in LP1 cells. We chose LP1 cells for these experiments because we previously demonstrated that these cells robustly activate SREBP2 in response to statin exposure, and co-treatment with dipyridamole sensitizes them to statin-induced apoptosis (Pandyra *et al.*, 2014). We treated LP1 sublines expressing small guide RNAs (sgRNA) against *PRKACA* or a random locus on chromosome 10 (negative control) with a range of fluvastatin concentrations, as a single agent or in combination with a fixed, sub-lethal concentration of either dipyridamole or cilostazol. Consistent with our S49 data, both dipyridamole and cilostazol equally sensitized the control and PKA-depleted LP1 sublines to fluvastatin (**Figure 4C-D**), further supporting that PKA activation is not necessary for the ability of dipyridamole or cilostazol to potentiate statin-induced cancer cell death.

3.4 Cilostazol inhibits statin-induced SREBP2 cleavage and sterol metabolism gene expression

We previously demonstrated that dipyridamole functions as an inhibitor of statin-induced SREBP2 cleavage and activation, an effect which sensitizes cancer cells to statin-induced apoptosis (Longo *et al.*, 2019; Pandyra *et al.*, 2014). To test whether cilostazol similarly inhibited the cleavage and activation of SREBP2 in response to statin treatment, we treated LP1 cells with fluvastatin as a single agent or in combination with either dipyridamole or cilostazol, and then evaluated the expression of three SREBP2 target genes by qRT-PCR: *HMGCR*, HMG-CoA synthase 1 (*HMGCS1*) and insulin-induced gene 1 (*INSIG1*). As expected, treatment of LP1 cells with fluvastatin resulted in the induction of all three sterol-regulated genes, a response which was completely blocked by co-treatment with dipyridamole (**Figure 5A**). Cilostazol similarly inhibited

fluvastatin-induced expression of these SREBP2 target genes (**Figure 5A**). In line with these observations, both dipyridamole and cilostazol inhibited statin-induced cleavage of the SREBP2 protein (**Figure 5B**). Moreover, in line with our drug sensitivity data, both dipyridamole and cilostazol were able to inhibit statin-induced *HMGCS1* expression irrespective of PKA expression (**Figure 5C**).

4. Discussion

Our lab previously reported a novel role for the drug dipyridamole as an inhibitor of the SREBP family of transcription factors (Longo *et al.*, 2019; Pandyra *et al.*, 2014). As a result, dipyridamole can sensitize certain cancer cells to statin-induced apoptosis (**Figure 1**) (Longo *et al.*, 2019; Pandyra *et al.*, 2014); however, given the polypharmacology of dipyridamole, the mechanism by which it synergizes with statins remains poorly understood. As a step towards elucidating this mechanism, we evaluated individual compounds that phenocopied the different known functions of dipyridamole for their ability to sensitize AML and MM cell lines to statin-induced cell death. Through this approach, we were able to dissect the polypharmacology of dipyridamole and implicate its role as a cAMP-hydrolyzing PDE inhibitor in potentiating statin-induced cancer cell death.

The data we present here suggest that increasing intracellular cAMP levels inhibits statin-induced SREBP2 cleavage, and sensitizes AML and MM cells to statin-induced apoptosis. These data are consistent with a previous report, where the combination of lovastatin and db-cAMP was shown to enhance differentiation and cytotoxicity in embryonal carcinoma and neuroblastoma cell lines (Arnold *et al.*, 2010). We further provide evidence that cAMP-hydrolyzing PDE inhibitors, such as dipyridamole and cilostazol, can inhibit the SREBP2-regulated feedback mechanism of the MVA pathway. While cilostazol has previously been shown to inhibit insulin-induced expression of SREBP1 (a transcriptional regulator of fatty acid metabolism) (Jung *et al.*, 2014), this is the first report to demonstrate that cilostazol can inhibit statin-induced SREBP2 cleavage and expression of MVA pathway genes. Interestingly, this effect seemed to be independent of PKA activity, which was unexpected, as PKA is known to phosphorylate and negatively regulate SREBP1 *in vitro* at a residue that is conserved between SREBP1 and SREBP2 (M. Lu and Shyy, 2006). In our study, we observed that dipyridamole and cilostazol were able to inhibit SREBP2 activation and potentiate statin-induced apoptosis in cells that lacked PKA expression (**Figure 4,**

5C), thus ruling out PKA activation as the mechanism by which these PDE inhibitors sensitize cancer cells to statin-induced apoptosis.

In addition to PKA, cAMP is also known to regulate specific ion channels and the EPAC (exchange protein directly activated by cAMP) proteins, which are cAMP-dependent guanine-nucleotide exchange factors for the RAP GTPases (Bos, 2006). Interestingly, however, our lab previously reported that overexpression of myristoylated and constitutively active RAP1A did not modulate statin sensitivity in MCF10A cells (Yu *et al.*, 2018). Further investigation is required to delineate the mechanism by which an increase in cAMP levels converges on increased statin sensitivity, particularly the mechanism by which cAMP signalling inhibits activation of SREBP2.

Data in the literature are conflicting as to the role of PDEs in regulating lipid metabolism. A recent study demonstrated that combined inhibition of PDE4 and PDE8 in Leydig cells promotes SREBP2 signalling, cholesterol metabolism and steroidogenesis (Shimizu-Albergine *et al.*, 2016). By contrast, the data we present here clearly show that dipyridamole (a pan-PDE inhibitor) and cilostazol (a PDE3 inhibitor) can abrogate SREBP2 cleavage and activation in AML and MM cells exposed to a statin. It is therefore possible that different PDEs play unique roles in regulating SREBP2 signalling and sterol metabolism, and that PDE-mediated regulation of SREBP2 is tissue type- and context-dependent. In the context of cancer, dipyridamole has been shown to inhibit statin-induced SREBP2 processing in AML, MM, breast cancer and prostate cancer cells (Göbel *et al.*, 2019; Longo *et al.*, 2019; Pandyra *et al.*, 2014), suggesting similar regulation in many different cell types. Further work is needed to better understand the relationship between different PDEs and cholesterol metabolism in cancer.

The data presented here may have important clinical implications, as many cAMP-hydrolyzing PDE inhibitors are approved for several non-oncology indications (Maurice *et al.*, 2014). For example, cilostazol (marketed as Pletal) is currently approved and widely used to treat intermittent claudication. The overexpression of several PDEs has been observed in solid and hematological tumors, and the possibility of cAMP-hydrolyzing PDE inhibition as an anti-cancer strategy has been pre-clinically explored alone or in combination with chemo- and targeted molecular therapies (Lerner and Epstein, 2006; Lin *et al.*, 2013; Moon and Lerner, 2003; Noonan *et al.*, 2014; Zhang *et al.*, 2008; Zhou *et al.*, 2020). In haematological malignancies, primary chronic lymphocytic leukemia patient samples were characterized by PDE7B overexpression and found to be sensitive PDE7 inhibition in a cAMP-dependent manner (Zhang *et al.*, 2008). Another

study found a strong synergistic combinatorial effect between Adenosine A2A receptor agonists and cAMP-hydrolyzing PDE inhibitors in MM and diffuse large B-cell lymphoma cell lines and primary patient samples (Rickles *et al.*, 2010). Given that a number of PDE inhibitors are poised for repurposing, and since statins have demonstrated anti-cancer activity in early-phase clinical trials (Bjarnadottir *et al.*, 2013; Garwood *et al.*, 2010; Goss *et al.*, 2016; Hus *et al.*, 2011; Knox *et al.*, 2005; Kornblau *et al.*, 2007; Murtola *et al.*, 2018), studies are needed to further evaluate the therapeutic benefit of a statin in combination with various PDE inhibitors for the treatment of cancer. As the combination of cilostazol and statins has already been evaluated clinically in healthy subjects (Bramer *et al.*, 1999; J.-R. Kim *et al.*, 2019) and in patients with cardiovascular indications (Ari *et al.*, 2015; Hiatt *et al.*, 2008) without added adverse effects, there is the possibility that they can be effectively combined for the treatment of cancer.

5. Conclusion

In summary, we propose a working model where cAMP-hydrolyzing PDE inhibitors, such as dipyridamole and cilostazol, inhibit SREBP2 activation and potentiate statin-induced apoptosis in hematological cancer cells via a PKA-independent mechanism. Given that statins and a number of PDE inhibitors are already approved for various non-oncology indications, future studies are needed to thoroughly evaluate the potential therapeutic benefit of these agents for the treatment of hematological malignancies. Moreover, our experimental approach to dissect the polypharmacology of dipyridamole is one that may be useful when interrogating novel functions of other repurposed drugs.

Acknowledgments

We thank all members of the Penn lab for helpful discussions. This work was supported by funding from the Canada Research Chairs program (L.Z. Penn), Canadian Institutes of Health Research (CIHR) (FRN: 142263; L.Z. Penn), a CIHR Doctoral Research Award (J. Longo, A.A. Pandyra) and a Canadian Breast Cancer Foundation (CBCF) Doctoral Award (A.A. Pandyra). This work was also supported by the Office of the Assistant Secretary of Defense for Health Affairs, through the Breast Cancer Research Program under Award No. W81XWH-16-1-0068 (to L.Z. Penn). Opinions, interpretations, conclusions and recommendations are those of the author and are not necessarily endorsed by the Department of Defense.

Conflict of interest

The authors have no conflicts of interest to declare.

Author contributions

JL, AAP and LZP conceived and designed the study. JL and AAP performed experiments, as well as analyzed and interpreted the experimental data. MDM and ADS provided the primary AML cells and clinical expertise. JL, AAP and LZP wrote the manuscript. All authors read and approved the manuscript. LZP supervised the study.

References

Ari H, Emlek N, Ari S, Coşar S, Doğanay K, Aydin C, … Melek M (2015) The Effect of High Dose Cilostazol and Rosuvastatin on Periprocedural Myocardial Injury in Patients with Elective Percutaneous Coronary Intervention. *Acta Cardiol Sin* **31**, 292–300.

Arnold DE, Gagne C, Niknejad N, McBurney MW, and Dimitroulakos J (2010) Lovastatin induces neuronal differentiation and apoptosis of embryonal carcinoma and neuroblastoma cells: Enhanced differentiation and apoptosis in combination with dbcAMP. *Mol Cell Biochem* **345**, 1–11.

Baillie GS, Tejeda GS, and Kelly MP (2019) Therapeutic targeting of 3′,5′-cyclic nucleotide phosphodiesterases: inhibition and beyond. *Nat Rev Drug Discov* **18**, 770–796.

Barretina J, Caponigro G, Stransky N, Venkatesan K, Margolin AA, Kim S, … Garraway LA (2012) The Cancer Cell Line Encyclopedia enables predictive modelling of anticancer drug sensitivity. *Nature* **483**, 603–607.

Bender AT, and Beavo JA (2006) Cyclic nucleotide phosphodiesterases: Molecular regulation to clinical use. *Pharmacol Rev* **58**, 488–520.

Bjarnadottir O, Romero Q, Bendahl PO, Jirström K, Rydén L, Loman N, … Borgquist S (2013) Targeting HMG-CoA reductase with statins in a window-of-opportunity breast cancer trial. *Breast Cancer Res Treat* **138**, 499–508.

Boleti H, Coe IR, Baldwin SA, Young JD, and Cass CE (1997) Molecular identification of the equilibrative NBMPR-sensitive (es) nucleoside transporter and demonstration of an equilibrative NBMPR-insensitive (ei) transport activity in human erythroleukemia (K562)

cells. *Neuropharmacology* **36**, 1167–1179.

Bos JL (2006) Epac proteins: multi-purpose cAMP targets. *Trends Biochem Sci* **31**, 680–686.

Bouley R, Pastor-Soler N, Cohen O, McLaughlin M, Breton S, and Brown D (2005) Stimulation of AQP2 membrane insertion in renal epithelial cells in vitro and in vivo by the cGMP phosphodiesterase inhibitor sildenafil citrate (Viagra). *Am J Physiol - Ren Physiol* **288**.

Bramer SL, Brisson J, Corey AE, and Mallikaarjun S (1999) Effect of multiple cilostazol doses on single dose lovastatin pharmacokinetics in healthy volunteers. *Clin Pharmacokinet* **37**, 69–77.

Clendening JW, Pandyra A, Li Z, Boutros PC, Martirosyan A, Lehner R, … Penn LZ (2010) Exploiting the mevalonate pathway to distinguish statin-sensitive multiple myeloma. *Blood* **115**, 4787–97.

Dimitroulakos J, Ye LY, Benzaquen M, Moore MJ, Kamel-Reid S, Freedman MH, … Penn LZ (2001) Differential sensitivity of various pediatric cancers and squamous cell carcinomas to lovastatin-induced apoptosis: Therapeutic implications. *Clin Cancer Res* **7**, 158–167.

Garwood ER, Kumar AS, Baehner FL, Moore DH, Au A, Hylton N, … Esserman LJ (2010) Fluvastatin reduces proliferation and increases apoptosis in women with high grade breast cancer. *Breast Cancer Res Treat* **119**, 137–144.

Göbel A, Breining D, Rauner M, Hofbauer LC, and Rachner TD (2019) Induction of 3-hydroxy-3-methylglutaryl-CoA reductase mediates statin resistance in breast cancer cells. *Cell Death Dis* **10**, 91.

Goldman M, Craft B, Swatloski T, Cline M, Morozova O, Diekhans M, … Zhu J (2015) The UCSC cancer genomics browser: Update 2015. *Nucleic Acids Res* **43**, D812–D817.

Goss GD, Jonker DJ, Laurie SA, Weberpals JI, Oza AM, Spaans JN, … Dimitroulakos J (2016) A phase I study of high-dose rosuvastatin with standard dose erlotinib in patients with advanced solid malignancies. *J Transl Med* **14**, 1–11.

Hart T, Chandrashekhar M, Aregger M, Steinhart Z, Brown KR, MacLeod G, … Moffat J (2015) High-Resolution CRISPR Screens Reveal Fitness Genes and Genotype-Specific Cancer Liabilities. *Cell* **163**, 1515–1526.

Hiatt WR, Money SR, and Brass EP (2008) Long-term safety of cilostazol in patients with peripheral artery disease: the CASTLE study (Cilostazol: A Study in Long-term Effects). *J Vasc Surg* **47**, 330–336.

Hourani SMO, Boon K, Fooks HM, and Prentice DJ (2001) Role of cyclic nucleotides in vasodilations of the rat thoracic aorta induced by adenosine analogues. *Br J Pharmacol* **133**, 833–840.

Hus M, Grzasko N, Szostek M, Pluta A, Helbig G, Woszczyk D, … Dmoszynska A (2011) Thalidomide, dexamethasone and lovastatin with autologous stem cell transplantation as a salvage immunomodulatory therapy in patients with relapsed and refractory multiple myeloma. *Ann Hematol* **90**, 1161–1166.

Jung YA, Kim HK, Bae KH, Seo HY, Kim HS, Jang BK, … Park KG (2014) Cilostazol inhibits insulin-stimulated expression of sterol regulatory binding protein-1c via inhibition of LXR and Sp1. *Exp Mol Med* **46**, e73.

Keshwani MM, Klammt C, von Daake S, Ma Y, Kornev AP, Choe S, … Taylor SS (2012) Cotranslational cis-phosphorylation of the COOH-terminal tail is a key priming step in the maturation of cAMP-dependent protein kinase. *Proc Natl Acad Sci U S A* **109**, E1221-9.

Kim J-R, Jung JA, Kim S, Huh W, Ghim J-L, Shin J-G, and Ko J-W (2019) Effect of Cilostazol on the Pharmacokinetics of Simvastatin in Healthy Subjects. *Biomed Res Int* **2019**, 1365180.

Kim M-J, Park K-G, Lee K-M, Kim H-S, Kim S-Y, Kim C-S, … Lee I-K (2005) Cilostazol inhibits vascular smooth muscle cell growth by downregulation of the transcription factor E2F. *Hypertension* **45**, 552–6.

King AE, Ackley MA, Cass CE, Young JD, and Baldwin SA (2006) Nucleoside transporters: from scavengers to novel therapeutic targets. *Trends Pharmacol Sci* **27**, 416–425.

Knox JJ, Siu LL, Chen E, Dimitroulakos J, Kamel-Reid S, Moore MJ, … Oza AM (2005) A Phase I trial of prolonged administration of lovastatin in patients with recurrent or metastatic squamous cell carcinoma of the head and neck or of the cervix. *Eur J Cancer* **41**, 523–530.

Kornblau SM, Banker DE, Stirewalt D, Shen D, Lemker E, Verstovsek S, … Appelbaum FR (2007) Blockade of adaptive defensive changes in cholesterol uptake and synthesis in AML by the addition of pravastatin to idarubicin + high-dose Ara-C: A phase 1 study. *Blood* **109**, 2999–3006.

Lerner A, and Epstein PM (2006) Cyclic nucleotide phosphodiesterases as targets for treatment of haematological malignancies. *Biochem J* **393**, 21–41.

Lin DC, Xu L, Ding LW, Sharma A, Liu LZ, Yang H, … Phillip Koeffler H (2013) Genomic and functional characterizations of phosphodiesterase subtype 4D in human cancers. *Proc Natl*

435 *Acad Sci U S A* **110**, 6109–6114.
436 Longo J, Mullen PJ, Yu R, van Leeuwen JE, Masoomian M, Woon DTS, … Penn LZ (2019) An
437 actionable sterol-regulated feedback loop modulates statin sensitivity in prostate cancer. *Mol*
438 *Metab* **25**, 119–130.
439 Lu J, Montgomery BK, Chatain GP, Bugarini A, Zhang Q, Wang X, … Chittiboina P (2018)
440 Corticotropin releasing hormone can selectively stimulate glucose uptake in corticotropinoma
441 via glucose transporter 1. *Mol Cell Endocrinol* **470**, 105–114.
442 Lu M, and Shyy JYJ (2006) Sterol regulatory element-binding protein 1 is negatively modulated
443 by PKA phosphorylation. *Am J Physiol - Cell Physiol* **290**, 1477–1486.
444 Maurice DH, Ke H, Ahmad F, Wang Y, Chung J, and Manganiello VC (2014) Advances in
445 targeting cyclic nucleotide phosphodiesterases. *Nat Rev Drug Discov* **13**, 290–314.
446 Moon EY, and Lerner A (2003) PDE4 inhibitors activate a mitochondrial apoptotic pathway in
447 chronic lymphocytic leukemia cells that is regulated by protein phosphatase 2A. *Blood* **101**,
448 4122–4130.
449 Mullen PJ, Yu R, Longo J, Archer MC, and Penn LZ (2016) The interplay between cell signalling
450 and the mevalonate pathway in cancer. *Nat Rev Cancer* **16**, 718–731.
451 Murtola TJ, Syvälä H, Tolonen T, Helminen M, Riikonen J, Koskimäki J, … Tammela TLJ (2018)
452 Atorvastatin Versus Placebo for Prostate Cancer Before Radical Prostatectomy-A
453 Randomized, Double-blind, Placebo-controlled Clinical Trial. *Eur Urol* **74**, 697–701.
454 Noonan KA, Ghosh N, Rudraraju L, Bui M, and Borrello I (2014) Targeting immune suppression
455 with PDE5 inhibition in end-stage multiple myeloma. *Cancer Immunol Res* **2**, 725–31.
456 Orellana SA, and McKnight GS (1990) The S49 Kin- cell line transcribes and translates a
457 functional mRNA coding for the catalytic subunit of cAMP-dependent protein kinase. *J Biol*
458 *Chem* **265**, 3048–3053.
459 Pandyra A, Mullen PJ, Kalkat M, Yu R, Pong JT, Li Z, … Penn LZ (2014) Immediate utility of
460 two approved agents to target both the metabolic mevalonate pathway and its restorative
461 feedback loop. *Cancer Res* **74**, 4772–4782.
462 Pandyra AA, Mullen PJ, Goard CA, Ericson E, Sharma P, Kalkat M, … Penn LZ (2015) Genome-
463 wide RNAi analysis reveals that simultaneous inhibition of specific mevalonate pathway
464 genes potentiates tumor cell death. *Oncotarget* **6**, 26909–26921.
465 Rickles RJ, Pierce LT, Giordano TP, Tam WF, McMillin DW, Delmore J, … Lee MS (2010)

Adenosine A2A receptor agonists and PDE inhibitors: A synergistic multitarget mechanism discovered through systematic combination screening in B-cell malignancies. *Blood* **116**, 593–602.

Sassone-Corsi P (2012) The Cyclic AMP pathway. *Cold Spring Harb Perspect Biol* **4**, a011148.

Shakur Y, Fong M, Hensley J, Cone J, Movsesian MA, Kambayashi J-I, … Liu Y (2002) Comparison of the effects of cilostazol and milrinone on cAMP-PDE activity, intracellular cAMP and calcium in the heart. *Cardiovasc Drugs Ther* **16**, 417–27.

Shimizu-Albergine M, Van Yserloo B, Golkowski MG, Ong SE, Beavo JA, and Bornfeldt KE (2016) SCAP/SREBP pathway is required for the full steroidogenic response to cyclic AMP. *Proc Natl Acad Sci U S A* **113**, E5685–E5693.

Steinfelder HJ, and Joost HG (1988) Inhibition of insulin-stimulated glucose transport in rat adipocytes by nucleoside transport inhibitors. *FEBS Lett* **227**, 215–219.

Wood TE, Dalili S, Simpson CD, Hurren R, Mao X, Saiz FS, … Schimmer AD (2008) A novel inhibitor of glucose uptake sensitizes cells to FAS-induced cell death. *Mol Cancer Ther* **7**, 3546–3555.

Yu R, Longo J, Van Leeuwen JE, Mullen PJ, Ba-Alawi W, Haibe-Kains B, and Penn LZ (2018) Statin-induced cancer cell death can be mechanistically uncoupled from prenylation of RAS family proteins. *Cancer Res* **78**, 1347–1357.

Zhang L, Murray F, Zahno A, Kanter JR, Chou D, Suda R, … Insel PA (2008) Cyclic nucleotide phosphodiesterase profiling reveals increased expression of phosphodiesterase 7B in chronic lymphocytic leukemia. *Proc Natl Acad Sci U S A* **105**, 19532–19537.

Zhou S, Xu H, Tang Q, Xia H, and Bi F (2020) Dipyridamole Enhances the Cytotoxicities of Trametinib against Colon Cancer Cells through Combined Targeting of HMGCS1 and MEK Pathway. *Mol Cancer Ther* **19**, 135–146.

FIGURE LEGENDS

Figure 1: Dipyridamole inhibits the sterol-regulated feedback loop of the MVA pathway. Schematic representation of the mevalonate (MVA) pathway. Statins inhibit the rate-limiting enzyme of the pathway, HMG-CoA reductase (HMGCR), which catalyzes the conversion of HMG-CoA to MVA. MVA is converted into various metabolites that are important for cell survival and growth, including geranylgeranyl pyrophosphate (GGPP) and cholesterol. Statin-mediated cholesterol depletion induces the cleavage and activation of sterol regulatory element-binding protein 2 (SREBP2), which in turn induces the transcription of genes involved in MVA metabolism to restore homeostasis. We previously identified that the drug dipyridamole can inhibit statin-induced SREBP2 activation; however, the mechanism by which it inhibits SREBP2 cleavage remains poorly understood.

Figure 2: The cAMP-hydrolyzing PDE3 inhibitor cilostazol potentiates the anti-cancer activity of atorvastatin. (**A**) Schematic representation of the reported targets of dipyridamole and additional agents that target these proteins (bolded & italicized). ENT = equilibrative nucleoside transporter, GLUT = glucose transporter, PDE = phosphodiesterase, PKA = protein kinase A. (**B**) The glucose uptake inhibitor fasentin (at concentrations of 12.5 μM, 6.3 μM and 12.5 μM in OCI-AML-2, OCI-AML-3 and KMS11 cells, respectively), ENT inhibitor NBMPR (20 μM for all cell lines) and cGMP-hydrolyzing PDE5 inhibitor MBMQ (10 μM for all cell lines) did not potentiate the cytotoxic activity of atorvastatin (4 μM, 2 μM and 4 μM in OCI-AML-2, OCI-AML-3 and KMS11 cells, respectively) following 48 hr of treatment. The cAMP-hydrolyzing PDE3 inhibitor cilostazol (25 μM, 12.5 μM and 25 μM in OCI-AML-2, OCI-AML-3 and KMS11 cells, respectively) potentiated atorvastatin activity in all 3 cell lines. #$p < 0.05$ (comparing the atorvastatin alone group to atorvastatin + cilostazol group), *$p < 0.05$ (comparing the atorvastatin + cilostazol groups within each cell line to the corresponding atorvastatin alone and cilostazol alone groups). Statistical significance was determined via one-way ANOVA and Tukey's multiple comparisons tests. Data are represented as the mean + SD.

Figure 3: Statin-cilostazol-induced cancer cell death can be rescued by exogenous MVA or GGPP, and phenocopied by other inducers of cAMP. (**A**) Cilostazol (12.5 μM) potentiated fluvastatin-induced cell death (2 μM in KMS11 and 0.5 μM in OCI-AML-3 cells), which was fully

rescued by exogenous MVA (0.2 mM) or GGPP (2 μM). *p < 0.05 (one-way ANOVA with Tukey's multiple comparisons test, where the fluvastatin + cilostazol group of each cell line is significantly different from all other treatment groups). Data are represented as the mean + SD. (**B**) RNA expression of the different PDEs in a panel of human AML and MM cell lines. Data was mined from the Cancer Cell Line Encyclopedia (CCLE) database. (**C**) The PDE3 inhibitor cilostazol (20 μM), adenylate cyclase activator forskolin (10 μM) and db-cAMP (0.1 mM) in combination with fluvastatin (4 μM for OCI-AML-2 or 2 μM for OCI-AML-3) induced apoptosis after 48 hr of treatment as measured by Annexin V staining. *p < 0.05 (one-way ANOVA with Tukey's multiple comparisons test, where each group was compared to every other group within the same cell line). Data are represented as the mean + SD. (**D**) Primary AML cells were cultured in the presence of solvent controls, 5 μM fluvastatin, 20 μM cilostazol or the combination. After 48 hr, cells were labelled with FITC-conjugated Annexin V and analyzed by flow cytometry. Data from four independent AML patient samples are represented as box plots with whiskers depicting the maximum and minimum values. *p < 0.05 (one-way ANOVA with Dunnett's multiple comparisons test, where each treatment group was compared to the solvent controls group).

Figure 4: Potentiation of statin-induced cancer cell death by dipyridamole or cilostazol is independent of PKA. (**A**) Immunoblot for PKA C-α expression in S49 wildtype (WT) or kin- (PKA-null) cells. (**B**) S49 WT and kin- cells were treated with 5 μM fluvastatin alone or in combination with either 2.5 μM dipyridamole or 5 μM cilostazol for 48 hr, fixed in ethanol and assayed for DNA fragmentation (% pre-G1 population) as a marker of cell death by propidium iodide staining. Data are represented as the mean + SD. *p < 0.05 (one-way ANOVA with Tukey's multiple comparisons test, where the fluvastatin + dipyridamole or cilostazol groups are significantly different from the control and single agent groups). (**C**) Immunoblot for PKA C-α expression in LP1 cells expressing Cas9 and a sgRNA to a random locus on chromosome 10 (gC10 Random) or one of two different locations in *PRKACA*. (**D**) LP1 gC10 Random and g*PRKACA* sublines were treated with a range of fluvastatin concentrations (0-24 μM) ± either 5 μM dipyridamole (DP) or 10 μM cilostazol for 48 hr, after which cell viability was determined using an MTT assay. The area under each fluvastatin dose-response curve is plotted. Data are represented as the mean + SD. *p < 0.05 (one-way ANOVA with Dunnett's multiple comparisons test, where each group was compared to the fluvastatin alone group within each subline).

Figure 5: Cilostazol inhibits statin-induced SREBP2 cleavage and sterol metabolism gene expression. (**A**) LP1 cells were treated with 4 μM fluvastatin alone or in combination with 5 μM dipyridamole or 20 μM cilostazol for 16 hr, and RNA was then isolated to assay for *HMGCR*, *HMGCS1* and *INSIG1* expression by qRT-PCR. mRNA expression data are normalized to *GAPDH* expression. Data are represented as the mean + SD. *$p < 0.05$ (one-way ANOVA with Dunnett's multiple comparisons test, where each group was compared to the solvent controls group). (**B**) LP1 cells were treated with 4 μM fluvastatin alone or in combination with either 5 μM dipyridamole (DP) or 20 μM cilostazol for 8 hr, and protein was then harvested to assay for SREBP2 cleavage (activation) by immunoblotting. (**C**) LP1 g*PRKACA* sublines were treated with 4 μM fluvastatin alone or in combination with 5 μM dipyridamole or 20 μM cilostazol for 16 hr, and RNA was then isolated to assay for *HMGCS1* expression by qRT-PCR. mRNA expression data are normalized to *GAPDH* expression. Data are represented as the mean + SD. *$p < 0.05$ (one-way ANOVA with Sidak's multiple comparisons test, where each group was compared to the solvent controls group).

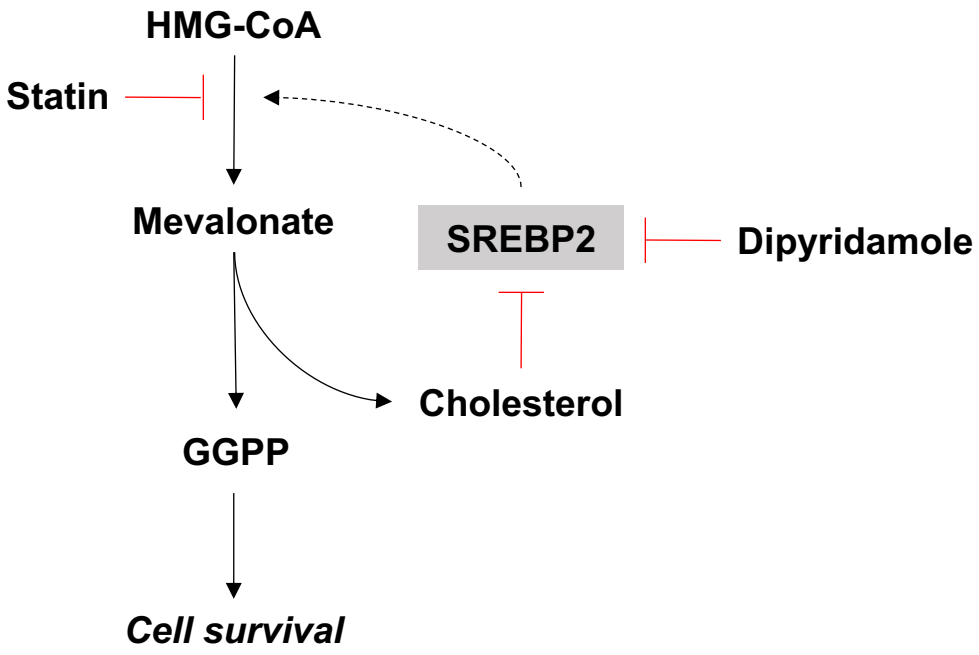
HMG-CoA
Statin
Mevalonate
SREBP2
Dipyridamole
Cholesterol
GGPP
Cell survival

FIGURE 1

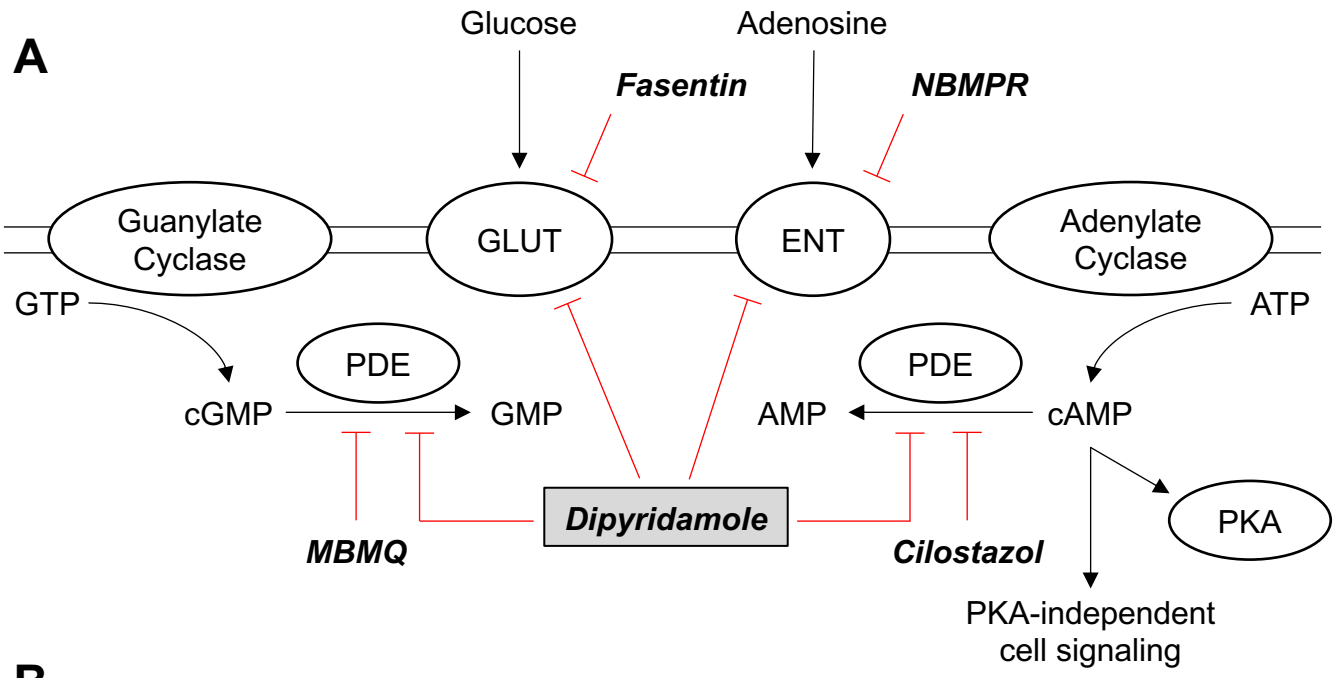
A
Glucose
Adenosine
Fasentin
NBMPR
Guanylate Cyclase
GLUT
ENT
Adenylate Cyclase
GTP
ATP
PDE
PDE
cGMP
GMP
AMP
cAMP
Dipyridamole
MBMQ
Cilostazol
PKA
PKA-independent cell signaling

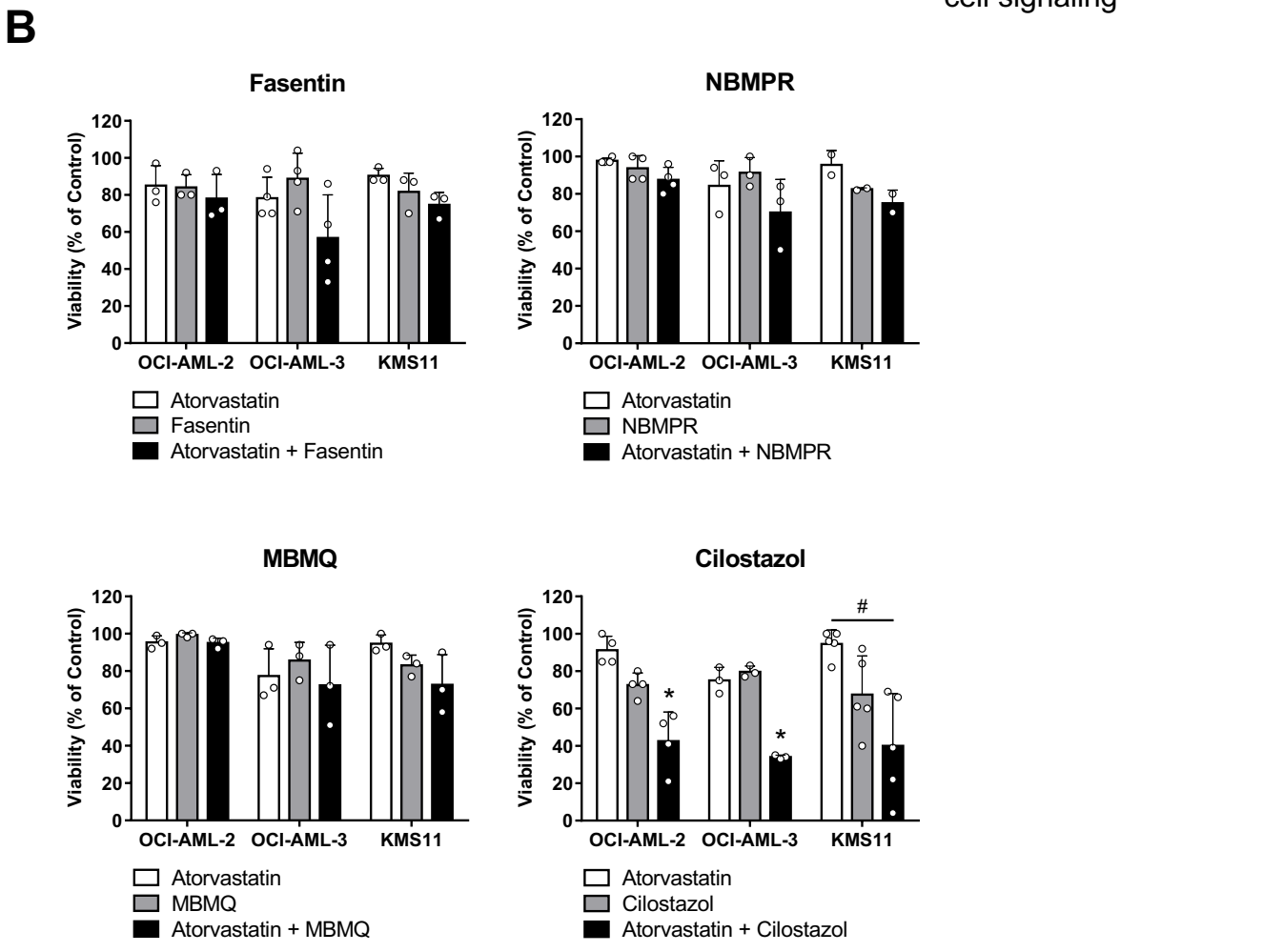
B
Fasentin
NBMPR
MBMQ
Cilostazol
Viability (% of Control)
OCI-AML-2
OCI-AML-3
KMS11
Atorvastatin
Fasentin
Atorvastatin + Fasentin
NBMPR
Atorvastatin + NBMPR
MBMQ
Atorvastatin + MBMQ
Cilostazol
Atorvastatin + Cilostazol
*
#

FIGURE 2

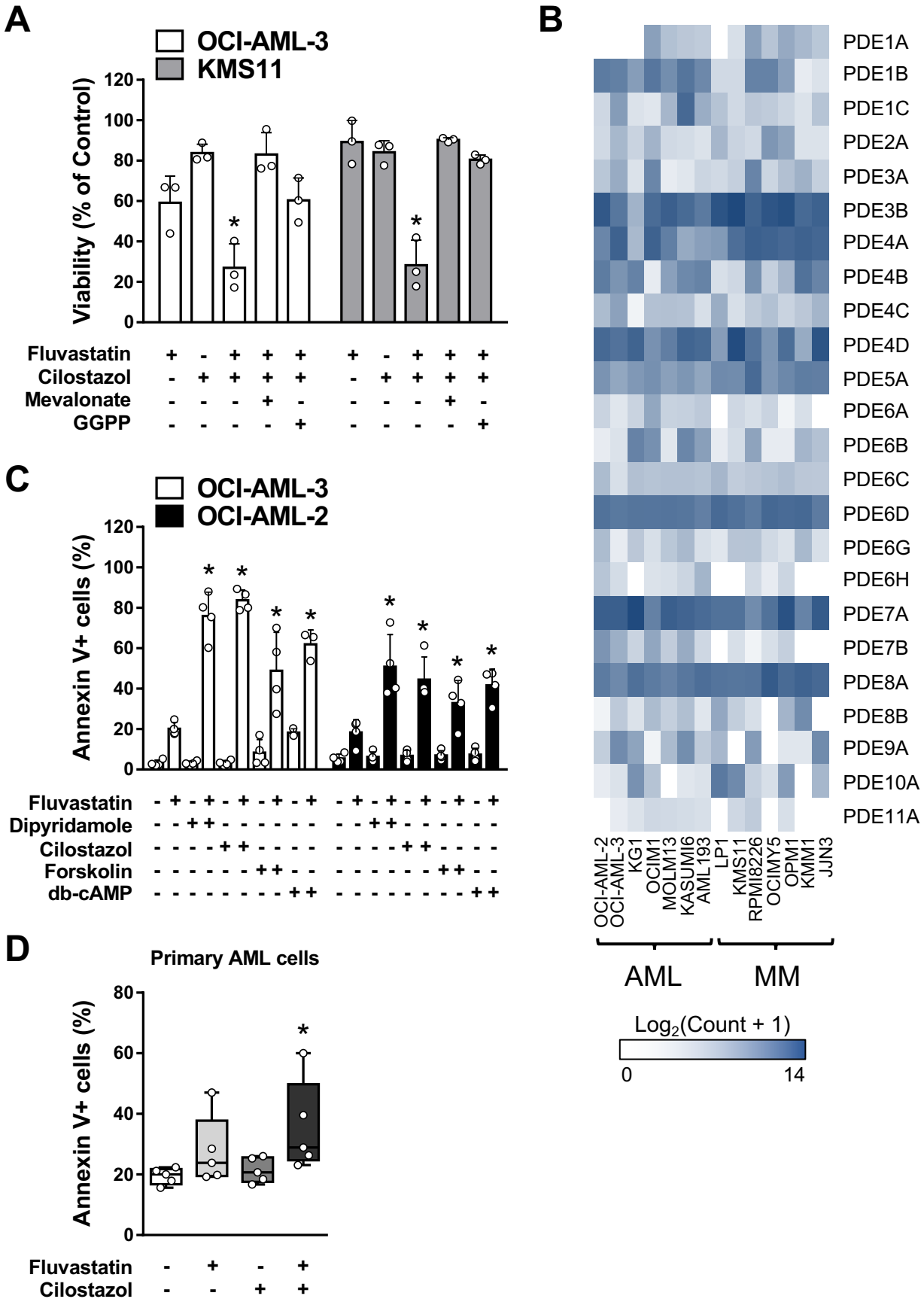
A
OCI-AML-3
KMS11
Viability (% of Control)
120
100
80
60
40
20
0
Fluvastatin + - + + + + - + + +
Cilostazol - + + + + - + + + +
Mevalonate - - - + - - - - + -
GGPP - - - - + - - - - +
B
PDE1A
PDE1B
PDE1C
PDE2A
PDE3A
PDE3B
PDE4A
PDE4B
PDE4C
PDE4D
PDE5A
PDE6A
PDE6B
PDE6C
PDE6D
PDE6G
PDE6H
PDE7A
PDE7B
PDE8A
PDE8B
PDE9A
PDE10A
PDE11A
OCI-AML-2
OCI-AML-3
KG1
OCIM1
MOLM13
KASUMI6
AML193
LP1
KMS11
RPMI8226
OCIMY5
OPM1
KMM1
JJN3
AML
MM
Log2(Count + 1)
0
14
C
OCI-AML-3
OCI-AML-2
Annexin V+ cells (%)
120
100
80
60
40
20
0
Fluvastatin - + - + - + - + - - + - + - + - + -
Dipyridamole - - + + - - - - - - - + + - - - - -
Cilostazol - - - - + + - - - - - - - + + - - -
Forskolin - - - - - - + + - - - - - - - + + - -
db-cAMP - - - - - - - - + + - - - - - - - + +
D
Primary AML cells
Annexin V+ cells (%)
80
60
40
20
0
Fluvastatin - + - +
Cilostazol - - + +

FIGURE 3

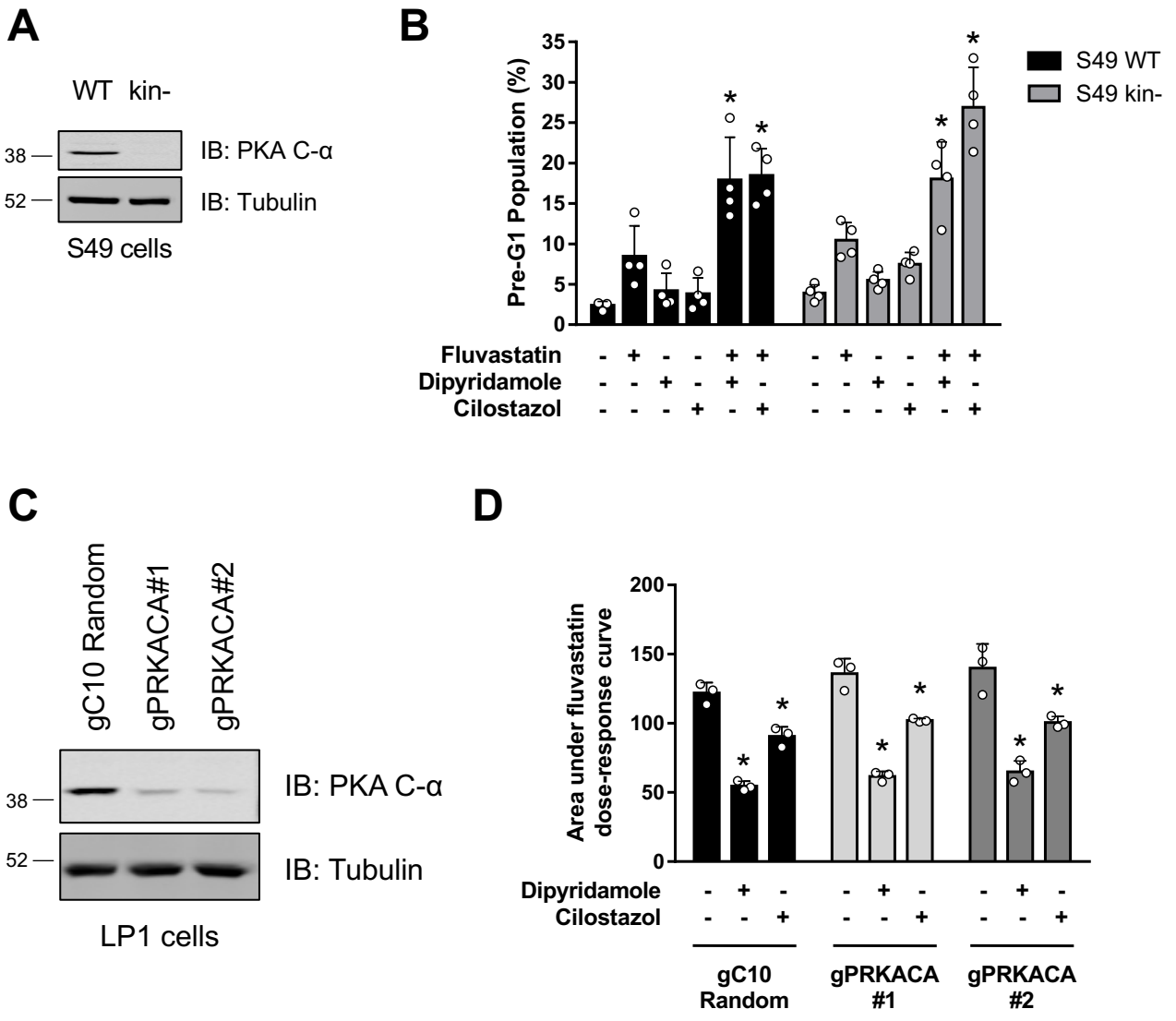
A
WT kin-
38
52
IB: PKA C-α
IB: Tubulin
S49 cells
B
Pre-G1 Population (%)
35
30
25
20
15
10
5
0
S49 WT
S49 kin-
Fluvastatin
Dipyridamole
Cilostazol
C
gC10 Random
gPRKACA#1
gPRKACA#2
38
52
IB: PKA C-α
IB: Tubulin
LP1 cells
D
Area under fluvastatin dose-response curve
200
150
100
50
0
Dipyridamole
Cilostazol
gC10 Random
gPRKACA #1
gPRKACA #2

FIGURE 4

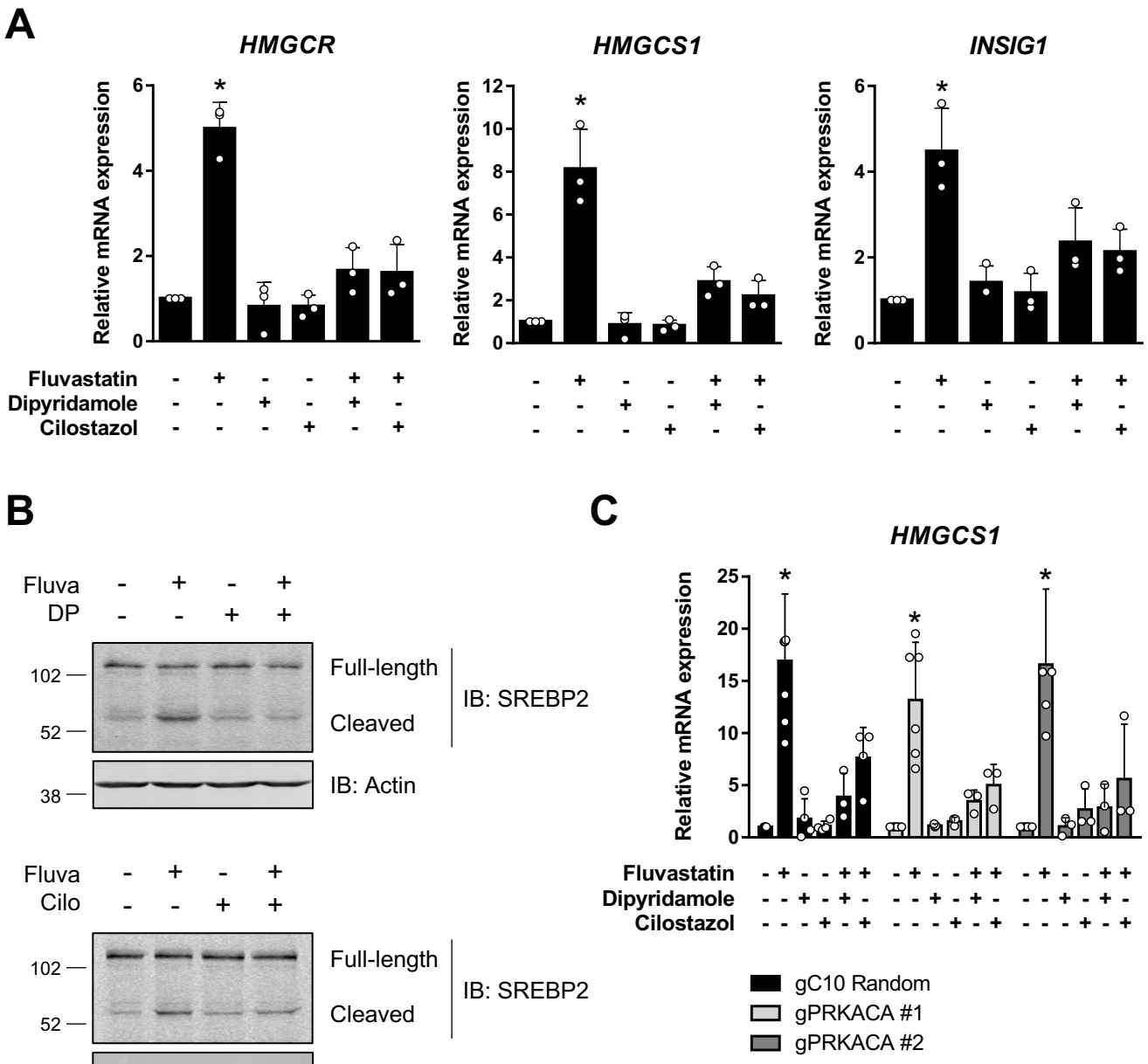
A
HMGCR
HMGCS1
INSIG1
Relative mRNA expression
Fluvastatin
Dipyridamole
Cilostazol
B
Fluva
DP
Cilo
102
52
38
Full-length
Cleaved
IB: SREBP2
IB: Actin
C
HMGCS1
Relative mRNA expression
gC10 Random
gPRKACA #1
gPRKACA #2

FIGURE 5

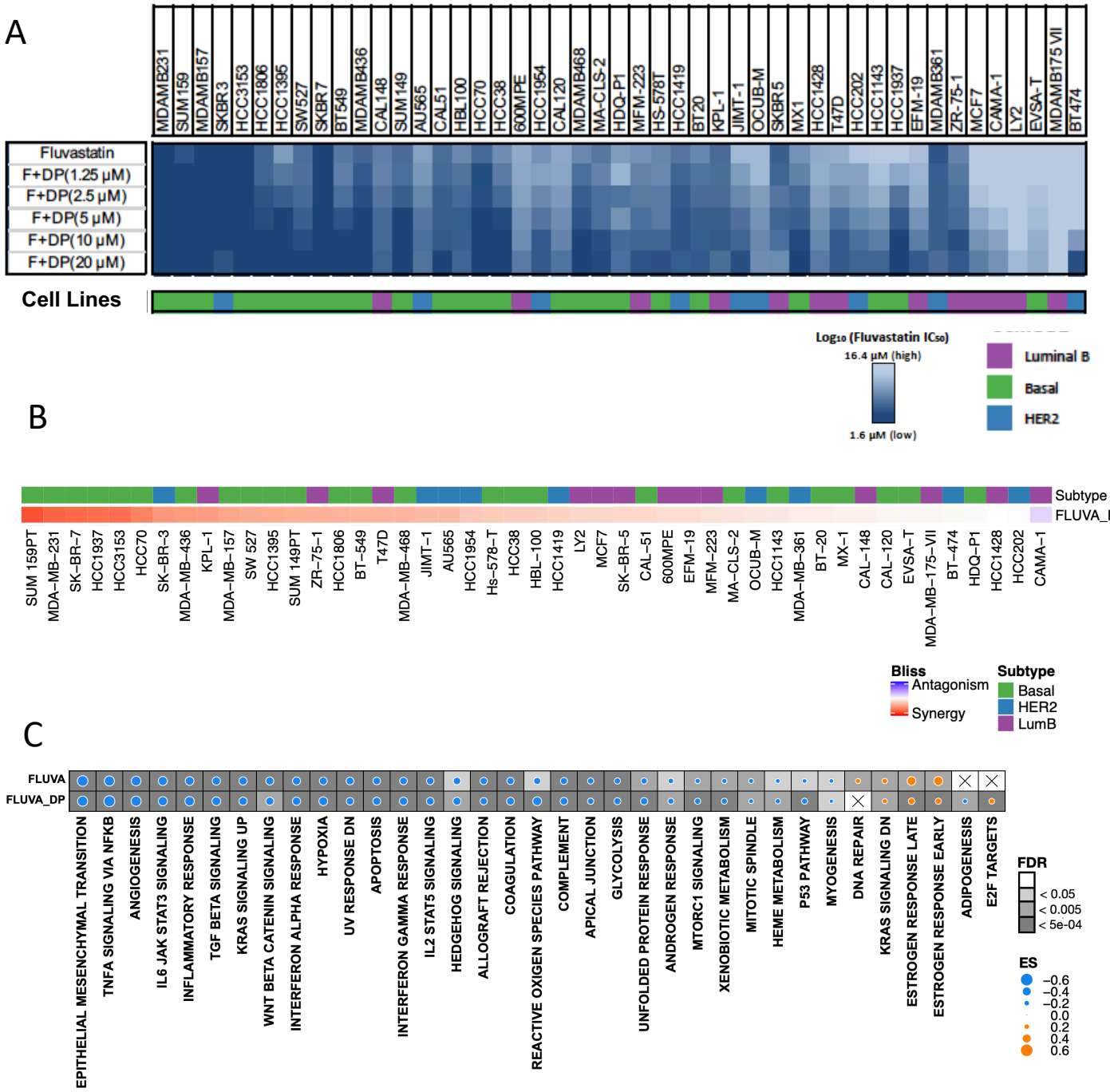

Figure. 1. Fluvastatin+DP combination synergy analysis (A)Heatmap of Log10(Fluvastatin IC50) values of a high-throughput drug synergy screen against 47 breast cancer (BC) cell lines visualizing the 15th to 85th percentile. BC cell lines were treated with a drug matrix of fluvastatin +/- dipyridamole. After 5 days of drug treatment, cell viability was assessed by SRB assay. SCMOD2 cell line subtyping was assigned to the BC cell line panel. Data presented are the average of 2 biological replicates (fluvastatin +/- dipyridamole). (B) Heatmap of synergy scores, measured using Bliss Index model, of the different drug combinations ordered by the synergy scores of fluvastatin and dipyridamole. Subtypes are based on SCMOD2 subtyping scheme. [fluvastatin (Fluva); dipyridamole (DP)]. (C) Gene set enrichment analysis using Hallmark gene set collection

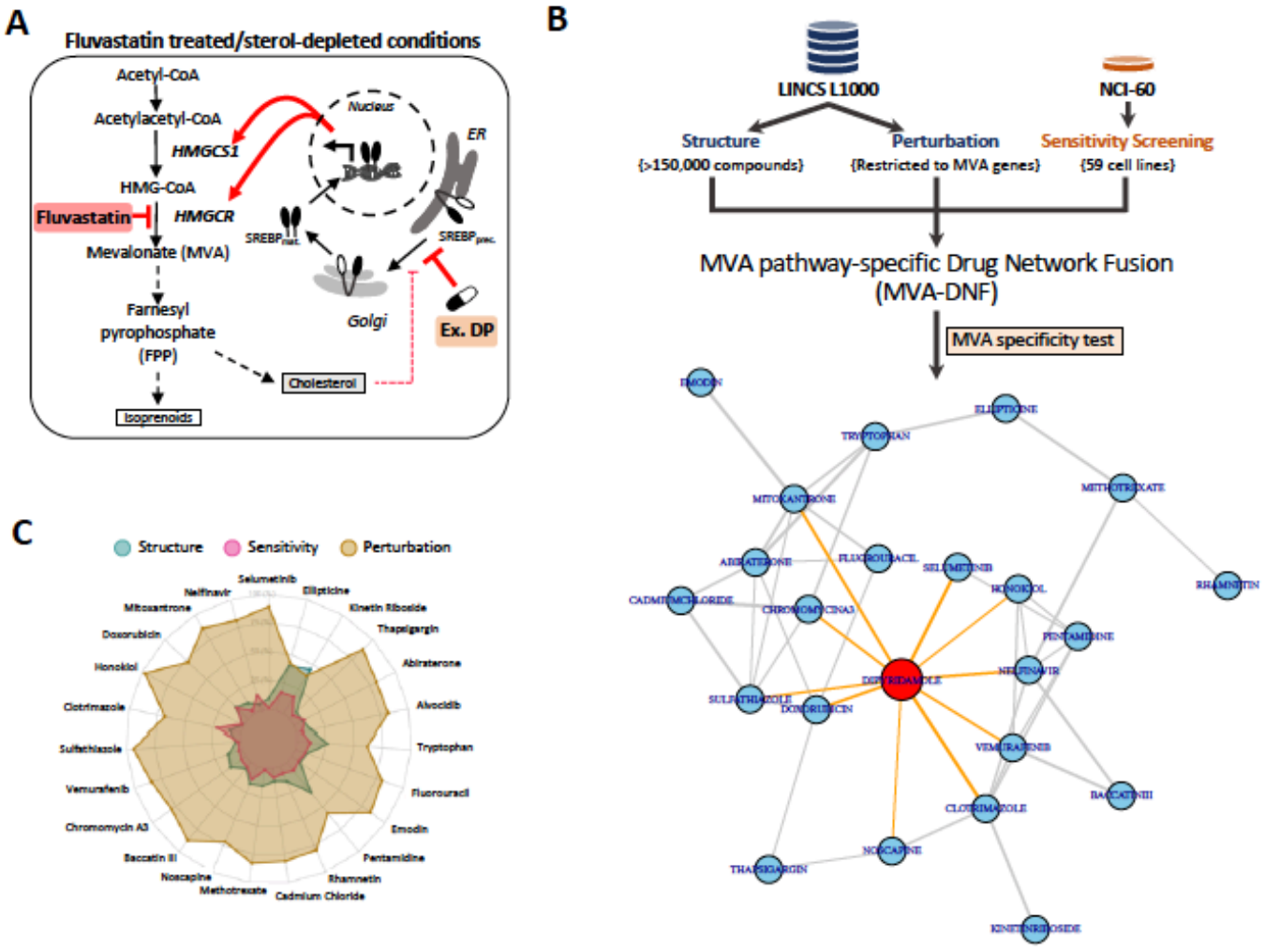

Fig. 2. A schematic of mevalonate (MVA) pathway and overview of the computational pharmacogenomics workflow. (A) Under Fluvastatin treatment/sterol-depleted conditions, MVA pathway end-products levels decrease, activating the SREBP-mediated feedback response to restore cholesterol and other non-sterol end-products levels by activating MVA-target genes transcription. Dipyridamole (DP) blocks the SREBP-mediated feedback response thereby potentiating fluvastatin induced cell death. (B) An overview of the computational pharmacogenomics approach, MVA-DNF, used to identify "dipyridamole-like" drug candidates. MVA-DNF combines drug structure, drug sensitivity, and drugperturbation datasets restricted to MVA-specific genes. Permutation testing was performed to assess the statistical significance of potential drug hits similar to DP (pvalue <0.05), compared to 1000 networks generated from random selection of 6 drugs within the perturbation layer. A drug network representation of dipyridamole and identified analogues is demonstrated. Each node represents a drug and edges connect drugs with based on statistical significance. (C) Radar plots of the top twenty-three DP-like drugs (p-val<0.05) to show individual layer contributions. Percentage contribution of each layer is shown from the center (0%) to the outer edges (100%).

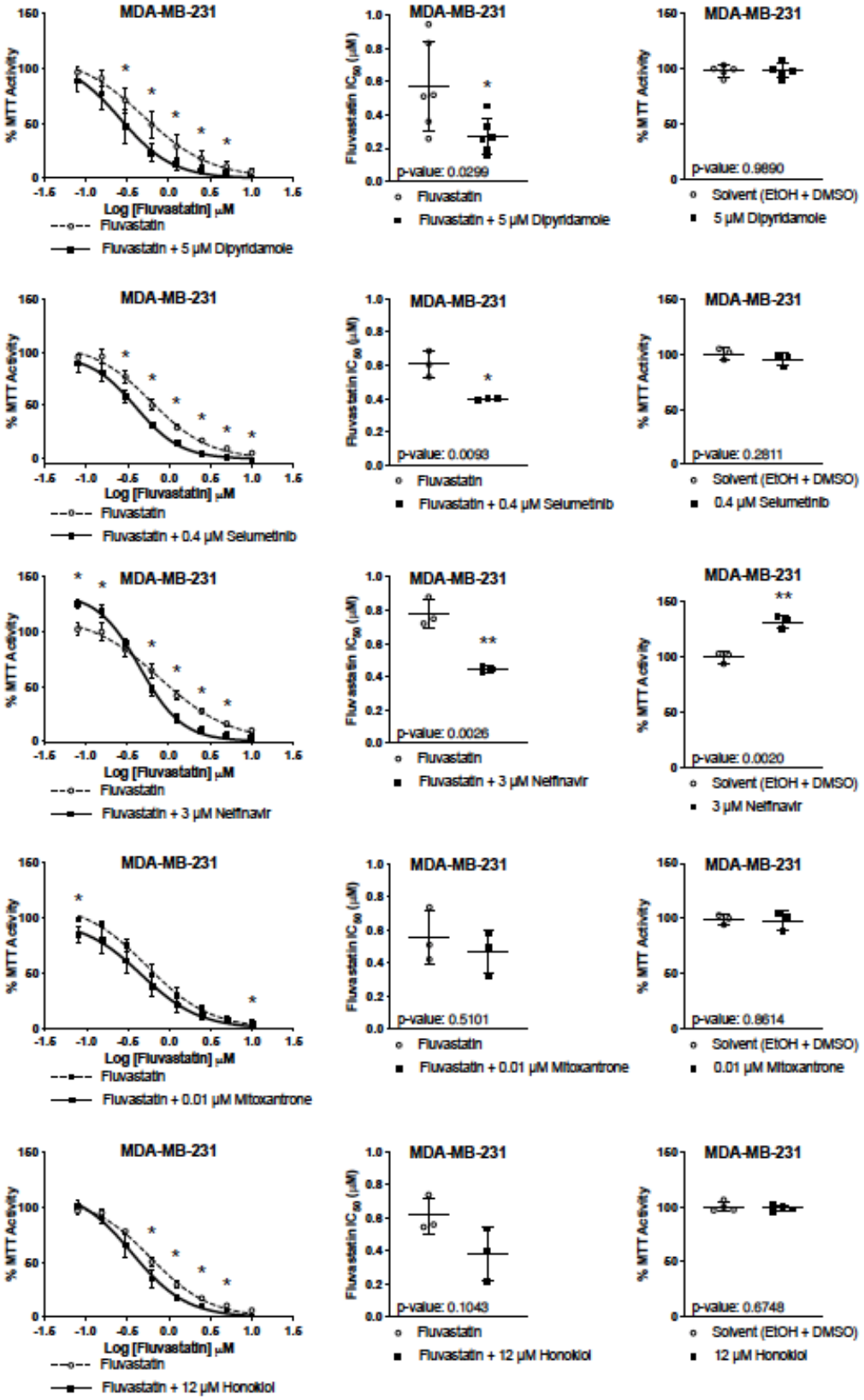

Fig 3. MDA-MB-231 cells were treated with a range of fluvastatin doses +/- a sublethal dose of dipyridamole (5 µM), nelfinavir (3 µM), honokiol (12 µM) or selumetinib (0.4 µM) for 72 hours, and cell viability was determined using an MTT assay. The dose-response curve and IC50 values and control values are plotted. Error bars represent the mean +/- SD, n > 3, *p <0.05, **p <0.01 (Students t test, unpaired, two-tailed).

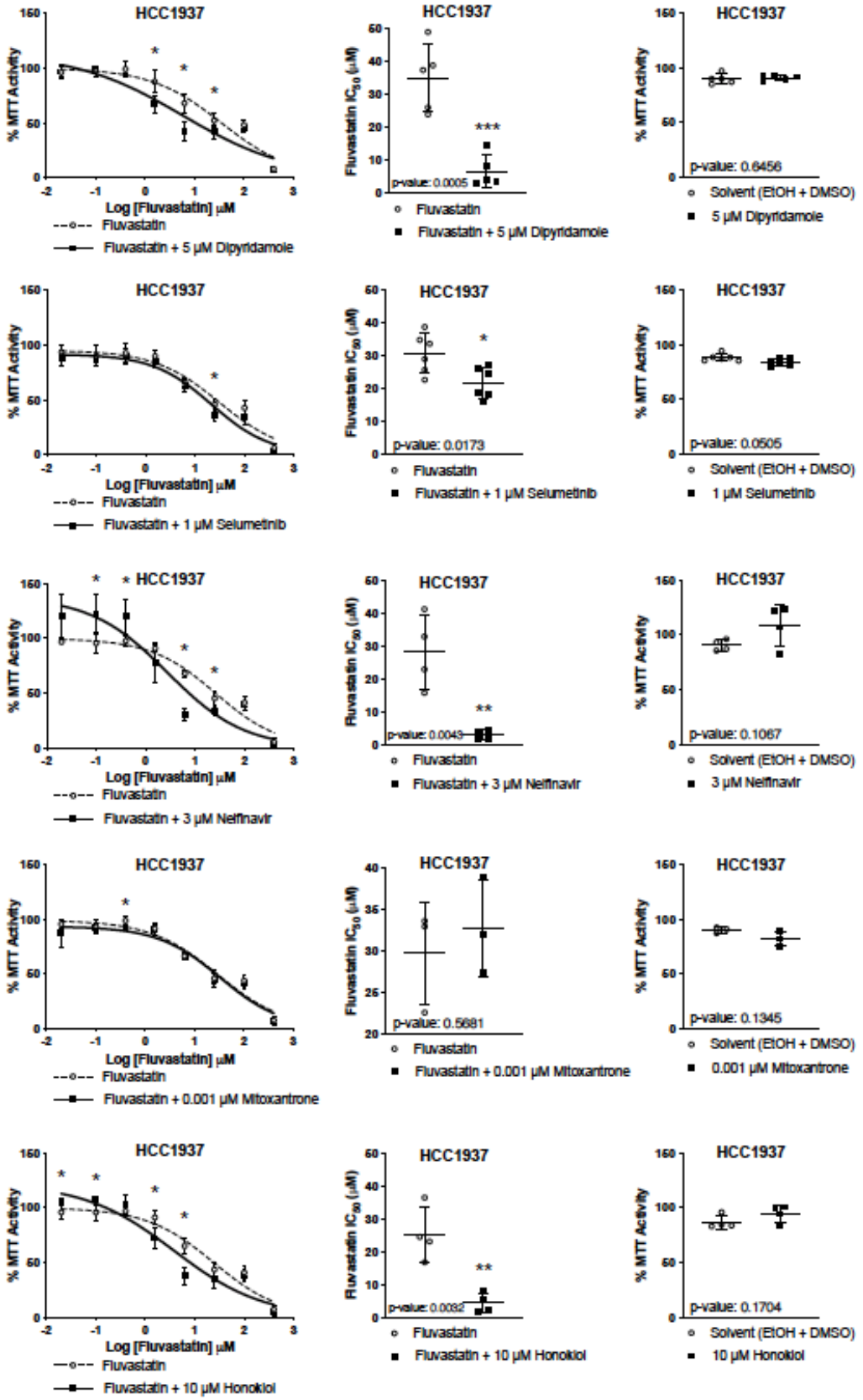

Fig. 4. HCC1937 cells were treated with a range of fluvastatin doses +/- a sub-lethal dose of dipyridamole (5 µM), nelfinavir (3 µM), honokiol (10 µM) or selumetinib (1µM) for 72 hours, and cell viability was determined using an MTT assay. The dose response curve and IC50 values and control values are plotted. Error bars represent the mean +/- SD, n > 3, *p <0.05, *p <0.01, ***p <0.001 (Students t test, unpaired, twotailed).

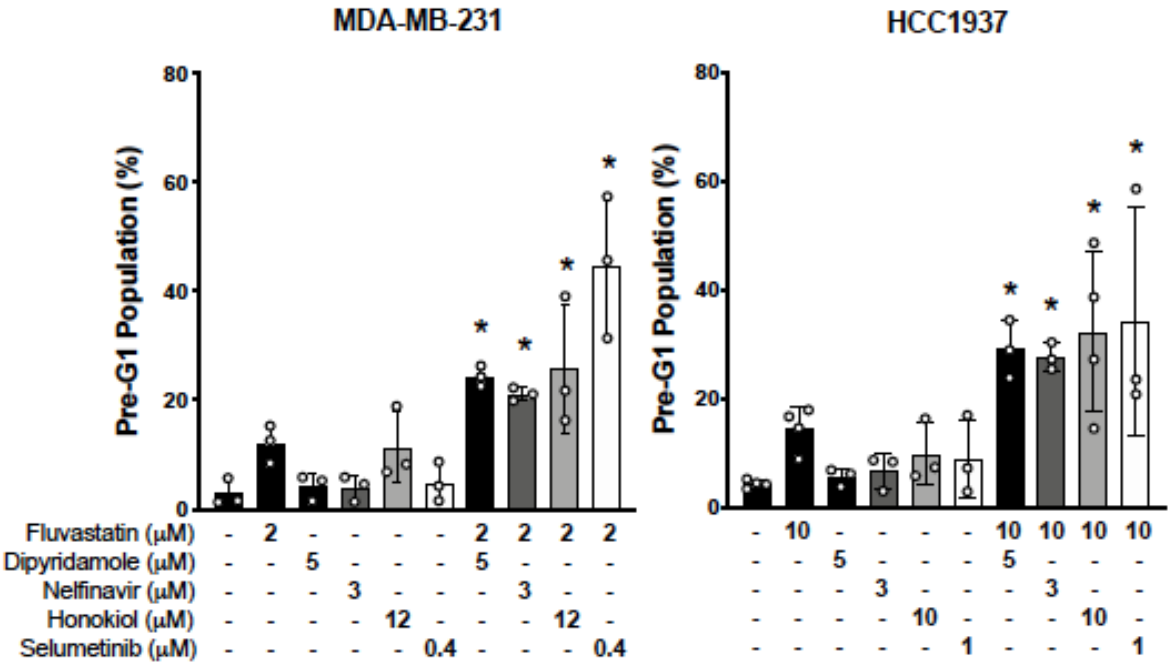

Fig. 5. Dipyridamole-like drugs potentiate fluvastatin induced cell death. (A) MDA-MB-231 and HCC1937 cells were treated with solvent controls or fluvastatin +/- dipyridamole (DP), nelfinavir (NFV), honokiol (HNK) or selumetinib (Selu) for 72 hours, fixed in ethanol and assayed for DNA fragmentation (% pre-G1 population) as a marker of cell death by propidium iodide staining. Error bars represent the mean + SD, n > 3, *p < 0.05 (one-way ANOVA with Bonferroni's multiple comparisons test, where each group was compared to the solvent controls group).